

TECHNISCHE UNIVERSITÄT MÜNCHEN  
Ingenieur fakultät Bau Geo Umwelt  
Lehrstuhl für Ingenieurgeologie

# Vegetation effects on avalanche dynamics

Thomas Feistl

Vollständiger Abdruck der von der Ingenieur fakultät Bau Geo Umwelt der Technischen Universität München zur Erlangung des akademischen Grades eines

Doktor der Naturwissenschaften

genehmigten Dissertation.

Vorsitzender: Univ.-Prof. Dr. M. Manhart

Prüfer der Dissertation: 1. Univ.-Prof. Dr. K. Thuro  
2. Univ.-Prof. Dr. M. Hanewinkel

Albert-Ludwigs-Universität Freiburg

3. Univ.-Prof. Dr. J. W. van de Kuilen

Die Dissertation wurde am 19.02.2015 bei der Technischen Universität München eingereicht und durch die Ingenieur fakultät Bau Geo Umwelt am 31.05.2015 angenommen.



# *Acknowledgements*

This work would not have been possible without the support of many people who I would like to thank first:

My direct supervisors Perry Bartelt and Peter Bebi always supported me, not only technically but also by encouraging me. It was a pleasure to work with them, to get insights in my field of studies from their different perspectives and to profit from their explicit knowledge on avalanche dynamics and mountain ecosystems.

I would like to thank Prof. Kuroschi Thuro and Prof. Marc Hanewinkel for their guidance throughout the last three years. They supported me in whatever direction my work developed and helped to bring it to a successful finish.

Bernhard Zenke, leader of the Bavarian avalanche service established the contact and cooperation with the SLF that led to the project “Dynamics of forest avalanches”. My thesis was mainly funded by this project and therefore by the Bavarian Environment Agency. Important input not only with data but also with knowledge was additionally provided by Hans Konetschny and Armin Fischer, who I especially would like to thank.

I thank my colleagues from the avalanche dynamics and risk management group for their friendship and the unique working atmosphere: Marc, Yves, Cesar, Walter, Anselm, Betty, Christina, Michi, Martina, Lisa, Linda, Jochen, James, Martin, Claudia, Lara and Juan Pablo. I want to thank Michaela who introduced me into this field of study and Lorenz and Irene who helped me with field work. Stefan Margreth, Lukas Stoffel and Mark Schaer gave me interesting insights into avalanche engineering and hazard mapping. The “Werkstatt” and the electronics group at SLF helped me whenever I needed them.

Thanks to all other colleagues and friends for the extraordinary four years at the SLF in Davos and for all the memorable moments we shared.

Finally I want to thank my parents who always believe in me, who support every decision in my life, who encouraged me to study, to climb mountains and to move to Davos.

*“In theory, theory and practice are the same. In practice, they are not.”*

Albert Einstein

# *Abstract*

Avalanches endanger people, destroy property and bury traffic routes in deep snow. Forests are an effective, economic and ecologic avalanche mitigation measure. The interaction between avalanches and forest vegetation represents the interaction between two dynamic systems with different time scales. One system is mechanical, the other system is biological. The biological system forest can prevent avalanches from starting, but long years of vegetation growth and evolution can be removed in seconds by fast moving flowing snow. Both natural hazard mitigation and forest management benefit from investigating and understanding the interaction between forests and avalanches. It facilitates the efficient planning of technical and organizational mitigation measures. Locating potential avalanche release areas in forested terrain as well as predicting avalanche runout distances and velocity as a function of forest type and structure is therefore key.

The interaction and interference of vegetation and avalanches starts with the first gliding motion of snow in forest gaps and ends with vegetation decelerating avalanches until snow piles up behind tree stands. This complex process is compounded by the fact that the protective capacity of forests undergoes permanent change. Quantitative knowledge of the governing processes is limited. This work contributes to the general understanding of forest-avalanche interaction and presents theoretical approaches and practical applications to facilitate the quantification and simulation of the governing physical processes. It consists of three ISI articles.

The first article investigates vegetation effects on glide-snow avalanche release. Full-depth glide-snow avalanches are identified to be the most critical forest avalanches. Their formation depends on the basal friction which changes with different vegetation covers. Glide-snow avalanche release is modeled by calculating the required threshold strain rate for failure of the snowpack below the release area which is commonly referred to as “stauchwall”. To this end the compression of the visco-elastic material snow is calculated with a Burgers model, where failure depends on snow characteristics, slope angle, slab length and basal friction. Field data, that was gathered within the framework of this thesis, was used to evaluate basal friction values for typical vegetation patterns on glide-snow avalanche release areas. The required ground roughness to prevent glide-snow avalanche release for a certain slope angle and forest gap length can be quantified with this model approach. For example, a forest gap in  $35^\circ$  steep terrain covered with long compacted grass should not exceed 15 m length, whereas shrubs or dead wood that penetrate into the snow cover prevent snow gliding on a  $40^\circ$  steep and 30 m long slope.

The second article shows that small to medium size avalanches are decelerated and stopped by forest, particularly because trees remove snow from the avalanche flow. A novel theoretical approach was developed to model the amount of snow that is extracted from the avalanche flow (the so-called “detrainment approach”). Because mass detrainment removes momentum from the avalanche, it can be considered a stopping (frictional) process. The detrainment approach was implemented in the avalanche simulation software RAMMS and was evaluated by back-calculating well-documented past events. Field observations of deposited avalanche snow behind single trees and tree

groups confirmed the detrainment approach. Snow detrainment by trees depends on forest structural parameters, the cohesive properties of snow and on the associated avalanche velocity. Stem density, tree species and forest composition were identified to be the crucial forest parameters. The application of the detrainment approach is limited to events where trees remain standing after avalanche impact. In contrast, the classical friction approach is based on the assumption that avalanches break, uproot, overturn and entrain trees. Thus, in order to apply the two different approaches one needs to distinguish forest destruction and non-destruction.

The third article investigates forest damage by avalanches. Tree breakage occurs if the bending stresses exerted by an avalanche exceed the bending strength of a tree stem. The bending stress in turn depends on the avalanche flow regime and the affected stem and crown area of the tree. Four loading cases for four different flow regimes were defined to derive formulas to calculate their bending stresses. Impact height, snow density, velocity and stem diameter are the crucial parameters to calculate the dynamic impact pressure on the tree. For slow moving plug-like wet snow avalanches, the static loading of snow on the tree is dominant in comparison to the velocity dependent dynamic loading. Trees break from the loading exerted by the powder cloud of a dry flowing avalanche even if the density and therefore the impact pressure is relatively small (less than 3 kPa). On the other hand slow moving wet snow avalanches that only affect the stem, exert bending stresses that are high enough to cause widespread damage. Different tree species have different bending strength. Birch, for example, can withstand higher impact pressures than spruce. Also their crown area is smaller as they lose their leaves in winter. Such differences in bending strength and crown area contribute to the explanation why certain tree species are dominant in avalanche paths, such as birch, larch or green alder. Predicting forest destruction - and therefore the stopping effect of the forest - requires consideration of both, avalanche flow regime and tree characteristics. A new tool was implemented in avalanche modeling to forecast forest destruction and consequently to distinguish between the friction and detrainment approaches.

The results of these articles show, that vegetation effects on avalanche dynamics depend not only on the avalanche flow regime, moving mass and velocity but also on forest stand characteristics. The interaction between the mechanical and biological systems is intricate. The plant composition in the release area and in the avalanche path can hinder the gliding motion of snow, affects the avalanche flow dynamics and leads to deceleration and runout shortening. The results of this thesis will assist decision-makers to quantify and optimize the effectiveness of forest to prevent damage caused by avalanches.

# *Zusammenfassung*

Lawinen gefährden Menschen, zerstören Häuser und verschütten Verkehrswege. Dagegen sind Wälder wirksame, ökonomische und ökologische Lawinenschutzmassnahmen. Lawinen und Vegetation sind zwei dynamische Systeme mit verschiedenen Zeitskalen, die sich gegenseitig beeinflussen. Das biologische System Wald kann einerseits Lawinen am Anbrechen hindern, aber andererseits kann über lange Jahre gewachsene Vegetation innerhalb von Sekunden von schnell fliessendem Schnee zerstört werden. Naturgefahren- und Forstmanagement profitieren beide von der Erforschung der Wechselwirkung zwischen Wald und Lawinen. Wachsendes Verständnis erleichtert die zielgerichtete Planung von technischen und strukturellen Schutzmassnahmen. Der Schlüssel dafür ist das Eingrenzen von möglichen Anrisszonen in Waldgebieten und die Vorhersage von Lawinenausläuflängen und Geschwindigkeiten in Abhängigkeit von Waldtyp und Struktur.

Die Wechselwirkung zwischen Vegetation und Lawinen beginnt mit der ersten Gleitbewegung von Schnee in Waldlücken, setzt sich mit erhöhter turbulenter Reibung fort und endet erst mit der Ablagerung von Lawinenschnee hinter Baumgruppen. Die Beschreibung dieser komplexen Vorgänge wird durch die Tatsache erschwert, dass sich die Schutzwirkung von Wald beständig verändert. Quantitatives Wissen über die entscheidenden Prozesse ist begrenzt. Diese Arbeit trägt zum grundsätzlichen Verständnis der Wechselwirkung zwischen Wald und Lawinen bei und es werden theoretische Ansätze und praktische Anwendungen vorgestellt, um die entscheidenden physikalischen Prozesse zu quantifizieren und zu simulieren. Sie setzt sich aus drei wissenschaftlichen ISI Artikeln zusammen.

Der erste Artikel befasst sich mit dem Einfluss von Vegetation auf Gleitschneelawinenanrisse. Gleitschneelawinen, die auf dem Boden abgleiten, werden als kritischste Waldlawinen identifiziert. Ob eine Lawine anreisst, hängt von der Bodenreibung ab, die sich mit der Vegetation verändert. Gleitschneelawinenanrisse werden modelliert, indem man den Grenzwert berechnet, ab dem der sogenannte "Stauchwall", die Schneedecke unterhalb der Anrisszone, versagt. Dafür wird das Zusammenstauchen des viskoelastischen Materials Schnee mit einem Burgers Modell berechnet. Das Versagen hängt von Schneeeigenschaften, Hangneigung, Anrisslänge und Bodenreibung ab. Werte für die Bodenreibung typischer Vegetationsarten konnten mit Hilfe von Feldmessungen bestimmt werden, die im Rahmen dieser Arbeit gesammelt wurden. Die benötigte Bodenrauigkeit, um Gleitschneelawinenanrisse zu verhindern, kann mit diesem Modellierungsansatz für eine bestimmte Hangneigung und Anrisslänge berechnet werden. Zum Beispiel sollte eine Waldlücke in  $35^\circ$  steilem Gelände, die mit langem niederliegendem Gras bewachsen ist, keine 15 m Länge überschreiten. Dagegen können Sträucher oder Totholz, die die Schneedecke durchdringen, Schneegleiten auf einem  $40^\circ$  steilen und 30 m langen Hang verhindern.

Im zweiten Artikel wird gezeigt, dass kleine und mittelgrosse Lawinen von Wald abgebremst und gestoppt werden können. Das passiert hauptsächlich, weil Bäume der Lawine Schneemasse entziehen. Ein neuer theoretischer Ansatz wurde entwickelt, der erlaubt, die Schneemenge zu berechnen, die von der Lawine entnommen wird (der sogenannte "Detrainment-Ansatz"). Da Schneedetrainment der Lawine Impuls entzieht, kann

dies als Reibungsvorgang beschrieben werden, der zum Stoppen der Lawine führt. Der Detrainment-Ansatz wurde in das Lawinensimulationsprogramm RAMMS eingebunden und mit Hilfe von Nachberechnungen gut dokumentierter Lawinenereignisse überprüft. Feldbeobachtungen von Lawinenablagerungen hinter einzelnen Bäumen und Baumgruppen haben den Detrainment-Ansatz bestätigt. Schneedetrainment hängt von der Waldstruktur, den kohäsiven Eigenschaften von Schnee und der damit verbundenen Geschwindigkeit der Lawine ab. Stammdichte, Baumart und Waldzusammensetzung wurden als entscheidende Waldparameter ermittelt. Die Anwendung des Detrainment-Ansatzes ist auf Ereignisse begrenzt, bei denen Bäume dem Lawinendruck standhalten. Dagegen basiert der klassische Reibungsparameteransatz auf der Annahme, dass Lawinen Bäume brechen, entwurzeln, umstürzen und mitreissen. Um die verschiedenen Ansätze anwenden zu können, muss man deshalb zwischen Waldzerstörung und Nichtzerstörung unterscheiden.

Im dritten Artikel wird Waldzerstörung durch Lawinen untersucht. Wenn die Biegespannung, die von einer Lawine auf einen Baum ausgeübt wird, die Biegefestigkeit des Baumstammes übertrifft, tritt Stammbruch auf. Die Biegespannung hängt wiederum von den Fliesseigenschaften der Lawine und von der Stamm- und Baumkronenfläche ab, die von der Lawine getroffen wird. Es wurden vier Belastungsfälle für vier verschiedene Fließregime definiert, um Gleichungen zur Berechnung der Biegespannungen herzuleiten. Anprallhöhe, Schneedichte, Geschwindigkeit und Stammdurchmesser sind die entscheidenden Parameter, um den dynamischen Lawinendruck auf einen Baum zu berechnen. Der statische Druck des Schnees auf den Baum ist bei langsam fließenden Nassschneelawinen im Vergleich zum geschwindigkeitsabhängigen dynamischen Druck erhöht. Bäume brechen unter dem Druck der Staubwolke einer Trockenschneelawine, obwohl die Dichte und damit der Anpralldruck vergleichsweise klein ist (kleiner als 3 kPa). Andererseits verursachen langsame Nassschneelawinen, die nur auf den Stamm wirken, hohe Biegespannungen und führen zu großflächiger Zerstörung. Verschiedene Baumarten haben unterschiedliche Biegefestigkeiten. Birken können zum Beispiel wesentlich höheren Anpralldrücken standhalten als Fichten. Ihre Kronen- und damit Angriffsfläche ist ausserdem kleiner, weil sie ihre Blätter im Winter abwerfen. Dies erklärt mit, warum gewisse Baumarten, wie Birken, Lärchen und Grünerlen in Lawinensturzbahnen vermehrt auftreten. Um Waldzerstörung und damit den vorherrschenden Bremsvorgang vorhersagen zu können, müssen Lawinenfließregime und Baumeigenschaften berücksichtigt werden. Es wurde ein neues Lawinendynamikmodul entwickelt, das die Modellierung von Waldzerstörung ermöglicht. Dementsprechend wird zwischen Reibungs- und Detrainment-Ansatz unterschieden.

Die Ergebnisse dieser drei Artikel zeigen, dass der Einfluss von Vegetation auf Lawinendynamik vom Fließregime der Lawine, ihrer Masse und Geschwindigkeit und insbesondere von der Vegetationszusammensetzung abhängt. Vegetation im Anrissgebiet und in der Lawinensturzbahn kann die Gleitbewegung des Schnees unterbinden, beeinflusst die Lawinenfließdynamik und führt zum Abbremsen und zu einer Verkürzung der Auslauflänge. Somit ist diese Arbeit eine Hilfe für Entscheidungsträger, um die Effektivität des Schutzwaldes zu quantifizieren und zu optimieren, um Lawinenschäden zu verhindern.

# Contents

<b>Acknowledgements</b>	<b>iii</b>
<b>Abstract/Zusammenfassung</b>	<b>v</b>
<b>Abbreviations</b>	<b>xiii</b>
<b>Symbols</b>	<b>xv</b>
<b>1. Introduction</b>	<b>1</b>
1.1 Avalanches in forested terrain . . . . .	1
1.2 Vegetation prevents avalanche release . . . . .	5
1.2.1 Snowpack in forest stands . . . . .	5
1.2.2 Forest gaps . . . . .	6
1.2.3 Technical prevention measures . . . . .	7
1.2.4 Stauchwall mechanics . . . . .	8
1.2.5 Basal friction . . . . .	10
1.3 Stopping behavior of avalanches in forest stands . . . . .	10
1.3.1 Avalanche modeling with RAMMS . . . . .	11
1.3.2 Avalanche dynamics models and forests . . . . .	12
1.4 Tree breaking . . . . .	14
1.4.1 Pressure forces on obstacles . . . . .	15
1.4.2 Failure mechanics . . . . .	16
1.5 Research goal . . . . .	16
1.6 Open research questions . . . . .	17
1.7 Outline . . . . .	18
<b>2. Quantification of basal friction for technical and silvicultural glide-snow avalanche mitigation measures</b>	<b>21</b>
2.1 Introduction . . . . .	23
2.2 Methods . . . . .	25
2.2.1 Observed glide-snow avalanche release areas . . . . .	25
2.2.2 Selection of avalanches with stauchwall . . . . .	28
2.2.3 Mechanical stauchwall model . . . . .	29
2.2.4 Technical guidelines . . . . .	30

2.3	Results and discussion . . . . .	31
2.3.1	Results of field observations, $l_g(\mu_m, \gamma)$ . . . . .	31
2.3.2	Results of model calculations $l_m(\mu_m, \gamma)$ . . . . .	33
2.3.3	Comparison of guidelines, model results and field observations . . . . .	35
2.4	Conclusion . . . . .	38
<b>3. Observations and modeling of the braking effect of forests on small and medium avalanches</b>		<b>41</b>
3.1	Introduction . . . . .	43
3.2	Observations . . . . .	45
3.2.1	Documented avalanches . . . . .	45
3.2.2	Deposition volume behind trees . . . . .	46
3.3	Modeling . . . . .	50
3.3.1	Avalanche modeling . . . . .	50
3.3.2	Modeling avalanche flow in forests . . . . .	52
3.3.2.1	Friction approach . . . . .	54
3.3.2.2	Detrainment approach . . . . .	54
3.4	Results . . . . .	55
3.4.1	Numerical experiment . . . . .	55
3.4.2	Simulations of documented avalanches with $\alpha = 0$ . . . . .	59
3.4.3	Simulations with $\alpha \neq 0$ . . . . .	62
3.5	Discussion and Conclusion . . . . .	64
<b>4. Forest damage and snow avalanche flow regime</b>		<b>69</b>
4.1	Introduction . . . . .	71
4.2	Avalanche loading . . . . .	73
4.2.1	Avalanche pressure and tree stress . . . . .	73
4.2.2	Four avalanche flow regimes $p_\Pi, p_g, p_\Phi^d, p_\Phi^w$ . . . . .	75
4.2.2.1	Powder cloud loading $p_\Pi$ . . . . .	76
4.2.2.2	Intermittent loading $p_g$ . . . . .	77
4.2.2.3	Dense flowing core loading $p_\Phi^d$ . . . . .	78
4.2.2.4	Creep Pressure Model $p_\Phi^w$ (CPM) . . . . .	79
4.2.2.5	Sliding Block Model $p_\Phi^w$ (SBM) . . . . .	80
4.2.3	Additional loading and tree breaking . . . . .	81
4.3	Modeling and results . . . . .	83
4.3.1	Forest destruction modeling . . . . .	83
4.3.2	Wet snow avalanche Monbiel, 2008 . . . . .	84
4.3.3	Powder snow avalanche Täsch, 2014 . . . . .	84
4.3.4	Powder snow avalanches Germany, 2009 . . . . .	87
4.4	Discussion . . . . .	87
4.5	Conclusions . . . . .	90
<b>5. Discussion</b>		<b>93</b>
<b>6. Conclusion</b>		<b>99</b>
6.1	Overview of results . . . . .	99
6.1.1	Vegetation effects on glide-snow avalanche release . . . . .	99
6.1.2	Detrainment approach to model forest-avalanche interaction . . . . .	99

6.1.3	Tree breakage and avalanche flow regime . . . . .	100
6.2	Main conclusions . . . . .	100
<b>7.</b>	<b>Applications and Outlook</b>	<b>103</b>
7.1	Applications for avalanche hazard management in forested terrain . . . .	103
7.2	Outlook . . . . .	104
	<b>Bibliography</b>	<b>109</b>



# Abbreviations

<b>CPM</b>	<b>C</b> reep <b>P</b> ressure <b>M</b> odel
<b>DEM</b>	<b>D</b> igital <b>E</b> levation <b>M</b> odel
<b>dGNSS</b>	<b>d</b> ifferential <b>G</b> lobal <b>N</b> avigation <b>S</b> atellite <b>S</b> ystem
<b>EAWS</b>	<b>E</b> uropean <b>A</b> avalanche <b>W</b> arning <b>S</b> ervices
<b>NaiS</b>	<b>N</b> achhaltigkeit im <b>S</b> chutzwald
<b>RAMMS</b>	<b>R</b> Apid <b>M</b> ass <b>M</b> ovement <b>S</b> ystem
<b>SBM</b>	<b>S</b> liding <b>B</b> lock <b>M</b> odel
<b>SLF</b>	<b>S</b> chnee und <b>L</b> awinen <b>F</b> orschung
<b>VS-model</b>	<b>V</b> oellmy <b>S</b> alm-model



# Symbols

$A$	area of impact	$\text{m}^2$
$A_f$	forest area	$\text{m}^2$
$A_r$	avalanche release area	$\text{m}^2$
$D$	magnification factor	
$E_k$	Kelvin elasticity	Pa
$E_m$	Maxwell elasticity	Pa
$E$	total strain	
$F$	force	N
$G$	force component of gravitational acceleration	$\text{m}^2/\text{s}^2$
$H$	tree height	m
$I$	moment of inertia	$\text{m}^4$
$K$	detrainment coefficient	Pa
$K_c$	creep factor	
$M$	bending moment	Nm
$M_d$	detrained snow mass per unit area	$\text{kg}/\text{m}^2$
$N$	gliding factor	
$\dot{Q}$	volumetric mass flux	$\text{m}/\text{s}$
$Rh$	mean fluctuation energy	$\text{J}/\text{m}^2$
$R_0$	activation energy	$\text{J}/\text{m}^2$
$S$	resistance	$\text{m}^2/\text{s}^2$
$U$	velocity in x direction	$\text{m}/\text{s}$
$V$	velocity in y direction	$\text{m}/\text{s}$

$W$	wedge volume	$\text{m}^3$
$\dot{W}_f$	frictional work rate	$\text{m}^3/\text{s}^3$
$Z$	elevation	m
$a$	correction factor	
$c$	cohesion	Pa
$c_d$	drag coefficient	
$c^*$	intensity factor	
$d$	stem diameter	m
$d_l$	lower width of wedge	m
$d_u$	upper width of wedge	m
$d_w$	base width	m
$e$	wedge length (slope parallel)	m
$g_x$	gravitational acceleration in x direction	$\text{m}/\text{s}^2$
$g_y$	gravitational acceleration in y direction	$\text{m}/\text{s}^2$
$g_z$	gravitational acceleration in z direction	$\text{m}/\text{s}^2$
$h$	mean avalanche flow height	m
$h_\lambda$	stagnation depth	m
$h_\Phi$	dense flowing core height	m
$h_\Pi$	powder cloud height	m
$h_a$	impact height	m
$h_d$	mean deposition height	m
$h_s$	snow cover height	m
$h_t$	terrain undulation height	m
$h_v$	vegetation height	m
$h_w$	wedge height	m
$l$	horizontal wedge length	m
$l_d$	defense structure distance	m
$l_f$	forest gap length	m
$l_g$	observed slab length	m

$l_m$	modeled slab length	m
$l_s$	stauchwall length	m
$l_v$	volume length	m
$m$	mass	kg
$p$	pressure	Pa
$p_g$	impact pressure of snow granule	Pa
$p_n$	pressure in vertical direction	Pa
$p_\Phi$	impact pressure of dense flowing core	Pa
$p_\Pi$	impact pressure of powder cloud	Pa
$r$	granule radius	m
$t$	time	s
$u$	flow velocity, displacement velocity of slab	m/s
$w$	effective crown width	m
$\mathcal{V}_0$	release volume	m <sup>3</sup>
$\alpha$	energy production	
$\beta$	energy decay	
$\delta$	top wedge angle	°
$\eta$	efficiency factor	
$\eta_k$	Kelvin viscosity	Pas
$\eta_m$	Maxwell viscosity	Pas
$\dot{\epsilon}$	strain rate	s <sup>-1</sup>
$\gamma$	slope angle	°
$\lambda$	stagnation constant	
$\nu$	slope angle below release	°
$\psi$	opening angle	°
$\rho$	density	kg/m <sup>3</sup>
$\rho_g$	density of snow granule	kg/m <sup>3</sup>
$\rho_\Phi$	density of dense flowing core	kg/m <sup>3</sup>

## *Symbols*

---

$\rho_{\Pi}$	density of powder cloud	kg/m <sup>3</sup>
$\mu$	Coulomb friction	
$\mu_0$	static Coulomb friction	
$\mu_d$	basal friction in guidelines	
$\mu_m$	modeled basal friction	
$\sigma$	bending stress, resisting stress	Pa
$\bar{\sigma}$	bending strength of tree	Pa
$\xi$	turbulent friction	m/s <sup>2</sup>
$\xi_0$	turbulent friction before fluidization	m/s <sup>2</sup>
$\xi_f$	turbulent friction in forests	m/s <sup>2</sup>

# 1. Introduction

The introduction is structured as followed: The first section (Sect. 1.1) introduces the reader into vegetation-avalanche interaction before the state of the art and gaps in knowledge of vegetation effects on avalanche release (Sect. 1.2), stopping behavior of avalanches in forests (Sect. 1.3) and tree breaking mechanics (Sect. 1.4) are depicted. The research goal is presented in Section 1.5 followed by questions and hypothesis that were formulated in the framework of this thesis (Sect. 1.6). Finally the content of the three main chapters is outlined in Section 1.7.

## 1.1 Avalanches in forested terrain

Avalanches threaten people and infrastructure in mountain communities in Europe, Asia and America. They destroy houses and infrastructure, disconnect traffic lines and endanger backcountry recreationists. As vegetation can prevent avalanche formation and stop moving snow, forests are one of the most cost-efficient mitigation measures against avalanches [*Olschewski et al.*, 2012]. The problem of forest-avalanche interaction is therefore a central theme in snow avalanche research and engineering [*de Quervain*, 1978; *Salm*, 1978; *Gubler and Rychetnik*, 1991].

Historically, the awareness of the importance of the protective function of forests against avalanches increases after deadly incidents. Many incidents are caused by human activities. For example, residents of Sakhalin (Russia) suffered from several deadly avalanche cycles after extensive logging decreased the protective capacity of forests above their settlements [*Kazakova and Lobkina*, 2013]. Some of the worst avalanche accidents ever recorded occurred in Sakhalin during this period of deforestation [*Podolskiy et al.*, 2014]. Presently, clear-cuts on steeper slopes in Canada and the USA have created new avalanche release areas that endanger existing roads and infrastructure [*Stethem et al.*, 2003; *McClung and Schaerer*, 2006; *Anderson and McClung*, 2012]. In the central European Alps, roads and ski runs are frequently endangered by small to medium size forest avalanches [*Zenke*, 1989]. Increasingly, mitigation methods and forest management guidelines are required to define the role of vegetation and forests in mitigating small, frequent avalanches. (Following the classification of *EAWS* [2013], small avalanches have less than 1,000 m<sup>3</sup> release volume and medium avalanches have 1,000 m<sup>3</sup> to 10,000 m<sup>3</sup> release volume.)

A sufficiently dense forest cover has the potential to protect mountain communities from avalanches and other natural hazards such as rockfall [de Quervain, 1978; Gubler and Rychetnik, 1991; Berger et al., 2002; Margreth, 2004; Dorren et al., 2005; Brang et al., 2006; Dorren and Berger, 2006; Teich et al., 2012a]. However, the composition and density of forest stands change continuously. Thus their protective capacity increases or decreases with time. Forest management on hazardous slopes requires reconciling economic demands for a valuable resource without decreasing the protective capacity of forests [Bebi et al., 2009]. Extensive alpine farming, firewood production and the construction of houses and infrastructure have reduced the area of protective forests, especially in densely populated areas such as the Alps [Germain et al., 2005]. Bark beetle outbreaks, partly facilitated by monocultures of fast growing tree species, overpopulation of deer due to the extermination of their natural enemies and changing climatic conditions are additional stress factors affecting the healthiness and resilience of mountain forests [Logan et al., 2003; Germain et al., 2005; Schoennagel et al., 2007; Bebi et al., 2009; Trujillo et al., 2012]. An expansion of the treeline to higher elevations and a densification of forest stands, however, has also been observed in the Alps in the last century. This emphasizes the potential of forests to increase their protective capacity, especially in a changing climate [Gellrich et al., 2007; Bebi et al., 2009].

Protection forests are managed proactively to assure their main function: to protect houses and infrastructure from natural hazards [Kräuchi et al., 2000; Schneebeli and Bebi, 2004; Dorren et al., 2004; Brändli, 2010]. It has a unique status in the Alps; human intervention and harvesting are limited to preserve and optimize its protective capacity [Margreth, 2004; Schneebeli and Bebi, 2004]. The first protection forest (Bannwald) in Switzerland was established above Andermatt in 1397 (Fig. 1.1) [Olschewski et al., 2012]. Both residents and the authorities agreed on the crucial protective function of this forest area and prohibited harvesting to guarantee forest regeneration. Today approx. 49% of the forest in Switzerland is classified as protection forest [Losey and Wehrli, 2013]. While physical processes of forest-avalanche interaction are assumed to be similar for mountain ranges worldwide, this thesis focuses on forests in the Alps, in particular in Switzerland and Germany.

Large avalanches break and/or uproot trees, causing widespread damage to mountain forests. They are common events in the Alps and contribute to the visual appearance of the mountain landscape [de Quervain, 1978]. Trees can be easily destroyed when avalanches exert sufficient force on the tree and a critical bending stress is reached in the stem [Mattheck and Breloer, 1994]. This creates distinct avalanche flow paths containing broken stems; avalanche tracks often have considerable woody debris. Large areas of protection and commercial forest are thus damaged each winter (e.g. 110 ha mountain forest in winter 2009 in Germany). Trim lines indicate differently aged vegetation covers, caused by avalanches, and therefore help specify return periods of avalanches [McClung and Schaerer, 2006]. Knowledge of the return period is, in turn, an important element for hazard mapping. Even though catastrophic events have been documented in the Alps for many centuries, observations of forest destruction and non-destruction still provide avalanche engineers with valuable additional information. To improve natural hazard management it is important to include release areas that evolve from newly opened forest



FIGURE 1.1: Avalanche protection forest above Andermatt and Hospental (Photo: Stefan Margreth).

gaps. The possibility of increased avalanche runouts due to missing or changing forest structure must be taken into account [Konetschny, 1990; Gubler and Rychetnik, 1991].

Recently, avalanche dynamics models have become an important tool to delineate hazard zones, to plan mitigation measures and to calculate risk scenarios for certain return periods. The influence of forest cover on avalanche runout distances is rarely included in model applications [Christen *et al.*, 2010a]. Traditionally, hazard assessment is based on extreme avalanche events in which the protective capacity of forests is not modeled [Christen *et al.*, 2010a]. Local decision-makers and natural hazard engineers need additional tools to quantify the effect of forests on avalanche runout areas, velocities and impact pressures. Especially at lower elevations (500 m - 2000 m), where most of the traffic routes and settlements are located in the Alps, forest-avalanche interaction must be considered for hazard mitigation. In order to minimize the risk of hazardous events, changes in forest structure and vegetation composition need to be taken into account and adequate countermeasures, often involving extensive field work, need to be planned and carried out. Local avalanche commissions and ski safety officers have to deal with frequent, small to medium size avalanches that run through forest and endanger roads and ski runs each winter (Fig. 1.2). Forests particularly influence flow dynamics of these small to medium size avalanches [Bartelt and Stöckli, 2001; Bebi *et al.*, 2009; Teich *et al.*, 2012a]. Teich *et al.* [2012a, 2014] showed that forest structure, composition, stem density, woody debris and ground vegetation are parameters that have an effect on the runout distance of small to medium size avalanches. Also, the influence of forest on avalanche dynamics depends on the flow regime. Cohesive snow clods are for example more adhesive and will facilitate jamming of avalanche snow above dense tree stands. Recent progress in the theoretical description of avalanche flow regimes, including the cohesive behavior of snow, snow temperature and the turbulent movement of particles, improved the performance of existing avalanche modeling software [Bartelt *et al.*, accepted; Vera

*et al.*, in press; *Buser and Bartelt*, 2009]. To understand and quantify the retarding and decelerating effect of forests with varying structure on avalanches with different flow regimes will be a further step to model avalanche flow from release to runout.



FIGURE 1.2: Road to Walchensee in Bavaria that is frequently endangered by avalanches that run through the forest uphill (Photo: Armin Fischer).

Avalanches and snow gliding have a strong effect on the vegetation on mountain slopes [*Rixen et al.*, 2007]. Young trees can survive avalanche impact if they are covered by deep snow or if the elasticity of their stems protects them from breakage [*Kajimoto et al.*, 2004]. However, they are often exposed to snow creep and glide that can lead to uprooting and overturning [*Zenke*, 1978; *Höller et al.*, 2009]. Stems of older trees can withstand higher bending stresses but they are more susceptible to powder blasts of dry flowing avalanches, especially if trees are evergreen, because their crown area is larger. Avalanches, or their woody and rocky cargo leave “scars” on tree stems and dendrochronological methods enable specialists to reconstruct the time frame of past events [e.g. *Potter*, 1969; *Schweingruber et al.*, 1996; *Casteller et al.*, 2008, 2011; *Corona et al.*, 2012]. Destructive avalanche events cause disturbances in the speed of tree growth and therefore in tree ring width. Forest damage, its documentation and the study of tree rings provide engineers and forest managers with valuable information on avalanche intensity and frequency. The vegetation cover itself adapts to disturbances, providing further information on avalanche activity [*Butler*, 1979; *Bebi et al.*, 2009]. For instance, certain tree species such as green alder or birch dominate in avalanche affected terrain [*Butler*, 1979; *Tiri*, 2009].

If the frequency and intensity of avalanche events is small, the forest may not be damaged or the trees can recover. Subsequently, a healthy and dense forest can prevent avalanche release or decelerate and stop it. Snow gliding is suppressed by a dense undergrowth, by rootstocks or lying tree stems; young trees are protected. Thus forests can reinforce themselves if conditions are favorable. Large avalanches that release high above the tree

line, however, develop destructive power and any kind of forest will be destroyed entirely [Schneebeili and Bebi, 2004; Bebi et al., 2009].

## 1.2 Vegetation prevents avalanche release

Avalanches release as slabs, or as loose snow avalanches [McClung and Schaerer, 2006]. The snow can be dry (below  $-2^{\circ}$ ), moist (between  $-2$  and  $0^{\circ}$ ) or wet ( $0^{\circ}$ ) [Steinkogler et al., 2014]. Whereas a large-area weak layer within the snow cover is mandatory for slab avalanche formation, loose snow avalanches release independent of the snow cover stratification. Loose snow avalanche formation depends predominantly on the steepness of the terrain and the mechanical properties (granular bonding) of snow granules. Point releases are characteristic for loose snow avalanche formation and large slopes are therefore not essential. Full-depth, glide-snow avalanches slide directly on the soil surface. A wet soil surface due to melt-water infiltration or melting of the snow cover caused by a warm underground usually triggers the gliding movement of the snow [Mitterer et al., 2011]. Prior to an acceleration of the slab and the following avalanche release, a glide-crack opens at the crown of the slab (a so-called “Fischmaul”). For the release of glide-snow avalanches the so called “stauchwall” at the lower boundary of a slab has to be overcome [Bartelt et al., 2012b]. Small-scale ground roughness can prevent glide-snow avalanche formation. These terrain undulations are smoothed out by a thick snow cover [Veitinger et al., 2014] and weak layers may form on entire slopes. A stable, inhomogeneous snow cover prevents slab avalanche formation, while glide-snow avalanches are still possible. For a detailed overview on avalanche formation see e.g. Schweizer et al. [2003] or McClung and Schaerer [2006].

The primary function of protection forests is the prevention of avalanche release [Salm, 1978; de Quervain, 1978; Gubler and Rychetnik, 1991; Meyer-Grass and Schneebeili, 1992; Höller, 2001, 2004; Viglietti et al., 2010]. A continuous stratification of the snowpack is suppressed below a dense forest canopy [Imbeck, 1987; Gubler and Rychetnik, 1991]. The spatial variability of weak layers in the snowpack is increased, thus the release of large area slab avalanches is prevented [Schweizer et al., 2008]. Loose snow and glide-snow avalanche formation is still possible [Imbeck and Meyer-Grass, 1988]. Loose snow avalanches rarely develop destructive power because snow is only collected from the uppermost layer and trees minimize the release area. In comparison, glide-snow avalanches mobilize the entire snowpack. In addition to slope angle and slab length, basal friction is an important factor. However, its role in the formation of glide-snow avalanches is not sufficiently quantified [Höller, 2014a; Teich et al., 2012a].

### 1.2.1 Snowpack in forest stands

The snowpack in forest stands is generally more stable, which means less distinct stratification is observed [Gubler and Rychetnik, 1991; McClung and Schaerer, 2006]. The following mechanisms lead to this inhomogeneous snow cover below forest canopy:

- Snow clumps fall from trees, penetrate into the snow cover and inhibit a continuous stratification [Löfvenius *et al.*, 2003]. The build-up of large-area weak layers is therefore hindered. In addition, increased melting and sublimation rates lower the snow depth in dense forest stands compared to open field [Imbeck, 1987; Bründl *et al.*, 1999; Schneebeli and Bebi, 2004; McClung and Schaerer, 2006].
- A dense forest canopy suppresses the outgoing long-wave radiation and therefore prevents the formation of surface hoar. Surface hoar potentially transforms into a weak layer after being covered by new snow [Schneebeli and Bebi, 2004].
- Trees deflect wind, which can be a builder of slabs, and splits into small-scale turbulences. The wind speed is generally lower in forests. The formation of large wind slabs is therefore prevented [Ragaz, 1972; de Quervain, 1978].

Full-depth glide-snow avalanches and loose snow avalanches occur in open forest stands [de Quervain, 1978; Imbeck and Meyer-Grass, 1988; Zenke, 1989]. Melt-water penetration through the snowpack is even facilitated along distinct snow clods or along branches and stems. The ground surface of forest areas is warmer in autumn and winter due to less outgoing longwave radiation and insulation effects caused by tree litter, such as leaves, needles and branches [MacKinney, 1929; Kienholz, 1940]. Melting of the snowpack from the soil surface is thereby supported. Grass, leaves or needles can form a smooth sliding surface for the snow on the ground.

### 1.2.2 Forest gaps

Forest gaps are potential avalanche release areas (Fig. 1.3). The gap length in the downhill direction, the slope angle and the basal friction are the crucial parameters that determine the probability of avalanche release. Avalanches release in steep, narrow forest gaps, especially in gullies and channels. Whereas slab avalanches have typically release widths of more than 10 m [Schweizer *et al.*, 2003], loose snow avalanches with point releases are common events in narrow forest gaps.

The required tree density to prevent avalanche release was defined by Salm [1978]; Frey *et al.* [1987]; Gubler and Rychetnik [1991] and Schneebeli and Bebi [2004]. They investigated the stabilizing effect of stems on the snow cover. The value for the critical slab length for the release of avalanches in forest gaps differs between studies. Salm [1978] and Teich *et al.* [2012a] mention 50 - 100 m long acceleration distances for avalanches that release above the treeline to develop destructive forces. Margreth *et al.* [2008] defines 30 m as critical length. In addition, the slab length depends on the slope angle. Thus, Frehner *et al.* [2005] and Gubler and Rychetnik [1991] define lengths between 25 and 60 m for slope angles between 30° and 45° to be critical. Schneebeli and Bebi [2004] assume that avalanches that accelerate for more than 150 m can not be stopped by forest. Bebi *et al.* [2009] conclude that the critical length of forest gaps lies between 20 and 200 m. The large range of critical slab lengths for the formation of destructive avalanches reported in the literature arises from varying basal friction parameter values. This conclusion will be highlighted in Chapter 2 of this dissertation.

The ground roughness and gap size depend on the formation history of the gap. Gaps develop for different reasons, such as forest fire, storm breakage, bark beetle outbreaks and logging. Once a gap has formed it can be extended by bark beetle, damage caused by game browsing, erosion, drought and snow gliding. Dead wood, remnant stems and upright root-plates in gaps support the snowpack and therefore prevent snow-gliding. However large amounts of dying or newly available dead wood after disturbances may facilitate the expansion of bark beetles to the surrounding trees [Frey and Thee, 2002; Kupferschmid Albisetti *et al.*, 2003]. Young trees hardly survive if bent and uprooted by snow gliding [Zenke, 1978] or if heavily damaged by ungulates or snow fungi [Ammer, 1996; Barbeito *et al.*, 2013].



FIGURE 1.3: Avalanche, that released in a forest gap (Photo, Armin Fischer). The slab length on the left hand side was large enough for glide-snow avalanche formation and the stabilizing effect of trees was missing. On the right hand side glide-cracks opened but the stauchwall did not fail because of trees below.

### 1.2.3 Technical prevention measures

Protection forest is the most cost-efficient avalanche protection measure [Olschewski *et al.*, 2012]. Where climatic conditions are favorable for the growth of trees, dense forest fulfills its protective function and artificial avalanche prevention measures are often unnecessary. Protection forest management must however support tree regeneration proactively.

The first task of technical defense structures is to prevent the release of avalanches, that means to hinder the downhill movement of the snow. Technical countermeasures against

avalanches are applied above the tree line or in forested terrain if the forest cannot meet its protective function anymore. Often additional measures such as nets or fences are installed temporarily to support the re-growth of trees until the protective effect is re-established [Leuenberger, 2003]. These fences or nets prevent avalanche formation and suppress snow-gliding. Leaving dead wood and stems in upright or horizontal position increases the roughness of the terrain [Kupferschmid Albisetti et al., 2003]. Root-stocks in upright position can be very effective in stopping the snow movement. Wooden tripods (timber jacks) are installed additionally to prevent gliding and to support single trees [Leuenberger, 2003]. The plantation of young trees to accelerate regeneration can be useful but the cost-effectiveness has to be evaluated [Rammig et al., 2007]. Additional technical avalanche prevention measures are only necessary until the young trees suppress snow gliding themselves. In the Alps protection from game animals is often required to support the growth of young plants. Forest managers use fences to protect their plantations.

Fences and nets stabilize the snow cover and stop the movement of snow in their immediate vicinity. The height of these measures is defined by the maximum snow height that can be expected for a particular slope. (Throughout this thesis snow height is defined in vertical direction, whereas snow depth is defined perpendicular to the slope.) For the assessment of avalanche defense structure dimensions, snow height measurements on the slope from the previous winters or at least from an adjacent measuring station are crucial.

Margreth [2007] introduced a procedure to calculate the maximum snow depth that can be expected for a particular slope in Switzerland. It is based on Gumbel statistics for extreme events. Variations in meteorological characteristics are addressed by applying a regional snow height gradient. Regional snow height gradients were determined for the Bavarian Alps by Feistl [2010]. Grown trees are normally higher than the maximum snow height and dense tree stands can therefore serve as a defense structure. Typically a “stauchwall” forms above technical defense measures and forest stands as the downhill movement of snow is hindered.

#### 1.2.4 Stauchwall mechanics

With “stauchwall” we denote the snow cover that is fixed to the ground and is situated below a moving slab. Besides the stauchwall, snow is always in motion and creeps and glides downhill [In der Gand and Zupančič, 1966; Häfeli, 1967; McClung, 1975; Höller et al., 2009]. In certain areas, where the slope is not steep enough, gliding is suppressed by high ground roughness or obstacles such as trees that fix the snow cover to the ground. The stauchwall is located in those areas. Typically the upper boundary of glide slabs is where the slope changes from flat to steep or where the ground surface changes from rough to smooth. A crack opens at the upper boundary of a slab, the crown, when the snow cover starts to glide. The compression of the stauchwall, from the weight of the snow cover above is simulated by Bartelt et al. [2012b] with a visco-elastic model [Mellor, 1974; Voytkovskiy, 1977; Salm, 1982; Von Moos et al., 2003; Scapozza and Bartelt, 2003; Bartelt et al., 2012b]. The stress response of snow is divided into an elastic (spring) and

viscous (dashpot) element in series (Fig. 1.4). The snow properties that are taken into account are Kelvin- and Maxwell elasticity  $E_k$  and  $E_m$ , viscosity  $\eta_k$  and  $\eta_m$  and density  $\rho$ . When a critical strain rate is reached, the stauchwall fails in brittle compression.

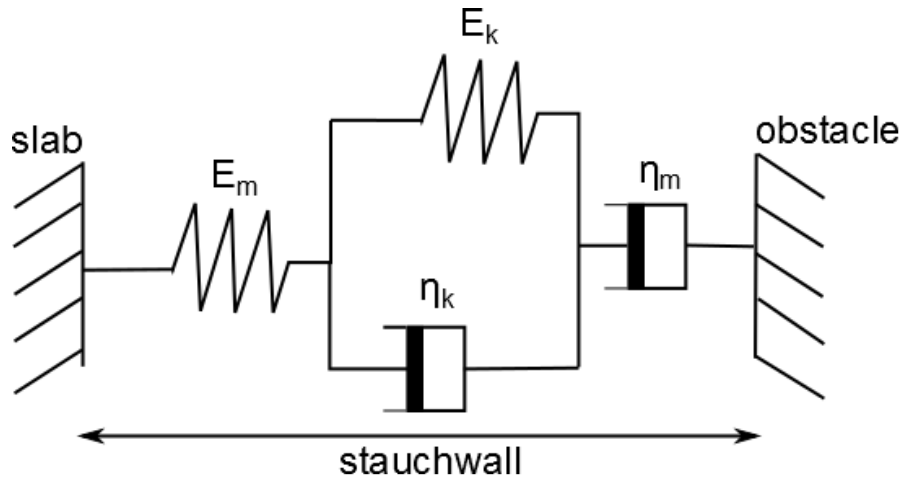


FIGURE 1.4: Simple Burgers model to describe visco-elastic behavior of stauchwall.

For the release of an avalanche the stauchwall has to fail. Stauchwall failure occurs when it can no longer support the weight of the snow above. Failure therefore depends on the slope angle, slab length and the friction between the slab and the weak layer or the slab and the ground for full-depth avalanches. To model snow cover failure, the location of the stauchwall must be defined in advance. As the snow cover is fixed to the ground by terrain roughness and vegetation, these surface features (in addition to walls, nets and fences) are helpful indicators to define the location of the stauchwall.

The distance between defense structures is a key engineering parameter in many guidelines to guarantee optimal protection [Margreth, 2007; Austrian Standard Institute, 2011; Matsushita et al., 2012; Leuenberger, 2003]. Full-depth glide-snow avalanches are common events in forest stands, especially if the soil is wet and smooth. Moreover, glide-snow avalanches have a high potential to develop destructive forces when the moving mass is large. Potential release areas in forest gaps with distinct upper and lower borders, with a defined slope angle and quantitative knowledge about the roughness of vegetation and terrain could be identified if stauchwall mechanics are understood and considered. As forest edges have the same effect as nets or fences (they stabilize the snow cover at the lower end of the release zone), forest gap size can be determined in a similar manner as defense structure distance. In contrast to open terrain where ground roughness remains constant, forested areas can change into potential avalanche release areas. As the vegetation changes, roughness changes, gaps can form and if not monitored frequently new hazard zones might develop. Quantitative knowledge about the basal friction, about slope angle and slab length enables the delineation of potential glide-snow avalanche release areas. It is therefore necessary to define the basal friction as a function of ground roughness to calculate the allowed forest gap length or distance between supporting structures.

### 1.2.5 Basal friction

Various studies underline the importance of basal friction for the release of glide-snow avalanches [Clarke and McClung, 1999; McClung and Schaerer, 2006]. Terrain undulations such as rocks, ridges, steps, holes or channels increase ground roughness and make glide-snow avalanche release unlikely. The height and distribution of these undulations are critical parameters [McClung, 1975]. Where climatic conditions are favorable, vegetation is another important factor [Newesely et al., 2000; Leitinger et al., 2008; Höller, 2012b]. The effective vegetation cover height below the snow cover depends on the dominant species and on the weight of the snow cover. Long grass is compressed by a relatively small load, whereas the compression of shrubs requires a thick snow cover, though a certain roughness will remain.

McClung [1975] defined ground roughness with the so-called stagnation depth. The stagnation depth depends only on the topography of the ground surface. Vegetation effects are not considered with this approach. Höller [2012b] applied the model of McClung [1975]; McClung et al. [1994] and Clarke and McClung [1999] to calculate the sliding velocity of a snowpack for varying ground roughness. Stagnation depth is defined according to the study of Salm [1977]. The wavelength and amplitude of surface undulations must be known to calculate the stagnation depth and therefore the ground roughness. These parameters are difficult to measure in the field as in most cases the ground surface is inhomogeneous. Leitinger et al. [2008] measured basal friction by pulling a glide shoe over areas with different vegetation covers. They concluded that the static friction coefficient is a sufficient indicator to characterize the complex influence of vegetation and land use on snow gliding. A wet surface was not included in their measurements. The basal friction of a wet vegetation cover is expected to be considerably lower than for dry ground [Mitterer et al., 2011]. Ground roughness depends on the effective penetration depth of vegetation into the snow cover. Rigid branches and strong lignified shrubs are more effective than grass, even if they have the same length. Different snow gliding velocities on tall or small shrubs were found by Newesely et al. [2000].

## 1.3 Stopping behavior of avalanches in forest stands

In the preceding section, the first important function of protection forests was presented; namely, how forests prevent avalanches from starting. A method was devised to determine the maximum forest gap length to prevent glide-snow avalanche formation. The approach involves a visco-elastic analysis of static forces. The second function of protection forests is now posed: how do protective forests hinder and stop avalanche motion? This is an avalanche dynamics problem. As numerical-based avalanche dynamics models are commonly applied to determine avalanche runout and velocity in three-dimensional terrain, it is first necessary to become familiar with the numerical approaches. Subsequently, the simulation of forest-avalanche interaction can be discussed.

### 1.3.1 Avalanche modeling with RAMMS

One of the first goals in snow science was to model avalanche motion. Fatal avalanche events in Russia, the European Alps, the Northwest territories of the USA and Canada convinced government authorities of the necessity of predicting avalanche behavior for safety measures. To this end, engineers developed formulas to estimate avalanche velocities, impact pressures and runout distances [Völlmy, 1955; Kozik, 1962; Briukhanov et al., 1967]. In Switzerland, Völlmy [1955] constructed a one-dimensional center-of-mass model to describe avalanche motion, the so-called “Voellmy-model”. The model was based on analytical solutions of equations of motion defined on three track segments: the release zone, the transition zone and the runout zone. Each zone was defined by a constant slope angle. The terminal velocity of the avalanche was reached at the end of the transition zone. Effective friction defined the runout distance of the avalanche. Avalanche modeling in Switzerland is still based on Voellmy’s frictional model. The model was further improved by Salm et al. [1990] by introducing relations that control the flow height of the avalanche (Voellmy-Salm model, VS-model). The analytical models were especially helpful in many practical mitigation problems because a set of calibrated friction parameters for extreme avalanche events was used. However, the models were restricted to simple avalanche tracks containing three well-defined track segments. In addition, the models required the specification of the avalanche flow width. For complex three-dimensional terrain analytical methods are difficult to apply. Therefore, numerical software approaches have been developed in recent years. Numerical approaches allow the consideration of complex two- and three-dimensional terrain [Bartelt et al., 1999; Christen et al., 2002; Sampl and Zwinger, 2004; Christen et al., 2010b]. Recently high resolution (1 - 2 m) digital elevation models (DEM) have been developed for Switzerland and Germany (and most other European countries). The high resolution of the terrain models have further increased the accuracy of avalanche dynamics simulations [Bühler et al., 2011; Bühler et al., 2012]. Terrain curvature effects [Fischer et al., 2012], granularization of flowing snow [Bartelt et al., 2006; Buser and Bartelt, 2009], cohesion of snow granules [Bartelt et al., accepted], snow cover entrainment [Sovilla et al., 2006; Christen et al., 2010b] and temperature effects [Vera et al., in press] are now included in avalanche dynamics models.

In this dissertation we applied the RAMMS modeling system (**RA**pid **M**ass **M**ovements **S**ystem) to investigate forest avalanche interaction [Christen et al., 2010b]. The snow avalanche model in RAMMS is based on numerical solutions of the depth-averaged mass, momentum and energy balance equations on general three-dimensional digital elevation models (DEM). A comprehensive overview of RAMMS equations is presented in Section 3.3. Model output includes the time histories of flow height, velocity and density at all positions along the three-dimensional avalanche track. Flow friction is parameterized according to the Voellmy-Salm law [Völlmy, 1955; Salm et al., 1990] which contains two parts, a normal stress dependent Coulomb friction (parameter  $\mu$ ) and a velocity-squared dependent turbulent friction (parameter  $\xi$ ):

$$S_x = \frac{U}{\|\mathbf{V}\|} \left[ \mu g'_z h + \frac{g \|\mathbf{V}\|^2}{\xi} \right] \quad (1.1)$$

and

$$S_y = \frac{V}{\|\mathbf{V}\|} \left[ \mu g'_z h + \frac{g \|\mathbf{V}\|^2}{\xi} \right]. \quad (1.2)$$

These friction parameters determine the maximum velocity of the avalanche ( $\xi$ ) and the slope angle, where avalanches stop ( $\mu$ ). The friction parameters  $\mu$  and  $\xi$  were calibrated from back-calculations of real avalanche events in the Vallée de la Sionne test site in the canton of Valais, Switzerland. Calibrated sets of friction parameters are used for hazard mapping in Switzerland. The friction recommendations for extreme events with varying return periods have been extensively tested by engineers in many applications (see *Gruber and Bartelt* [2007]). The standard approach recommends using constant  $\mu$  and  $\xi$  values for extreme events. However, procedures have been developed to vary the friction parameters based on terrain and avalanche characteristics: gullies, channels, flat terrain, avalanche volume, return period and elevation. In a model extension, the energy associated with random movements of particles is considered ( $\mu(R)$  and  $\xi(R)$ ). The friction parameters  $\mu$  and  $\xi$  represent the static friction values (avalanche snow at rest), but dynamically change during the avalanche movement according to avalanche speed and avalanche free energy (see *Bartelt et al.* [2011]; *Platzer et al.* [2007]). This is a type of velocity-weakening in which granular fluctuations increase with increased shear rate. The granular fluctuations locally decrease the volume fraction, decreasing frictional dissipation.

The RAMMS model formulation includes snow uptake by the avalanche and mass removal behind trees. These are denoted entrainment and detrainment, respectively. Snow temperature defines snow quality and therefore the avalanche flow parameters as well as avalanche flow regime. The flow parameters control the velocity weakening and therefore the avalanche runout. Advanced model formulations (for example *Vera et al.* [in press]) account for the mean avalanche temperature and phase transitions leading to melt-water lubrication of basal surfaces. Cohesion is considered to be a binding process operating on the random particle motions within the avalanche and therefore it can have a large effect on shearing [*Bartelt et al.*, accepted]. Cohesion is parameterized with an additional parameter  $c$ . Vertical density variations in avalanche flows are the basis to model powder clouds in RAMMS and two studies on this topic are currently under preparation [*Dreier et al.*, submitted; *Buser and Bartelt*, submitted]. A first test version of RAMMS that allows the simulation of powder cloud heights, densities, velocities and impact pressures was released recently. The avalanche simulations in this thesis were conducted with RAMMS.

### 1.3.2 Avalanche dynamics models and forests

Both analytical and numerical models concentrated on avalanche flow in open non-forested terrain. Avalanche flow in forests requires introducing new frictional processes to account for tree breaking, overturning, uprooting and entrainment of trees. The first

attempts to model forest-avalanche interaction were based on a so-called friction approach. Forest-avalanche interaction was modeled by lumping all the different processes (breaking, overturning, etc.) to an increase in turbulent friction [Salm, 1978; Gubler and Rychetnik, 1991; Bartelt and Stöckli, 2001; Christen et al., 2010a]. Avalanche terrain containing forests was locally assigned a higher friction value in the avalanche calculations [Schaerer, 1973; Buser and Frutiger, 1980; Sampl and Zwinger, 2004; Takeuchi et al., 2011]. Bartelt and Stöckli [2001] demonstrated that the velocity dependent friction increases by a factor two because of entrainment of heavy tree stems and trunks. Therefore, there is physical motivation to increase the turbulent friction and not the Coulomb term of the Voellmy model. However, the key idea behind the friction approach is the assumption that the forest is destroyed by the avalanche. The avalanche slows down, not because of the energy required to break trees, but because considerable energy is required to entrain the heavy woody debris.

To date, forest areas are modeled in RAMMS (and other numerical programs) by reducing the turbulent friction parameter  $\xi$  from approx.  $1000 \text{ m/s}^2$  to  $400 \text{ m/s}^2$ . (Recall that  $\xi$  is in the denominator of the turbulent friction and therefore  $\xi$  must be *reduced* to increase the turbulent flow friction.)

Different forest densities and structures have not been considered in avalanche modeling to date. Problems when characterizing forest-avalanche interaction with increased turbulent friction have been addressed in recent publications.

For example, increased turbulent friction cannot explain runout shortening of avalanches in forested terrain [Teich et al., 2012b, 2014]. Recent investigations of Teich et al. [2012a, 2014] showed that the primary influence of forests and their structural characteristics is to reduce avalanche runout distances. The avalanche is decelerated by an increased turbulent friction, but the runout distance does not vary significantly, especially if simulating small avalanche events where the forests are not destroyed. Forest destruction is a necessary condition to apply a turbulent friction modeling approach.

Christen et al. [2010a] suggested to disregard forest cover when simulating large avalanche events. They back-calculated an avalanche event (release volume:  $175,000 \text{ m}^3$ ) where forest was destroyed entirely. Based on their results, it is now common practice to disregard forest cover when simulating large avalanches that start high above the tree line. Therefore, there are few case studies that confirm that the value of  $\xi = 400 \text{ m/s}^2$  is appropriate.

Another problem with the friction approach is that velocity measurements are rare. Trees enable or at least complicate the documentation and the tracking of the avalanche front and make assumptions on the deceleration of the avalanche, caused by forest, difficult. In modeling, however, deceleration caused by increased turbulent friction is widely assumed to characterize forest-avalanche interaction if trees are broken or uprooted [Salm et al., 1990; Bartelt and Stöckli, 2001; Margreth, 2004; Takeuchi et al., 2011].

Observations show, that a considerable amount of avalanche snow is stopped uphill of single trees and tree stands [McClung and Schaerer, 2006] (Fig. 1.5). This effect is large if trees remain standing after avalanche impact. Simulations of avalanches that run

through forest do not result in increased depositions in forest areas if assuming increased turbulent friction. The amount of snow that is removed by trees can be observed and measured. The effect of forest on avalanche dynamics can therefore be quantified. The removal of snow by trees is referred to as “detrainment” throughout this thesis. A novel approach to model the detrainment of avalanche snow by trees is introduced in Chapter 3 (the so-called “detrainment approach”).



FIGURE 1.5: Avalanche snow stopped by trees.

Increased turbulent friction and detrainment of avalanche snow are the main (and equivalent) processes that govern the stopping behavior of avalanches in forests [McClung and Schaerer, 2006; Teich *et al.*, 2012a, 2014].

## 1.4 Tree breaking

Avalanches break, uproot, overturn and entrain trees if the bending stress is sufficiently high [Johnson, 1987; Peltola and Kellomäki, 1993; Peltola *et al.*, 1999; Mattheck and Breloer, 1994]. Tree destruction does not only depend on avalanche velocity, flow height and snow density but also on avalanche flow regime, stem diameter and tree species. The avalanche impact area of the tree is an important factor that depends on the avalanche flow regime and tree characteristics such as height of the lowest branches, foliation and position relative to other trees. Slow moving wet snow avalanches that exert impact pressure only on the tree stem, break trees as well as fast moving low density powder clouds (Fig. 1.6). In a catastrophic avalanche winter in 1999, 160,000 m<sup>3</sup> of wood were destroyed by avalanches in Switzerland [SLF, 2000].

To be able to distinguish between detrainment and friction approach in the modeling of avalanche dynamics, a prediction of forest damage is required. A unified theory of tree damage by avalanches with different flow regimes is needed to predict forest destruction.



FIGURE 1.6: Broken trees after avalanche impact (Photo: Frank Krumm).

#### 1.4.1 Pressure forces on obstacles

Various authors studied avalanche impact pressures on obstacles [Pedersen *et al.*, 1979; Lang and Brown, 1980; Faug *et al.*, 2004, 2010; Gray *et al.*, 2003; Hauksson *et al.*, 2007; Naaim *et al.*, 2004, 2008; Sheikh *et al.*, 2008; Teufelsbauer *et al.*, 2011; Baroudi *et al.*, 2011]. These measurements provide insights on flow patterns of avalanches around tree-like obstacles. The measured impact pressures vary according to the measurement method, e.g. the size of the pressure sensor [Sovilla *et al.*, 2008]. The Swiss guidelines on the calculation of avalanche dynamics [Salm *et al.*, 1990] and the report from the European commission on the design of avalanche protection dams [Johannesson *et al.*, 2009] recommend Eq. 4.6 (Chapter 4) to calculate the impact pressure exerted by a fast moving avalanche past a slender obstacle. When applied to model wet snow pressures, the formula requires unrealistic and clearly non-physical drag coefficients [Sovilla *et al.*, 2010, 2014].

Tree destruction is accompanied by minimum bending stresses that can be calculated if the forest structure prior to the destructive event is known. As measurements or observations of the avalanche velocity, flow height and density are rare, damage of forests and buildings are often the only sources of information. Models of avalanche dynamics enable the reconstruction of past events. Simulation results can be confirmed if compared to forest destruction patterns.

### 1.4.2 Failure mechanics

*Mattheck and Breloer* [1994] state that tree stems and root plates are designed to withstand bending stresses of the same magnitude. This implies that uprooting and tree breakage consume comparable amounts of energy. Various authors found impact pressures of the same magnitude for tree breaking and uprooting [*Peltola et al.*, 2000; *Stokes et al.*, 2005; *Tiri*, 2009] and therefore confirm *Mattheck and Breloer's* observations. An abrupt pressure loading of a tree may favorably lead to stem breakage instead of uprooting [*Lundström et al.*, 2009]. Most of the time trees break at low stem heights [*Peltola et al.*, 2000; *Kajimoto et al.*, 2004]. Stem breakage in the crown occurs in powder snow avalanches in exceptional cases. For fast moving avalanches the impact pressure is classically calculated with Eq. 4.6 (Chapter 4) [*Mears*, 1975; *Salm et al.*, 1990; *Johannesson et al.*, 2009].

Trees break if the bending stress exerted by the avalanche exceeds the bending strength of the tree. The bending strength of trees is highly variable, it depends on the tree species, their location in the forest, the soil characteristics and its nutrient content, the trees' health, the temperature and the moisture content of the wood [*Grosser and Teetz*, 1985; *Götz*, 2000; *Peltola et al.*, 2000; *Lundström et al.*, 2009]. Bending strengths of wood provided in literature vary according to stand and tree characteristics and depend on the measuring method. For example whether the load is applied dynamically or statically. Tree pulling experiments [*Peltola et al.*, 2000; *Stokes et al.*, 2005], rock impact experiments [*Lundström et al.*, 2009], fractometer measurements by [*Götz*, 2000] and material testing procedures by *Lavers* [1983] showed different values for bending strength. The bending stress of avalanches to destroy mature trees must exceed a minimum value of  $\sigma > 30 \text{ MN/m}^2$ . According to *Peltola et al.* [2000]; *Götz* [2000] and *Stokes et al.* [2005] spruce is the species with the lowest strength ( $\sigma \approx 36 \text{ MN/m}$ ), whereas birch is the strongest of the investigated tree types ( $\sigma \approx 41 \text{ MN/m}$ ).

## 1.5 Research goal

The fundamental processes of forest-avalanche interaction must be understood to improve management guidelines for protection forests. The aim of this thesis is to re-investigate the mechanical interaction between vegetation and avalanches using modern state-of-the-art numerical methods. New numerical methods allow a more accurate physical description of mechanical interactions between forests and avalanches. This facilitates a better quantification of the primary vegetation and forest parameters that influence avalanche flow dynamics. Avalanches can be simulated from release to runout, including vegetation effects.

How vegetation influences basal friction must be first quantified to delineate potential glide-snow avalanche release areas in forest gaps. A general mechanical model is constructed to link terrain characteristics, such as slope angle and slab length, with vegetation cover and ground roughness. Snowpack properties and terrain characteristics

are defined to predict a potential failure of the stauchwall which results in a glide-snow avalanche release. By comparing the occurrence of certain vegetation patterns and glide-snow avalanche release areas with slope angles, slab lengths and topographical characteristics, basal friction values can be obtained (Chapter 2). This result can be used in forest management guidelines to establish the allowable size of forest gaps.

In the next chapter (Chapter 3), the effect of different forest cover characteristics on avalanche flow dynamics is investigated. The aim of this investigation is to develop a modeling approach that facilitates the consideration of different forest types in a snow hazard analysis. As soon as an avalanche runs through forest, observations reveal that snow is extracted from the flow. How much snow is dependent on the forest structure. Avalanche deceleration is therefore associated with mass detrainment in forests. Field observations of snow depositions behind trees coupled with the back-calculation of the observed events can be used to link mass detrainment and avalanche runout shortening.

Runout shortening implies that forest stands can withstand the avalanche impact pressure. Therefore, defining the threshold when trees break and overturn is necessary to distinguish between detrainment-based runout shortening and frictional deceleration based on tree-breakage, overturning and entrainment (Chapter 4). This information can be used to define the maximum size of an avalanche that can be stopped by a forest. It is assumed that tree-breakage depends on avalanche flow regime. Therefore, the protective capacity of a forest depends on climatic conditions that define the prevailing temperature and moisture content of the avalanche snow. As before, the consideration of flow regime in understanding the forest-avalanche interaction problem is made possible by new numerical models that consider the influence of temperature on snow quality. With this approach it is possible to account for the full range of forest-avalanche interaction - from minor tree stem breakage to large scale forest destruction.

## 1.6 Open research questions

The following four open research questions and related hypothesis are formulated in this dissertation. These arise from gaps in knowledge about the complex interaction between forest vegetation and the downhill motion of flowing snow.

1. *What physical processes prevent snow gliding in forests?*

Hypothesis: Trees stabilize the snow cover, fix it to the ground and therefore prevent snow gliding. The compression of the visco-elastic snow cover behind tree stands can be described with stauchwall mechanics and allows the prediction of snow cover failure due to overloading. The failure of the stauchwall is the precondition for glide-snow avalanche release. The basal friction in the release area is a crucial parameter and is influenced by the vegetation cover. By quantifying the basal friction, the minimum forest gap size for avalanche release can be determined.

2. *What is the influence of forest density and structure on avalanche dynamics? How can it be quantified?*

Hypothesis: The influence of forest stands on avalanche dynamics depends on the capability of trees to survive avalanche impact forces and therefore on the stress threshold between tree-survival and tree-breakage. The destruction of forest consumes kinetic energy of the avalanche, which leads to a deceleration. In contrast trees that remain standing extract mass from the flow. The amount of snow that is extracted from the avalanche volume can be calculated in simulations and is verified with observations.

3. *How can forest-avalanche interaction be calculated and implemented in existing avalanche modeling systems?*

Hypothesis: Depending on the damage, forest can be implemented in avalanche simulation software by either applying a higher turbulent friction for forest destruction (tree breakage, uprooting, overturning, entrainment) or by extracting snow mass according to forest stand characteristics.

4. *What are the crucial forest parameters that define the protective effect against avalanches?*

Hypothesis: Stand density, vertical structure, ground roughness and tree species are the crucial factors defining the amount of mass extracted by forests. Forest damage is governed by the avalanche flow regime, by the flow parameters density, flow height, velocity, by the terrain and by stem diameter, tree species and tree arrangement.

## 1.7 Outline

To achieve the overall goal to answer the research questions, theoretical and field studies were conducted and the main results were summarized in three chapters. Each chapter consists of one peer reviewed journal article.

**Chapter 2:** Quantification of basal friction for technical and silvicultural glide-snow avalanche mitigation measures *T. Feistl, P. Bebi, L. Dreier, M. Hanewinkel and P. Bartelt, 2014: Quantification of basal friction for technical and silvicultural glide-snow avalanche mitigation measures. Natural Hazards and Earth System Sciences, 14 (11), 2921-2931.* Reprinted from the Journal of Natural Hazards and Earth System Sciences with permission of the European Geosciences Union.

In this chapter we present a new approach to quantify basal friction as roughness of terrain and vegetation and its effects on glide-snow avalanche formation. The approach is based on the prediction of stauwall failure which depends on slope angle, slab length and ground friction. Field observations are used to validate our calculations.

**Chapter 3:** Observations and modeling of the braking effect of forests on small and medium avalanches *T. Feistl, P. Bebi, M. Teich, Y. Bühler, M. Christen, K. Thuro and P. Bartelt, 2014: Observations and modeling of the braking effect of forests on small and medium avalanches. Journal of Glaciology, 60 (219), 124-138.* Reprinted from the Journal of Glaciology with permission of the Glaciological Society.

In this chapter we calculate the amount of snow that is stopped behind trees to predict the runout shortening caused by forest-avalanche interaction. The assumption behind the theory is that trees withstand the avalanche impact pressure and remain rigid obstacles in the avalanche flow. We present simulations of documented avalanche events and proof the applicability of this new modeling approach.

**Chapter 4:** Forest damage and snow avalanche flow regime *T. Feistl, P. Bebi, M. Christen, S. Margreth, L. Diefenbach and P. Bartelt, submitted. Forest damage and snow avalanche flow regime. Natural Hazards and Earth System Sciences Discussions, 3, 535-574.* Reprinted from the Journal of Natural Hazards and Earth System Sciences Discussions with permission of the European Geosciences Union.

In this chapter we calculate bending stresses of different avalanche flow regimes on trees. Wet snow avalanche pressure cannot be calculated with dynamic impact scenarios but static loading explains observed forest damage. We test our theoretical assumptions by simulating real events and are able to predict forest damage by the dense flowing core and powder cloud.



## 2. Quantification of basal friction for technical and silvicultural glide-snow avalanche mitigation measures

Thomas Feistl<sup>[1,2]</sup>, Peter Bebi<sup>[1]</sup>, Lisa Dreier<sup>[1]</sup>, Marc Hanewinkel<sup>[3,4]</sup> and Perry Bartelt<sup>[1]</sup>

<sup>[1]</sup> WSL Institute for Snow and Avalanche Research SLF, Flüelastrasse 11, 7260 Davos Dorf, Switzerland

<sup>[2]</sup> Technical University Munich (TUM), Engineering Geology and Hydrogeology, Arcisstrasse 21, 80333 Munich, Germany

<sup>[3]</sup> Swiss Federal Institute for Forest, Snow and Landscape Research WSL, Zürcherstrasse 111, 8903 Birmensdorf, Switzerland

<sup>[4]</sup> University of Freiburg, Forestry Economics and Planning, Tennenbacherstrasse 4, 79106 Freiburg, Germany

## Abstract

A long-standing problem in avalanche engineering is to design defense structures and manage forest stands such that they can withstand the forces of the natural snow cover. In this way glide-snow avalanches can be prevented. Ground friction plays a crucial role in this process. To verify existing guidelines, we collected data on the vegetation cover and terrain characteristics of 101 glide-snow release areas in Davos, Switzerland. We quantified the Coulomb friction parameter  $\mu_m$  by applying a physical model that accounts for the dynamic forces of the moving snow on the stauchzone. We investigated the role of glide length, slope steepness and friction on avalanche release. Our calculations revealed that the slope angle and slab length for smooth slopes corresponds to the technical guidelines for defense structure distances in Switzerland. Artificial defense structures, built in accordance with guidelines, prevent glide-snow avalanche releases, even when the terrain is smooth. Slopes over 40 m length and  $45^\circ$  steepness require a ground friction of  $\mu_m = 0.7$  corresponding to stumps or tree regeneration to assure protection. Forest management guidelines which define maximum forest gap sizes to prevent glide-snow avalanche release neglect the role of surface roughness and therefore underestimate the danger on smooth slopes.

## 2.1 Introduction

Full-depth, glide-snow avalanches are common events on the steep, smooth slopes of the European Alps [*In der Gand and Zupančič*, 1966; *Höllner*, 2014a]. Although these slides have relatively small release areas, they endanger roads, railways and other infrastructure. Because glide-snow avalanches are difficult to predict [*Dreier*, 2013], hazard engineers rely on mitigation measures to stabilize the snow cover and prevent glide-snow avalanches from starting. These measures include both technical defense structures and forests [*Margreth*, 2007; *Höllner*, 2012a]. A critical problem for decision makers is to define potential release areas in real terrain and understand how terrain and vegetation characteristics influence release and can be managed to defend against glide-snow avalanche hazard.

The mechanics of glide-snow avalanches involves two principle components: the compressive strength of the stauchwall and the frictional properties of the ground [*In der Gand and Zupančič*, 1966; *Häfeli*, 1967; *McClung*, 1975; *Bartelt et al.*, 2012b]. Glide-snow avalanches typically occur when water accumulates on the snow-soil interface either by melting (because of a warm soil surface) or by melt-water penetration through the snow cover [*In der Gand and Zupančič*, 1966; *Mitterer et al.*, 2011]. As the ground friction decreases because of the melt-water, the lost frictional forces must be taken up in the tensile or compressive zone of the snow cover, otherwise it begins to glide (Fig. 2.1). Typically, the snow cover breaks first in the tensile zone and a glide-crack (a so-called “Fischmaul”) opens. This causes an additional redistribution of stress within the snow cover and leads to a fragile stability governed by the strength of the compressive zone. This zone is termed the stauchwall [*Lackinger*, 1987; *Bartelt et al.*, 2012b]. The stauchwall is fixed to the ground, either because the basal surface is rough, or because the slope is flatter leading to large compressive stresses. Any obstacles, such as trees, will help stabilize the snow cover by consuming the additional stress. The distance between obstacles in large part determines the stress redistribution: if the distances are too large, the natural strength of the snow cover will be overcome and snow slides will result [*de Quervain*, 1978; *Höllner*, 2004].

A key parameter in the mitigation of glide-snow avalanches is therefore the distance between defense structures and the allowable forest clearing size. Different approaches have been addressed to define distances between defense structures and maximum forest gap sizes. The Swiss guidelines on sustainable management of protective forests NaiS [*Frehner et al.*, 2005] for example are based on a statistical evaluation of data mostly gained on a field campaign in Switzerland from 1985 to 1990 [*Gubler and Rychetnik*, 1991; *Meyer-Grass and Schneebeli*, 1992]. Statements on possible avalanche formation as a function of slope angle and gap length could be drawn, taking ground roughness qualitatively into account [*Frehner et al.*, 2005]. These guidelines were successfully applied in the past by foresters. *Leitinger et al.* [2008] developed a spatial snow glide model based on data of two study areas in Austria and Italy. It takes slope angle, surface roughness, slope aspect, winter precipitation and forest stand characteristics into account. Likewise, the technical guidelines for avalanche prevention structures in release areas in Switzerland are based on calculations of the pressure that a slab exerts

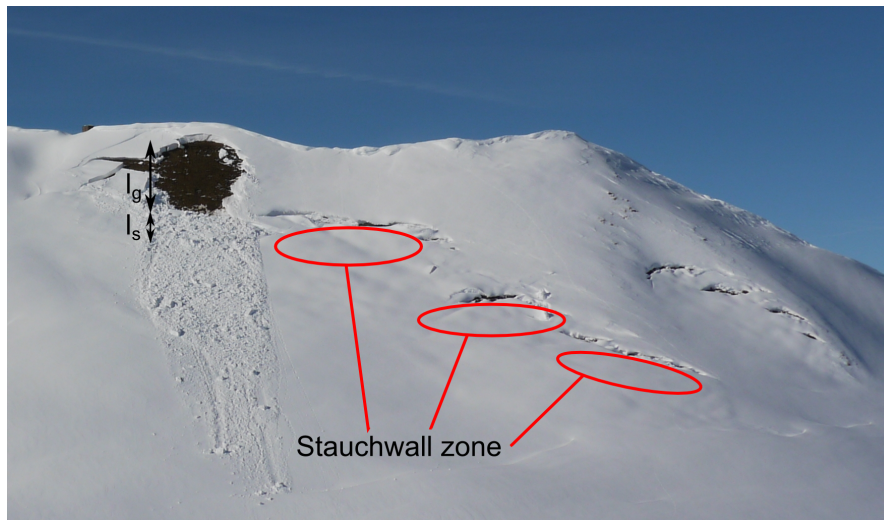


FIGURE 2.1: Opening of glide-cracks (Fischmaul) near Davos. The left slope released, probably because the slope is steeper than the right part.

on an avalanche prevention bridge [de Quervain and Salm, 1963; Margreth, 2007]. Slope angle, snow depth and the Coulomb friction of the snow on the ground are taken into account.

Although the relationship between slab length and slope angle at which glide-snow avalanches release is well understood [Fiebiger, 1978; Imbeck, 1984; Imbeck and Meyer-Grass, 1988; Gubler and Rychetnik, 1991; Meyer-Grass and Schneebeli, 1992; Leitinger et al., 2008], the important role of ground roughness remains an unknown parameter. Ground friction dictates the force redistribution and therefore the loading on the stauchwall [In der Gand and Zupančič, 1966; McClung, 1975; Höller, 2004; Bartelt et al., 2012b]. Vegetation can increase the ground roughness significantly [de Quervain, 1978; Fiebiger, 1978; Newesely et al., 2000; Höller, 2001; Leitinger et al., 2008; Schneebeli and Bebi, 2004; Weir, 2002]. Although all authors agree that glide-snow avalanche activity is retarded by dense forest stands, the quantification of basal friction as a function of vegetation structure is missing.

In this paper we aim to combine a physical ground friction – stauchwall model with data on glide-snow avalanche release areas to quantify the role of technical and silvicultural avalanche protection measures. To this end, we collected and analyzed data of the characteristic vegetation cover, terrain and snow characteristics of glide-snow avalanche release areas on the Dorfberg, near Davos, Switzerland. We compare the glide-snow avalanche data with model results and test if existing guidelines are in accordance with our measurements. As the glide-snow avalanche model includes the important role of ground roughness – which is strongly influenced by the vegetation cover – we are able to link the observed terrain roughness and ground vegetation to specific Coulomb friction values. Finally we attempt to answer the questions where, when and what elements of terrain roughness are most appropriate for glide-snow avalanche prevention.

## 2.2 Methods

### 2.2.1 Observed glide-snow avalanche release areas

Glide-snow avalanches are observed on the Dorfberg, above Davos, Switzerland every season and were documented via time lapse photography in the winters 2011/2012 and 2012/2013 [van Herwijnen and Simenhois, 2012]. Their occurrence depends on meteorological conditions such as temperature, snow depth, snow stratification and ground temperature [Dreier, 2013; Dreier et al., 2013] but their location in the terrain is almost similar each year. Dreier [2013] mapped the release zones according to the photos (see Fig. 2.2). These photos were not georeferenced and a small uncertainty concerning the location of the release areas in the terrain exists but we suppose the error to be relatively small. We performed a field campaign in autumn 2013 where we collected data on the characteristic vegetation cover, vegetation height  $h_v$ , distance to the next obstacle and terrain characteristics of 101 glide-snow avalanche release areas on Dorfberg. The compaction of vegetation due to the snow cover weight was documented on a second field campaign in February 2014.

The south to east facing slope below the Salezer Horn (2536 m) covers 200 ha. The elevation of the observed release areas ranges from 1700 m a.s.l. to 2300 m a.s.l. Grassy slopes, shrubs and forest alternate with stones and small rock walls. We calculated the mean slope angles  $\alpha$  and slab lengths  $l_g$  of all avalanche release areas using ArcGIS. Release height was estimated with the snow depth  $h_s$  measured at the meteorological station in Davos. The station is situated at a lower elevation (1560 m a.s.l.) but is not exposed to the sun. The snow depth on Dorfberg and therefore the release height of the glide-snow avalanches resemble the snow depth measured at the meteorological station in the investigated winters.

We documented the typical vegetation cover of the 101 release areas (Fig. 2.3) and found four characteristic types of vegetation:

1. long grass (*Calamagrostis villosa*)
2. short grass (*Nardion* spp.)
3. low dwarf shrubs (Ericaceae, Vaccinium, Empetrum)
4. strong lignified shrubs (Rhododendron, Juniperus).

No avalanches were observed in forested terrain. We recorded the dominating vegetation species, if more than one vegetation type was present on a single release area.

The vegetation height  $h_v$  was measured in November 2013 and February 2014 (Fig. 2.4). Our first field study took place in autumn, therefore this vegetation height represents the surface that the first snow fell on. In February 2014 the vegetation heights were measured below the snow cover at representative locations on Dorfberg. We observed a mean height of long compacted grass  $h_v < 1$  cm, in contrast to short upright grass with

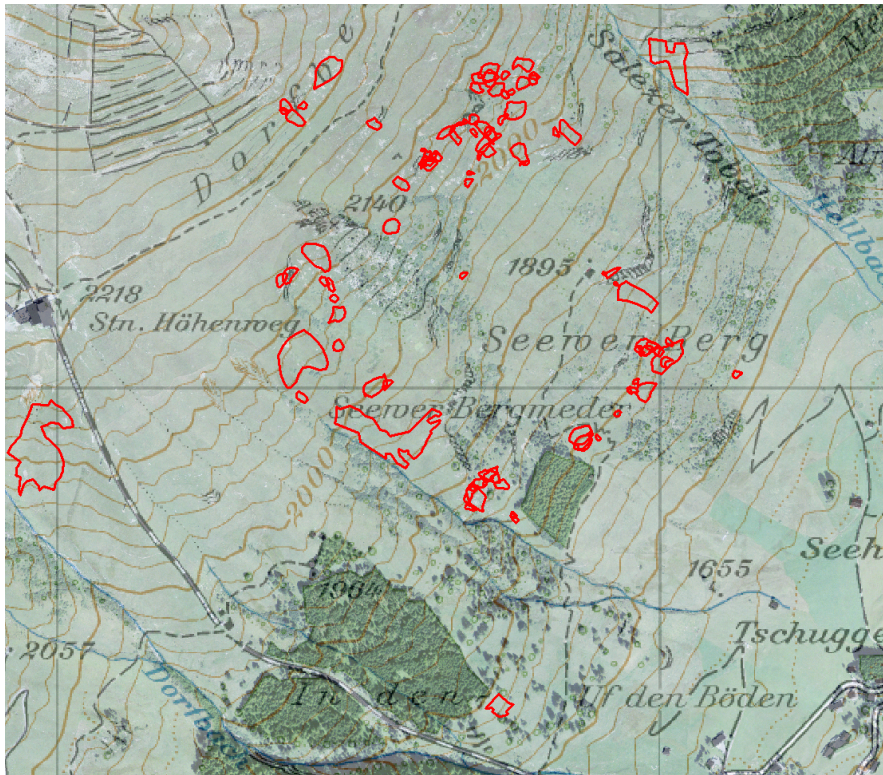


FIGURE 2.2: Glide-snow avalanche release zones on Dorfberg, Davos. (Swissimage ©, DV 033594, 2013).



FIGURE 2.3: Different vegetation types were observed at our field campaign. The main types were long grass, short grass, low dwarf shrubs and strong lignified shrubs.

$h_v = 3$  cm, low dwarf shrubs  $h_v = 4$  cm and strong lignified shrubs  $10 \text{ cm} < h_v < 20$  cm (Fig. 2.4). The snow cover of depth  $h_s = 0.5$  m compacted long grass to one tenth of the height in autumn. Short grass, low dwarf shrubs and strong lignified shrubs were compacted to one fourth of their original height.

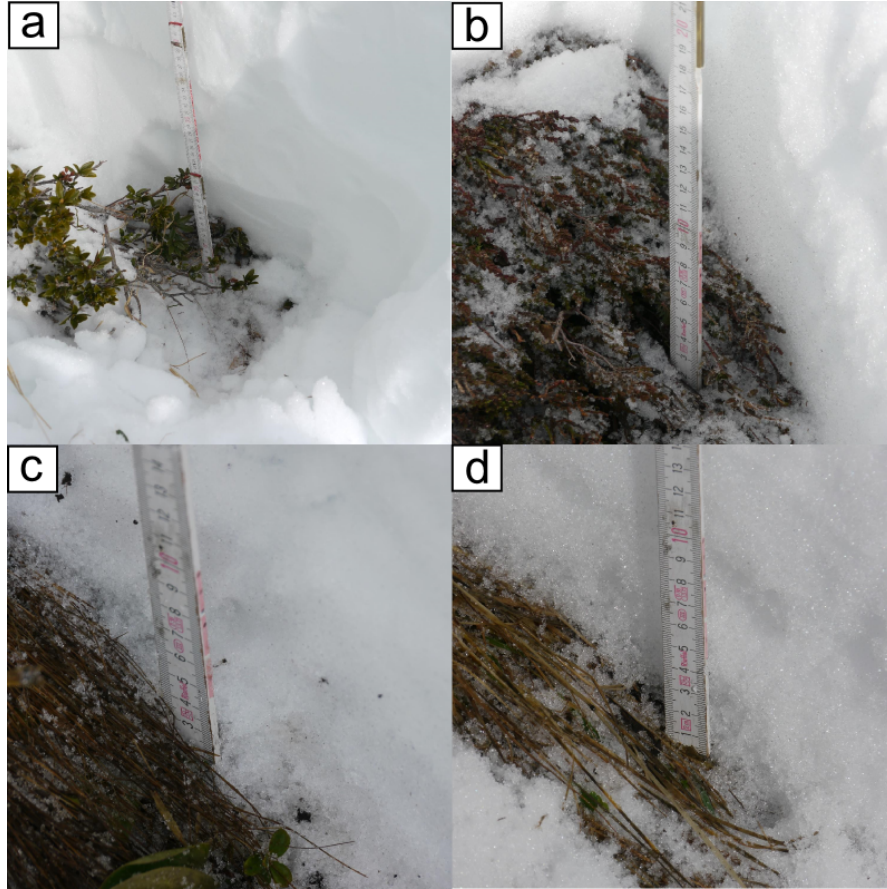


FIGURE 2.4: Vegetation below the snow cover. Vegetation heights  $h_v$  are smaller in winter than in autumn: 10–20 cm for strong lignified shrubs (a), 4 cm for low dwarf shrubs (b), 3 cm for short grass (c) and less than one centimeter for long grass (d).

As topography contributes to roughness we assume the underlying terrain of the release areas to play an important role in glide-snow avalanche release. Therefore we documented the dominating terrain types and their height  $h_t$  for each release area. Typical features we found were smooth, steps, rocks and ridges. We performed a Mann–Withney  $U$  test in order to test if these different vegetation- and terrain types in release areas correlate with slope angle, slab length and snow depth.

We parameterized surface roughness using the measured terrain irregularity heights  $h_t$  and vegetation heights  $h_v$ . This allowed us to relate the observed heights to the calculated friction parameter  $\mu_m$ . The heights  $h_v$  and  $h_t$  are assigned values characteristic to the observed vegetation and terrain types. This is necessary in order to transfer the model results to other field locations.

### 2.2.2 Selection of avalanches with stauchwall

We selected events where we assume the snow cover below the release area to be fixed to the ground, the so called stauchwall. The mechanical stauchwall model (Sect. 2.2.3) is applicable for these events. A flatter slope, higher surface roughness or an obstacle (Fig. 2.5) below the release area are cases where a fixed stauchwall is probable. Several events without stauchwall were neglected in further studies. In particular events with either a drop or with a steeper slope below the release area (Fig. 2.6) were disregarded. These events were found by comparing the slope angle of the release areas  $\gamma$  with the slope angle of the areas below  $\nu$ . If  $\gamma < \nu$  we assume no stauchwall to be present. Out of 101 glide-snow avalanches, 67 events were considered with stauchwall. Of these 67 events 31 released on compacted long grass, 4 on upright short grass, 31 on low dwarf shrubs and one on strong lignified shrubs.

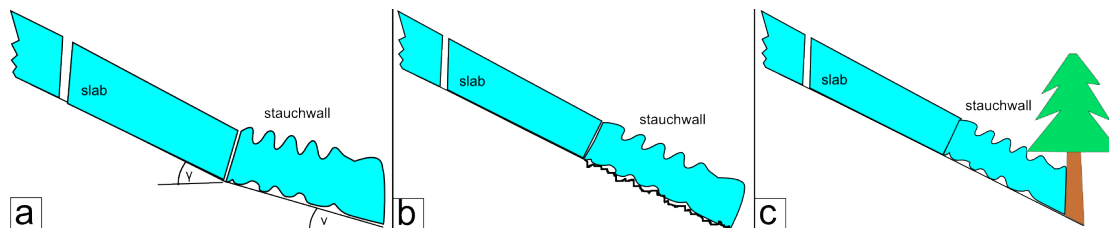


FIGURE 2.5: Cases where a stauchwall forms: in (a) the area below the release zone is flatter, than the release area. Rougher surface below the release zone fixes snow to the ground (b) and a tree can be an effective obstacle stabilizing the snow cover below the release area (c).

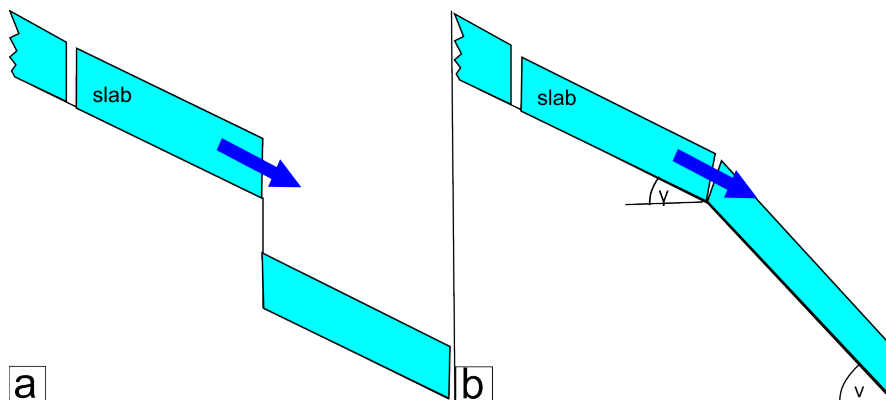


FIGURE 2.6: Cases where no stauchwall forms: either there is a terrain drop (a) or the area below the release is steeper than the release area (b).

Vegetation cover and terrain both contribute to ground roughness. We defined three combined categories (see Sect. 2.3.1) to enable a simplified classification:

1. smooth terrain covered with long compacted grass
2. smooth terrain covered with short upright grass or low dwarf shrubs
3. rocky or stepped terrain covered with shrubs

Only avalanches with stauchwall were considered for this categorization. Long compacted grass always had smooth terrain underneath. We assume this combination of long grass and smooth terrain to form the surface with the lowest friction. Short grass or low dwarf shrubs on smooth terrain was defined as the second category. And the third category was shrubs on steps or rocks. On stepped terrain or on rocky slopes we did not find any grass dominated vegetation.

### 2.2.3 Mechanical stauchwall model

To predict glide-snow avalanche release we apply the two-dimensional visco-elastic continuum model of *Bartelt et al.* [2012b]. The model divides the snow cover into two regions: the sliding zone and the stauchwall (Fig. 2.7). The sliding zone has length  $l_m$ ; the stauchwall has length  $l_s$  and is fixed to the ground. We assume a snow cover with depth  $h_s$  and a homogenous density  $\rho$ . Therefore, the total mass per unit width of the slab is  $m = \rho h_s \cos \gamma l_m$ . The snow cover starts to slide downwards once the frictional force on the ground can not withstand the gravitational force of the snow pack and a tensile crack opens at the crown. Static equilibrium is lost and the tensile force at the crown must be transferred to the sliding zone and the stauchwall. The avalanche releases if a critical strain-rate is reached. It is possible that the lost force is balanced entirely by an increase in shear stress at the base of the snow cover. In this case no avalanche will release, but this scenario requires high friction  $\mu_m$  to transfer the lost tensile force into the ground. Moreover, the driving force and the friction resistance are in balance:

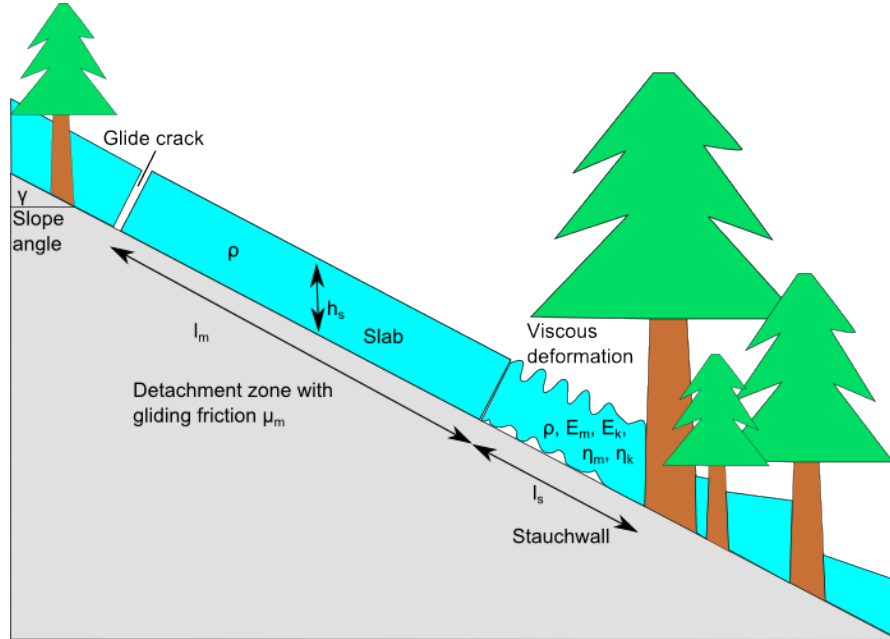


FIGURE 2.7: Model description: a slab with length  $l_m$ , snow density  $\rho$  and snow depth  $h_s$  starts to glide on a slope with angle  $\gamma$ . A glide crack opens and the weight of the slab  $m$  is balanced by the friction of the snow on the ground  $\mu_m$  and the stauchwall with length  $l_s$ , snow density  $\rho$  and material parameters  $E_k, E_m, \eta_k, \eta_m$ .

$$mg_x = \mu_m mg_z; \quad (2.1)$$

where  $g_x$  and  $g_z$  are the gravitational accelerations in the slope parallel and normal directions, respectively. These depend on the slope angle  $\gamma$ . It is also possible that the lost force is taken up by the stauchwand. In this case there is an out-of-balance stress  $\sigma$  that must be resisted by the stauchwand:

$$m\dot{u}(t) = mg_x - \mu_m mg_z - \sigma(t)h_s \cos \gamma \quad (2.2)$$

where  $u(t)$  is the displacement velocity of the slab. Because snow is a visco-elastic material, the stauchwand resisting stress  $\sigma$  is time dependent. A simple Burgers model is used to calculate the resisting action of the stauchwand:

$$\ddot{\sigma}(t) + \left[ \frac{E_m}{\eta_m} + \frac{E_m}{\eta_k} + \frac{E_k}{\eta_k} \right] \dot{\sigma}(t) + \left[ \frac{E_m E_k}{\eta_m \eta_k} \right] \sigma(t) = \frac{E_m}{2l_s} \dot{u}(t) + \frac{E_m E_k}{2\eta_k l_s} u(t). \quad (2.3)$$

The visco-elastic constants ( $E_m$ ,  $E_k$ ,  $\eta_m$ ,  $\eta_k$ ) are density and temperature dependent [Von Moos *et al.*, 2003; Scapozza and Bartelt, 2003].

Equations (2.2) and (2.3) are a system of two coupled ordinary differential equations that can be solved numerically. Numerical solutions are presented in Bartelt *et al.* [2012b]. The model predicts the strain-rate  $\dot{\epsilon} = u/2l_s$  in the stauchwand. The total strain  $E$  and therefore total deformation is calculated by summing the strain-rates at every calculation step with length  $\Delta t$ :  $E(t + \Delta t) = \epsilon(t) + \dot{\epsilon}\Delta t$ . When the strain-rates exceed a critical value, we consider the stauchwand to fail and an avalanche is released.

#### 2.2.4 Technical guidelines

For further analysis we refer to the technical guidelines for avalanche prevention structures in release areas in Switzerland [Margreth, 2007], the Swiss guidelines on sustainable management of protective forests NaiS [Frehner *et al.*, 2005] and on the Austrian norm on avalanche prevention structures [Austrian Standard Institute, 2011]. These guidelines specify the maximum allowable length between defense structures and the maximum allowable length of forest clearings. For clarity, we denote these allowable lengths  $l_d$  and  $l_f$ , respectively. The stauchwand is within these lengths. The guidelines require knowledge of the ground friction, which we have designated  $\mu_d$  for guidelines. The distance between prevention bridges is calculated according to  $l_d = \frac{2 \tan \gamma}{\tan \gamma - \mu_d} h_s$ . For example, the allowable defense structure distance  $l_d$  in Switzerland is calculated with friction values between  $0.5 \leq \mu_d \leq 0.6$ . Therefore  $l_d(\mu_d, \gamma)$  and  $l_f(\mu_d, \gamma)$  as the guidelines depend on the slope angle  $\gamma$ .

Although the technical and forest guidelines are based on different approaches, the aim of all guidelines is similar: within the distance  $l_d(\mu_d, \gamma)$  or  $l_f(\mu_d, \gamma)$  no avalanche should release. On the Dorfberg we have measured the distance between fracture crown and stauchwand; we denote the observed lengths  $l_g$ . We have documented the terrain features

and vegetation associated with each  $l_g$ . Furthermore we have quantified the mean slope angle of each slide observed in the field. That is, we have  $l_g(\mu_m, \gamma)$ . If the guidelines are correct, we should have

$$l_d(\mu_d, \gamma) \leq l_g(\mu_m, \gamma) + l_s \quad (2.4)$$

and

$$l_f(\mu_d, \gamma) \leq l_g(\mu_m, \gamma) + l_s. \quad (2.5)$$

where the stauhwall length is denoted  $l_s$  and added to the measured slab length  $l_g$ . These comparisons should also hold for the mechanical model. To distinguish between measured and modeled slab length we denote the modeled slab length by  $l_m$ . That is,

$$l_d(\mu_d, \gamma) \leq l_m(\mu_m, \gamma) + l_s \quad (2.6)$$

and

$$l_f(\mu_d, \gamma) \leq l_m(\mu_m, \gamma) + l_s. \quad (2.7)$$

We calculated the critical slab lengths (the slab lengths at failure,  $l_m$ ) for all slope angles mentioned in guidelines. Different friction parameters  $\mu_m$  were applied in the model calculations. By comparison we could quantify the friction values we observed in the field. In the model calculations we tested different snow densities and snow depths to investigate the role these parameters had on strain-rates and therefore glide-snow avalanche formation.

## 2.3 Results and discussion

### 2.3.1 Results of field observations, $l_g(\mu_m, \gamma)$

Most releases in the Dorfberg study area were found on long grass (45 avalanches) and on low dwarf shrub vegetation (49 avalanches), whereas only few avalanches released on the vegetation categories “short grass” and strong “lignified shrubs” (Table 2.1). The categories “short grass” and “low dwarf shrubs” had comparable vegetation heights  $h_v$  (Table 2.1). We subsequently combined these two categories in our data analysis. The mean vegetation height of long grass was 10 cm, whereas the mean vegetation height of short grass was 13 cm, of low dwarf shrubs 14 cm and of strong lignified shrubs 50 cm. These values were measured before the first snowfall. Below the snow cover (measurements taken in February 2014) the heights decreased to  $h_v < 1$  cm for long grass,  $h_v = 3$  cm and  $h_v = 4$  cm for short grass and low dwarf shrubs and  $10 \text{ cm} < h_v < 20$  cm for strong lignified shrubs. We combined also different terrain types according to their measured irregularity heights  $h_t$  (Table 2.2). Irregularities of smooth terrain and ridges had a mean height of approximately 20 cm in contrast to stepped and rocky terrain with approximately 30 cm. We note, that in autumn, only 5 cm separates the vegetation types and 10 cm separates the two terrain classes. Below the snow cover the differences

are even smaller. This is an indication that small height variations can lead to a large difference in surface friction.

TABLE 2.1: The observed vegetation types on Dorfberg. Mean vegetation height  $h_v$  in autumn and winter, slope angle  $\gamma$ , slab length  $l_g$  and a photo of a typical example case are added.

Vegetation type	Long compacted grass	Short upright grass	Low dwarf shrubs	Strong lignified shrubs
Number of avalanches	45	6	49	1
Mean $\gamma$ [°]	35	36	39	35
Mean $l_g$ [m]	26	42	28	38
Mean $h_v$ [m] in autumn	0.10	0.13	0.14	0.5
Mean $h_v$ [m] in winter	0.01	0.03	0.04	0.15

Photo



TABLE 2.2: The observed terrain on Dorfberg. Mean slope angle  $\gamma$ , slab length  $l_g$ , terrain height  $h_t$  and a photo of a typical example case are added. Note the high number of smooth terrain cases.

Terrain	Ridge	Smooth	Steps	Rocks
Number of avalanches	1	79	9	12
Mean $\gamma$ [°]	36	37	38	40
Mean $l_g$ [m]	40	26	36	34
Mean $h_t$ [m]	0.15	0.19	0.31	0.32

Photo



The release of glide-snow avalanches on Dorfberg depended strongly on surface characteristics. Releases occurred in steeper terrain in areas with shrubs compared to areas with long grass (Mann–Whitney  $U$  Test,  $p = 0.008$ ) and on areas with the terrain type “smooth” compared to other terrain types (79 events out of 101). The combination of vegetation- and terrain categories led to clear correlations between glide-snow avalanches and surface characteristics. This suggests the importance of basal properties. For example, we found that glide-snow avalanches can release on relatively flat slopes and had the shortest slab lengths if the terrain was smooth and was covered with long grass. Higher slope angles and longer slab lengths were observed for the slopes covered with short grass or shrubs growing on smooth terrain. The highest slope angles and release

lengths were necessary for cases where the terrain was rocky or stepped and covered with shrubs. In this case the mean slope angles and slab lengths increased.

Snow depth  $h_s$  (at the release) correlated weakly with the slab length  $l_g$  (Fig. 2.8). Avalanches with a release length of  $l_g > 50$  m were observed only for snow depths of more than one meter,  $h_s > 1$  m. Note that slope angle  $\gamma$  and snow depth  $h_s$  could not be correlated. The mean snow depth was slightly higher for short grass, low dwarf shrubs and strong lignified shrubs ( $h_s = 94$  cm) than for long grass ( $h_s = 84$  cm). Snow depth has an influence on the mean vegetation height as vegetation is compressed by the snow mass (Table 2.1, Fig. 2.4). Long grass is already compressed with a relatively small load. However, shrubs need more weight for a similar effect. We observed glide-snow avalanche release on less steep slopes covered with low dwarf shrubs only for snow depths  $h_s > 1$  m. No such effect was found for slopes covered with grass.

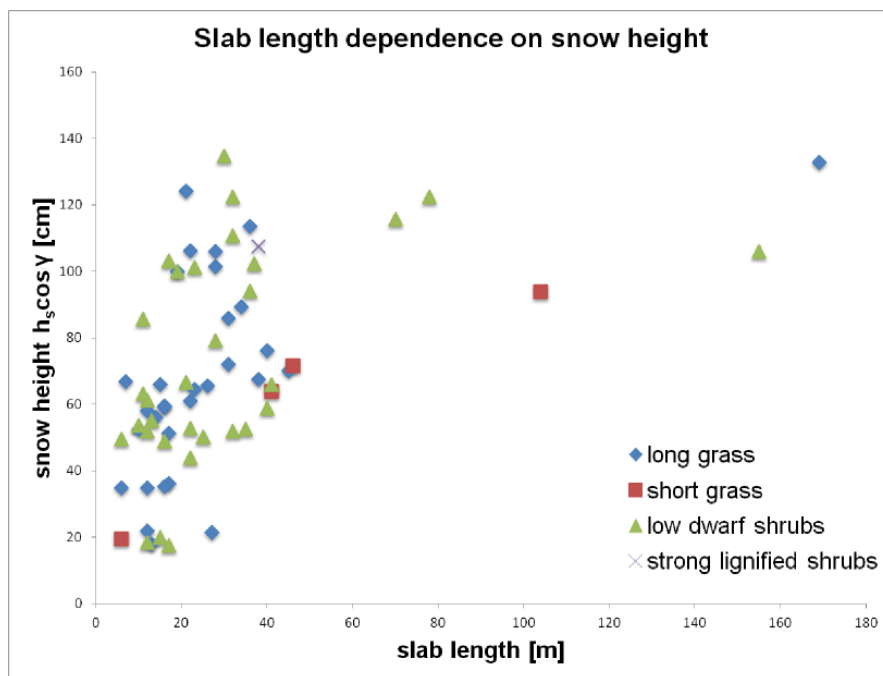


FIGURE 2.8: Slab length and snow height correlate weakly (Pearson coefficient of correlation squared:  $R^2 = 0.25$ ). The longest slabs  $l_g$  were observed for snow heights  $h_s \cos \gamma > 90$  cm. Whereas short release areas, (up to 50 m) are possible for any snow height, long slabs are characteristic for large snow heights. Here we only look at the 67 events where we assume a stauwall to be present.

### 2.3.2 Results of model calculations $l_m(\mu_m, \gamma)$

We performed a series of model calculations to establish a correlation between strain-rate, slab length, slope angle and ground friction. We studied the influence of ground roughness  $\mu_m$  on slab length  $l_m$  and slope angle  $\gamma$  by modeling the resistance and failure of the stauwall (Sect. 2.2.3). We kept the material parameters of snow ( $E_m = 1.5 \times 10^8 Pa$ ,  $E_k = 1.5 \times 10^7 Pa$ ,  $\eta_m = 1.4 \times 10^9 Pas$ ,  $\eta_k = 2.5 \times 10^6 Pas$ ) constant and defined a critical strain rate in compression ( $\dot{\epsilon} = 0.01 s^{-1}$ ) which leads to the collapse of the

stauchwall. The material parameters and the critical strain rate were defined according to the work of *Von Moos et al.* [2003], *Scapozza and Bartelt* [2003] and *Bartelt et al.* [2012b]. Model results for different slope angles, slab lengths and friction parameter values are depicted in Fig. 2.9. We varied density  $\rho$  and the stauchwall length  $l_s$  which depends on the snow depth  $h_s$ . We found friction values between  $\mu_m = 0.33$  and  $\mu_m = 0.81$  for a density  $\rho = 300 \text{ kg m}^{-3}$  and a stauchwall length  $l_s = 2 \text{ m}$ . The lowest values are necessary for a slope angle  $\gamma = 30^\circ$  and slab length  $l_m = 30 \text{ m}$  to prevent the stauchwall from failing. The highest values are necessary for a slope angle  $\gamma = 45^\circ$  and a slab length  $l_m = 60 \text{ m}$ . Clearly, the calculated slab lengths and slope angles at failure depend strongly on the friction parameter  $\mu_m$ .

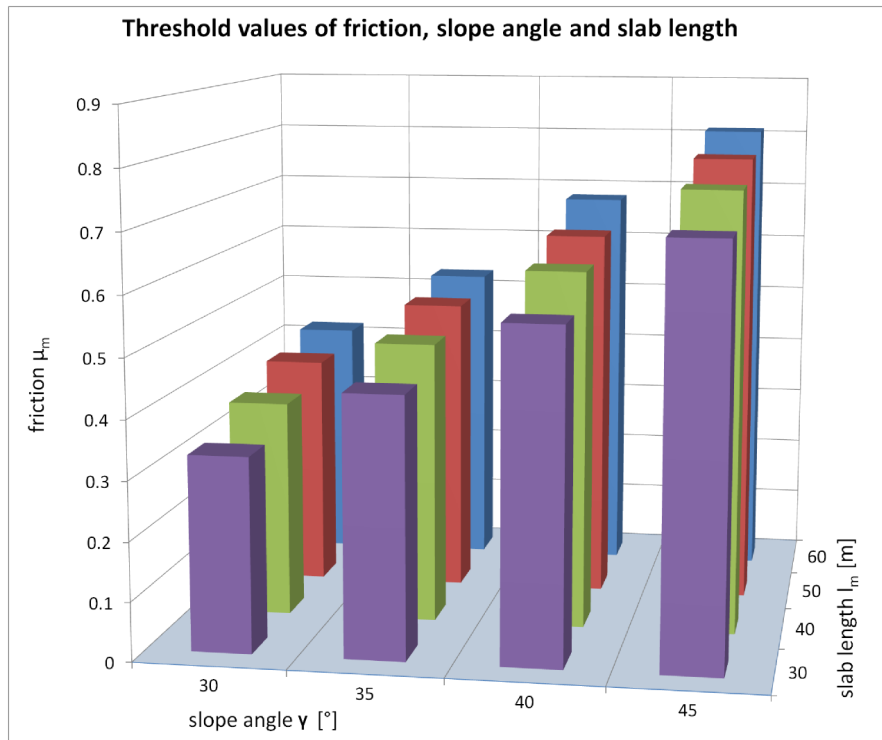


FIGURE 2.9: Three-dimensional plot showing combinations of friction  $\mu_m$ , slope angle  $\gamma$  and slab length  $l_m$  for a critical strain-rate  $\dot{\epsilon} = 0.01 \text{ s}^{-1}$ . The higher the slope angle, the higher the friction  $\mu_m$  must be to prevent a failure of the stauchwall. The larger the slab length  $l_m$ , the larger the friction  $\mu_m$  must be to prevent failure.

We investigated the role of snow density  $\rho$  and snow depth  $h_s$  on the model results. We kept the slab length  $l_m$  and slope angle  $\gamma$  constant. The model results revealed that a change in density of  $\Delta\rho = 50 \text{ kg/m}^3$  needs a corresponding change in friction parameter  $\Delta\mu$  of approximately 0.03. Therefore, we find that higher density snowpacks require higher surface roughness in order for the stauchwall to withstand the higher pressure. Moreover, the process of densification by snow settling coupled with melt-water (decrease of  $\mu$ ) could be a critical combination leading to glide-snow avalanche release. Thus, the process of densification, which can stabilize the high winter snowpack, must not automatically lead to a reduction of glide-snow avalanche activity. For further studies we kept the density constant,  $\rho = 250 \text{ kg/m}^3$ .

The pressure on the stauchwall also depends on snow depth  $h_s$ . We assumed the stauchwall length to be twice as long as the snow depth. This assumption is based on observations, for example Fig. 2.1, in which the stauchwall length can be discerned as the zone with wavelike perturbations on the surface of the snowpack. No systematic measurements exist since the stauchwall is typically destroyed during an avalanche release. We therefore varied the snow depth  $h_s$  and the stauchwall length  $l_s$  respectively and found that an increase of approximately  $\Delta\mu = 0.05$  is necessary to compensate for one additional meter of snow,  $\Delta h_s = 1.0$  m. This result suggests that snow cover stability is relatively robust to changes in snow height. Moreover, the model results are in accordance with the observations which show a similar trend (Fig. 2.8). For example, we found very little correlation between avalanche release and snow depth: glide-snow avalanches can have both large and small fracture heights.

### 2.3.3 Comparison of guidelines, model results and field observations

We compared observed slab lengths  $l_g(\mu_m, \gamma)$  from the Dorfberg with our calculated model results  $l_m(\mu_m, \gamma)$  (Fig. 2.10). For this analysis we only used data of the events with stauchwall (see Section 2.2.2). To be able to compare these to guidelines, the stauchwall length  $l_s$  was added to the observed slab length  $l_g + l_s$  and modeled slab lengths  $l_m + l_s$ . We divided the observed release areas in the three different categories (1) smooth terrain with long grass, (2) smooth terrain with short grass or shrubs and (3) stepped or rocky terrain with shrubs (Table 2.3). Friction values between  $0.1 \leq \mu_m \leq 0.5$  were tested. A lower ground friction of the observed events is indicated if the length  $l_m + l_s$  of the three terrain and vegetation categories is lower than the model calculation curves in Fig. 2.10. We found release areas with smooth terrain and long grass below the  $\mu_m = 0.1$  curve, whereas smooth terrain with shrubs or short grass was mostly (87%) above the  $\mu_m = 0.1$  curve. 92% of rocky or stepped terrain with shrubs was above the  $\mu_m = 0.3$  curve. The same analysis was performed for vegetation cover only. Whereas release areas with long grass are found even below the  $\mu_m = 0.1$  curve, 86% of all other vegetation types are above the  $\mu_m = 0.2$  curve.

TABLE 2.3: Vegetation and terrain combined in three categories. The least roughness was observed for smooth terrain with long grass and the roughest surface was observed when stepped or rocky terrain was covered with shrubs. The second category was smooth terrain covered with short upright grass or shrubs.

Terrain + Vegetation	Smooth + long grass	Smooth + short grass or shrubs	Stepped or rocky + shrubs
Number of avalanches	31	23	13
Mean $\gamma$ [°]	35	39	40
Mean $l_g$ [m]	27	27	42
Mean $h_v + h_t$ [m] in autumn	0.30	0.33	0.54
Mean $h_v + h_t$ [m] in winter	0.20	0.22	0.41

Guidelines on defense structure distances and forest gap sizes were formulated in Switzerland and Austria to prevent avalanches from releasing. We compared our observations with these guidelines to check on their performance. Guidelines on technical avalanche

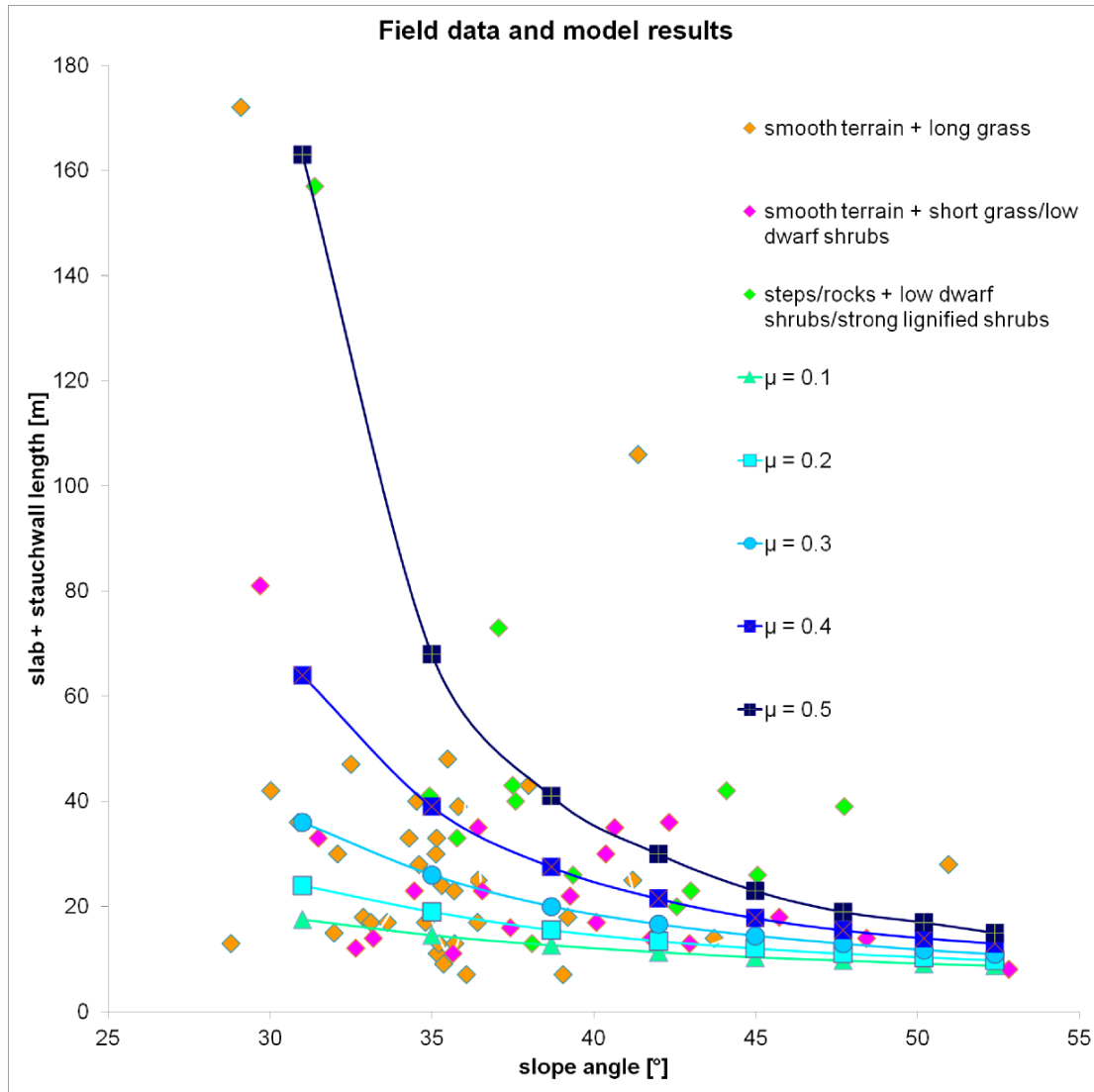


FIGURE 2.10: Comparison of glide-snow avalanche release length and stauchwand  $l_g + l_s$  from Dorfberg with model results. The graph shows slope angle against slab length of the 67 avalanches with stauchwand. We divided the data in three roughness categories: smooth terrain + long grass; smooth terrain + short grass or shrubs and stepped or rocky terrain + shrubs.

defense in Switzerland distinguish between different ground roughness and assume friction parameter values between  $0.5 \leq \mu_d \leq 0.6$ . For the same slope angle this variation leads to a change in allowable slab length of maximum three meters. The values for slab length and slope angle for small snow depths (1.5 m) are in the range of almost all events on Dorfberg of the winters 2011–2013 (Fig. 2.11). Deviations due to smooth or rough surface are small. Guidelines in Austria which do not distinguish between different snow depths recommend larger distances between defense structures.

In contrast most of the events on Dorfberg are below the tolerable forest gap sizes. Lower slope angles and shorter slab lengths than proposed in the guidelines are sufficient to allow the release of glide-snow avalanches, especially if assuming a smooth surface.

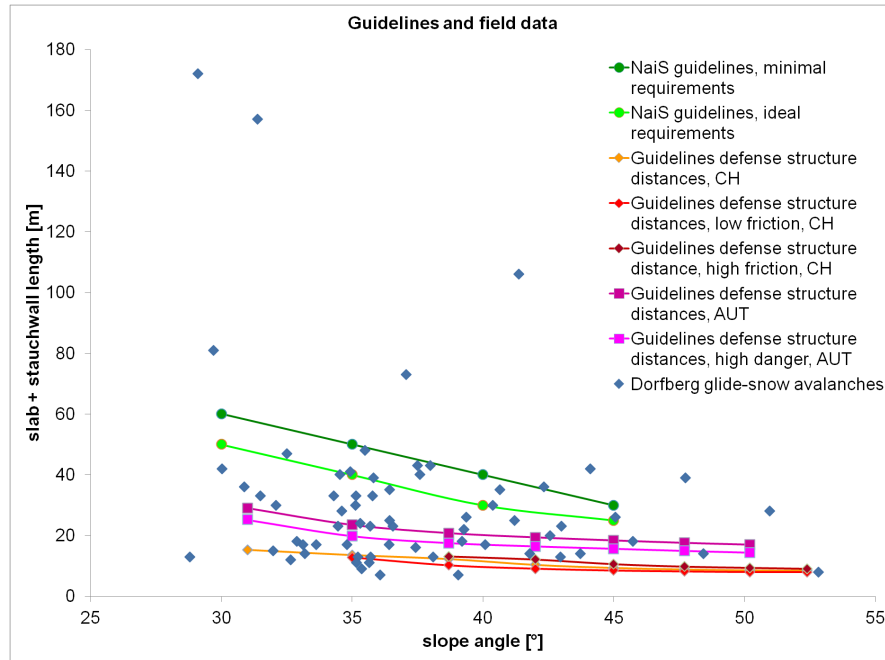


FIGURE 2.11: Comparison of guidelines with Dorfburg data. Note that most of the Dorfburg glide-snow avalanches had longer slab lengths and released on steeper slopes than proposed by the defense structure guidelines of Switzerland. In contrast forest gaps with slope angles and lengths in accordance with the Swiss guidelines on sustainable management of protective forests NaiS would not have hindered avalanche formation in a lot of cases on the Dorfburg.

We then compared the guideline values with the model results and found a good correspondence when comparing the technical guidelines for defense structures and stauhwall model results with low friction, i.e. for friction values  $\mu_m = 0.1$ . This indicates that the guidelines assume low friction values, which is essential for the safe design of supporting structures. However, for higher friction values the stauhwall model is more sensitive to the slab length and slope angle. Thus, for high friction values, we can devise slopes that are stable for slope angles up to  $35^\circ$ . The technical guidelines are again conservative since they do not assume such high friction values. In comparison correspondence between the forest management recommendations and the model results was poor. This indicates that the guidelines are not consistent for the same ground roughness and slope angle (Fig. 2.12). The calculated maximum slab length for  $\mu_m = 0.4$  and a slope angle  $\gamma = 35^\circ$  corresponds to the guideline values for gap sizes in ideal conditions. However, the model results for lower slope angles overestimate the guideline values and underestimate the guideline values for high slope angles. Moreover, the forest guidelines are appropriate for low slope angles and high friction, but appear to miscalculate the acceptable gap length in steep terrain.

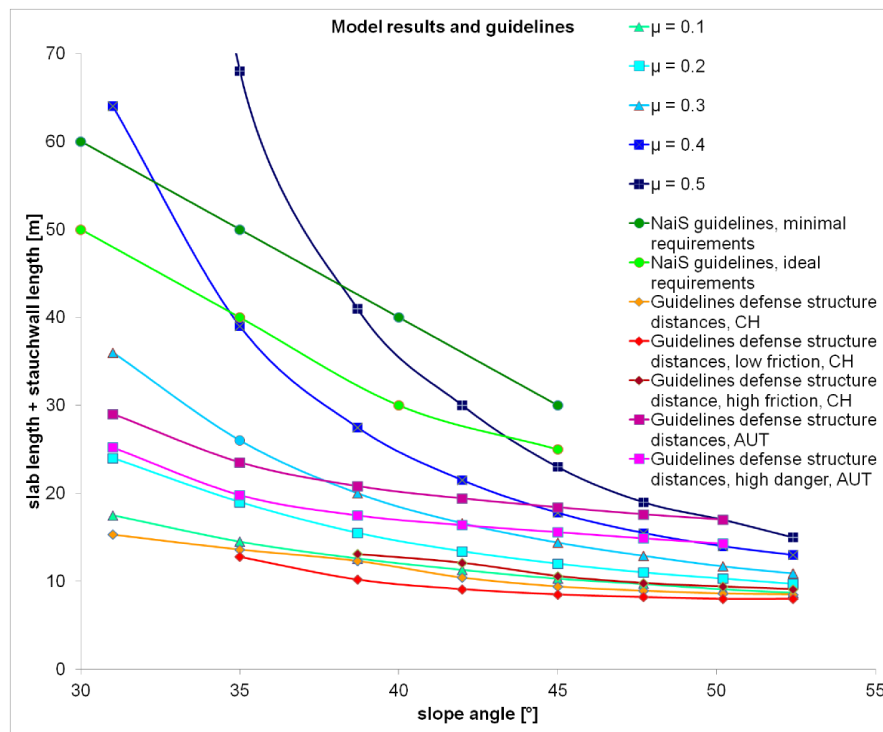


FIGURE 2.12: Comparison of guidelines with model results. Model calculations with friction values  $\mu_m = 0.1$  correspond to the technical guidelines for avalanche prevention bridges. Maximum forest gap sizes proposed by the Swiss guidelines on sustainable forest management (NaiS) are appropriate for low slope angles and high friction.

## 2.4 Conclusion

In this study we quantified the effect of ground roughness on glide-snow avalanche release with data on typical vegetation cover and topographical characteristics of 101 release areas. Additionally we employed a physical model which accounts for stauchwail mechanics and predicts failure or resistance depending on the slab length, snow depth, snow density and basal friction. We defined a critical strain rate which in turn defines the maximum slab length and slope angle allowable to prevent glide-snow avalanche release. The material parameters elasticity  $E_m$ ,  $E_k$  and viscosity  $\eta_m$ ,  $\eta_k$  were kept constant. The model results indicate a strong dependence of maximum slab length and slope angle on the Coulomb friction  $\mu_m$  of the snow on the ground which we were able to quantify by comparing the model results with our observations.

Our field study revealed that glide-snow avalanches release on grass or shrubs and on smooth, stepped or rocky terrain. The release angle and observed slab length depend on vegetation and terrain. We were able to define three roughness categories which have different characteristic vegetation and terrain heights. On the one hand smooth terrain with long grass has the least roughness and the release of avalanches is possible on relatively flat slopes with short slab lengths. On the other hand avalanches release on stepped or rocky terrain with shrubs only if the slope is steep and long. Snow depth plays an important role as vegetation is compressed by the snow's weight and therefore

the friction is lowered significantly. Whereas long grass is compressed with a small load, for shrubs to be pressed together a higher snow cover is needed.

We were able to draw conclusions on the Coulomb friction of the snow–soil interface by comparing the field data with stauchwall model calculations. Assuming stauchwall strength to be the crucial factor for glide-snow avalanche release, we selected data of release areas where the presence of a stauchwall could be expected. We defined approximate friction values  $\mu_m$  for the categories “smooth terrain with long grass” ( $\mu_m = 0.1$ ), “smooth terrain with short grass or shrubs” ( $\mu_m = 0.2$ ) and for “stepped or rocky terrain with shrubs” ( $\mu_m = 0.4$ ). These values represent the minimum Coulomb friction for a wet snow–soil interface that lead to glide-snow avalanche formation. They are slightly lower than the values *Leitinger et al.* [2008] found for abandoned meadows but in the same range as the values *In der Gand and Zupančič* [1966] estimated for wet grass. These values are in good agreement with previous studies and indicate that melt-water is the crucial factor leading to glide-snow avalanches. In contrast the friction values proposed in the Swiss guidelines on artificial avalanche defense structures ( $0.5 \leq \mu_d \leq 0.6$ ) are questionable if we assume snow gliding on wet smooth soil. We expect the friction  $\mu_m$  to depend on terrain, vegetation cover and wetness of the snow–soil interface and therefore covers a wide range of values ( $0.1 \leq \mu_m \leq 1.0$ ).

Guideline values for the distance of technical defense structures are in accordance with the data and the model calculations for low friction ( $\mu_m = 0.1$ ). Our results indicate, that the release of glide-snow avalanches in between defense structures is unlikely. According to the Swiss guidelines the distance between structures depends strongly on the assumed maximum snow depth. A larger snow depth leads to a larger spacing. This is in accordance with our model calculations. However, this conclusion is based on the model assumption that higher snow covers are associated with longer stauchwall lengths. This assumption is supported by the field observations. The important relationship between snow cover height and structure spacing is central to ongoing discussions [*Matsushita et al.*, 2012]. Austrian guidelines do not account for varying snow depths, therefore relatively large distances are recommended for small snow depths [*Austrian Standard Institute*, 2011]. Guidelines on maximum forest gap sizes in Switzerland fit our observations and calculations only if the ground roughness is relatively high. For  $\mu_m \approx 0.4$  the guidelines ensure safety for slope angles below  $35^\circ$ . To prevent avalanche formation on such slopes, we assume that a terrain roughness corresponding with stepped or rocky terrain and dwarf shrubs (e.g. *Vaccinium vaccinium* or *Rodhodendron ferrugineum*) is necessary in addition to the minimal required forest cover characteristic given in existing guidelines. Higher slope angles would even require a higher terrain roughness corresponding to strong lignified shrubs, stumps or piles of dead wood to hinder gliding. To leave logs of dead wood and high stumps in clearings is already often considered as safety measure in silvicultural management [*Frehner et al.*, 2005; *BAFU*, 2008]. This study underlines the importance of these measures, in particular for protective forests with low roughness and little ground vegetation.

## **Acknowledgements**

The authors thank the Austrian Research Center for Forests for organizing the meeting on protection forest and natural hazards in January 2014. We profited from interesting presentations and conversations rich in content on the topic of this work. Professor Kuroschi Thuro, Chair of Engineering Geology at the Technical University Munich supported our work and made it possible. This research was funded by the Bavarian Environment Agency.

### 3. Observations and modeling of the braking effect of forests on small and medium avalanches

Thomas Feistl<sup>[1,2]</sup>, Peter Bebi<sup>[1]</sup>, Michaela Teich<sup>[1,3]</sup>, Yves Bühler<sup>[1]</sup>, Marc Christen<sup>[1]</sup>, Kuroschi Thuro<sup>[2]</sup> and Perry Bartelt<sup>[1]</sup>

<sup>[1]</sup> WSL Institute for Snow and Avalanche Research SLF, Flüelastrasse 11, 7260 Davos Dorf, Switzerland

<sup>[2]</sup> Technical University Munich (TUM), Engineering Geology and Hydrogeology, Arcisstrasse 21, 80333 Munich, Germany

<sup>[3]</sup> Planning of Landscape and Urban Systems PLUS, Swiss Federal Institute of Technology ETH, Wolfgang-Pauli-Strasse 15, 8093 Zurich, Switzerland

## **Abstract**

A long-standing problem in avalanche science is to understand how forests stop avalanches. In this paper we quantify the effect of forests on small and medium avalanches, crucial for road and ski-run safety. We performed field studies of seven avalanches where trees affected the runout. We gathered information concerning the release zone location and dimension, deposition patterns and heights, runout distance and forest structure. In these studies the trees were not destroyed, but acted as rigid obstacles. Wedge-like depositions formed behind (1) individual tree stems, (2) dense tree groups and (3) young trees with low-lying branches. Using the observations as a guide, we developed a one-parameter function to extract momentum corresponding to the stopped mass from the avalanche. The function was implemented in a depth-averaged avalanche dynamics model and used to predict the observed runout distances and mean deposition heights for the seven case studies. The approach differs from existing forest interaction models which modify avalanche friction to account for tree breakage and debris entrainment. Our results underscore the importance of forests in mitigating the danger from small to medium avalanches.

### 3.1 Introduction

The protective capacity of mountain forests has been traditionally quantified assuming that avalanches do not start in dense forest stands [de Quervain, 1978; Gubler and Rychetnik, 1991; Newesely et al., 2000; Gruber and Bartelt, 2007]. Forests act to stabilize the snow cover and prevent destructive avalanches from releasing. They serve as a natural defense against avalanches where meteorological conditions and the terrain enable trees to grow.

The ability of forests to stop avalanches that start above the timberline is limited. Observations show that trees cannot withstand the dynamic forces of large, fast moving avalanches [de Quervain, 1978; Margreth, 2004] (Fig. 3.1). The energy required to break, uproot trees and entrain the woody debris is small in comparison to the overall flow energy of the avalanche [Bartelt and Stöckli, 2001]. The braking effect of forests is small for extreme avalanches. Avalanche experts therefore often neglect forests, assuming extreme large avalanches (that easily destroy the forest), or, that the forest has been removed by previous events [Christen et al., 2010a]. Consequently, avalanche dynamics calculations typically ignore forests completely or prescribe only minor changes to the flow friction [Gruber and Bartelt, 2007].



FIGURE 3.1: Uprooted trees in Val Prada (Switzerland) in winter 2009. The avalanche destroyed the whole forest and does not seem to be stopped or even decelerated by the forest. (Photo: Stefan Margreth)

Modeling how mountain forests stop small to medium avalanches<sup>1</sup> has recently become a critical question in avalanche hazard mitigation [Casteller et al., 2008; Anderson and McClung, 2012]. Frequent (not extreme) avalanches are often the primary hazard for roads, railways and ski-runs, particularly in climates where wet snow avalanches are common [Gruber and Bartelt, 2007]. Local authorities must deal with the risk of small to medium avalanches hitting infrastructure, and therefore people, numerous times during

---

<sup>1</sup>According to the European avalanche classification scale, small avalanches are defined to have less than 1,000 m<sup>3</sup> release volume, medium avalanches are between 1,000 m<sup>3</sup> and 10,000 m<sup>3</sup> in release volume [EAWS, 2013].

a winter season. Forests can stop these avalanches and are an important protective measure [Teich *et al.*, 2012a].

There is subsequently an urgent need in practice to quantify the braking effect of forests on small to medium avalanches [Bebi *et al.*, 2009; Teich and Bebi, 2009; Takeuchi *et al.*, 2011; Teich *et al.*, 2012a]. In this case, trees remain standing after avalanche impact. They withstand dynamic forces and thus work as effective obstacles to decelerate the flow. The effect is similar to avalanche dams [Naaim *et al.*, 2003; Faug *et al.*, 2003; Naaim *et al.*, 2004; Faug *et al.*, 2008, 2010]; however, the working mechanism differs because the forest is not a single, rigid man-made defense structure, but a natural and inhomogeneous array of slender obstacles (trees, tree groups). If the trees are not broken or uprooted, forest structure – stem density, gaps, crown coverage, age and low lying vegetation – is of crucial importance.

Much of the existing forest avalanche data contains material with valuable observational content, especially regarding the effect of different forest structures to hinder avalanche formation [Schneebeli and Meyer-Grass, 1993; Viglietti *et al.*, 2010]. However, information on forest structure and avalanche flow, such as velocity, flow heights and deposition patterns, is limited and has concentrated on the extreme avalanche case [Bartelt and Stöckli, 2001; Casteller *et al.*, 2008; Christen *et al.*, 2010a; Takeuchi *et al.*, 2011]. A first step to model avalanche flow in forests is to understand how forests stop avalanche snow. To this end, we recorded data of six forest avalanches near Davos and within the Bavarian Prealps (Section 3.2) in the winter 2011/12. One more Bavarian case study of the winter 2008/09 completes our data set. In these events, the avalanche paths were partially or completely covered by forest. The focus of this data collection was to document release areas and fracture depths, snow conditions, forest structure, flow perimeter and deposition patterns. The events were special in that we collected data on forests that were *not* destroyed by avalanches. Of particular importance was to quantify the mass deposition behind trees.

Based on the observations, we develop an forest-avalanche interaction function (detrainment function) to be used within the framework of a depth-averaged avalanche dynamics model [Christen *et al.*, 2010b]. Our goal is to simulate the observed events. We assume that the trees stop the granular snow flow by a combination of processes: impact followed by jamming resulting in a sudden and local dissipation of flow energy behind trees or tree groups. We address forest-avalanche interaction by specifying snow detrainment rates instead of using higher friction values to represent the highly non-linear braking effect of trees. The friction approach has been applied by several authors for extreme avalanches within the framework of Voellmy-type models [Völlmy, 1955; Bartelt and Stöckli, 2001; Christen *et al.*, 2010b]. This approach is justifiable for extreme avalanches where the braking effects are small and occur over longer flow distances. For the small avalanche case, Voellmy-type relations represent the avalanche forest interaction poorly [Teich *et al.*, 2012b]. The detrainment function is parameterized by a single coefficient representing forest structure. This coefficient determines the braking power of the forest. Both the friction and detrainment approaches have the same goal: to explain the deceleration and quantify the amount of mass stopped by the forest. The detrainment approach, however, is more direct in the sense that we extract mass from the avalanche

volume, removing momentum directly from the flow, rather than indirectly by friction coefficients. Furthermore, it is easier to calibrate as the detrainment function provides users with the total mass per unit area stopped in the forest. Therefore we are able to compare calculated deposition volumes with observations and measurements of the seven case studies and to demonstrate the potential and limitations of the detrainment approach.

## 3.2 Observations

### 3.2.1 Documented avalanches

Field campaigns in the Swiss and German Alps were performed to investigate how avalanche mass is stopped by forests. The stopped mass can be estimated by calculating the difference between the volume of the initial release area and the deposition zone and by determining the volume of deposited snow behind trees. As we assume forest structure to have a crucial impact on the mass balance and the runout distance we also gathered information on stem density and vegetation cover. Although single small trees and low branches were sometimes destroyed when hit by the avalanches, we focused on small to medium avalanches flowing through the forest where the trees acted as obstacles. This was the main selection criteria for the observation of an event. Such events are rarely documented by forest managers. Field studies have to be conducted before changing weather conditions (snowfall or melting) affect the deposits. Spotting such avalanches and reaching the tracks on time, if at all accessible, is generally challenging.

In the winters 2008/9 and 2011/12 data on seven avalanche events was collected: five in the region of Davos, Switzerland (ID-I to ID-V); two in the region of Spitzingsee, Germany (ID-VI and ID-VII). The observed avalanche sites cover a wide range of terrain, snow and forest characteristics (Table 3.1), with altitude levels ranging between 1,000 m a.s.l. (runout, Hagenberg, ID-VII) and 2,100 m a.s.l. (release area, Dischma, ID-IV). The differences in altitude from release to runout vary from 50 m (Junkerboden, ID-I) to 450 m (Dischma, ID-IV). The smallest release volume was calculated to be approximately 320 m<sup>3</sup> (Junkerboden, ID-I), whereas the largest release area covers approximately 7,400 m<sup>2</sup> with a release volume of 5,190 m<sup>3</sup> (Monstein, ID-V). Different terrain features in the avalanche track, such as gullies and flat slopes, could be distinguished. Slope angles vary from 50° steep release areas to flat runout zones. As the avalanche deposits could generally not be reached on time, we classified snow characteristics according to qualitative criteria such as dry, moist and wet, based on meteorological data from the nearest weather station. The meteorological conditions prior to the events and therefore the causes of the avalanches differed, resulting in wet snow avalanches (for example, Filisur, ID-I) as well as dry snow avalanches (for example, Brecherspitz, ID-VII). Forests penetrated by the avalanches we studied consist mainly of conifers with varying stand densities and age. For modeling we distinguished between a canopy density of > 50% for dense forests and < 50% for open forests. Canopy density was identified by analysing ortho-images (from 2011 with 25 cm grid resolution) of each event [Bebi *et al.*, 2001].

TABLE 3.1: Characteristics of forest avalanches documented during the winters 2008/2009 and 2011/2012

Internal ID	Switzerland				Germany		
	Junkerboden	Filisur south	Filisur north	Dischma	Monstein	Hagenberg	Brecherspitz
Date	1 Jan. 2012	~23 Feb. 2012	~23 Feb. 2012	~27 Feb. 2012	1 Mar. 2012	24 Feb. 2009	14 Feb. 2012
Temperature (dry, moist, wet)	moist	wet	wet	wet	wet	dry	dry
Terrain features (upper part/ track/ runout)	unchanneled/ unchanneled/ flat	channeled/ unchanneled/ unchanneled	channeled/ unchanneled/ unchanneled	unchanneled/ channeled/ unchanneled	channeled/ unchanneled/ unchanneled	channeled/ unchanneled/ unchanneled	unchanneled/ unchanneled/ unchanneled
Forest structure (upper part/ track/ runout)	dense/ open/ no forest	no forest/ open/ dense	no forest/ open/ dense	open/ no forest/ dense	open/ no forest/ dense	open/dense/ dense	open/dense/ dense
Tree age	mixed	mixed	mixed	mixed	mixed	mixed	mixed
GPS measurements of deposits	✓	✓	✓	✓	✓	X	✓
GPS measurements of release area	✓	X	X	✓	X	X	✓
Image of release	✓	X	X	✓	✓	✓	✓
Altitude [m a.s.l.]	1540-1500	1320-1080	1360-1058	2093-1642	2070-1640	1419-1027	1472-1327
Slope angle, release to runout [°]	39-0	50-25	50-20	42-15	50-10	50-25	45-23
Release volume [m <sup>3</sup> ]	320	1080	1390	3690	5190	3460	690

To document the exact shapes of the release and deposition areas was essential and allowed the comparison with simulation results (Section 3.3). We used a hand-held differential Global Navigation Satellite System (dGNSS) device whenever possible such that we could map the runout areas precisely. For safety reasons or lack of accessibility the release area could not always be reached. For these cases we used images of the release area from the opposite slope or from a helicopter and matched these with maps of the area. For the two events near Filisur, Switzerland, we performed a terrain analysis with a spatial resolution of 2 m. Terrain features such as gullies, ridges and slope angle were taken into account to identify probable release areas. The GIS analysis is only accurate up to a scale of several meters whereas the error of measurements with the dGNSS device is in the range of a few centimeters.

We collected information about the deposition patterns of avalanche snow within the forest which allowed us to quantify the stopped mass. Photographs were taken which document the significant amount of avalanche snow that remained behind the trees. Not only do tree trunks stop considerable amounts of avalanche snow but also root plates of upturned trees, low-lying branches and dead woody debris. Depositions in forests were mainly concentrated at the outer edges of the avalanche tracks where the flow velocities were small (see Fig. 3.2). We observed differences in deposited snow amounts due to slope angle, snow temperature (wet, moist or dry), stand density and age of trees (see Section 3.2.2).

### 3.2.2 Deposition volume behind trees

In all the case studies (ID-I to ID-VII) we observed wedge-like depositions behind single trees as well as tree groups (Fig. 3.3). Wedge shaped depositions have been observed behind obstacles in chute experiments with granular materials [Gray *et al.*, 2003]. Deposition wedges have also been observed behind pressure measurement pylons at the Swiss



FIGURE 3.2: Avalanche track near Filisur, Switzerland (ID-III). Note the main avalanche channel in the foreground with little snow on the ground in comparison to the dense forest in the background.

Vallée de la Sionne [Sovilla *et al.*, 2010] and Italian Seehore [Bovet *et al.*, 2011] avalanche test sites. Although the deposition wedges had different dimensions, depending on the snow properties and tree stand characteristics, a general geometry could be determined (Fig. 3.3). Typically the upper and lower width of the wedge at the base (ground),  $d_u$  and  $d_l$  are the same,  $d_u = d_l = d_w$ . The base width  $d_w$  is determined by the base width of the obstacle: (1) the stem diameter (Fig. 3.3a), or (2) the total width of a dense group of trees (Fig. 3.3b). Small trees with low-lying branches have base widths much greater than the stem diameter (Fig. 3.3c) because additional snow can be stopped by the branches. For single tree impacts, the width of the upper wedge surface at the tree was sometimes smaller than the stem diameter, resulting in a pyramid shaped wedge (Fig. 3.3 a). The angle  $\delta$  defines the top wedge angle of the pyramid (Fig. 3.3a). In general, the exterior side planes were parallel to the primary flow direction of the avalanche: the planes are nearly vertical, especially close to the tree. For large stem diameters, the trees' sides are often rubbed clean of snow, indicating snow is stopped behind the tree, while the avalanche continues to move forward. This suggests that strong velocity gradients can develop when the avalanche flows within the forest. Shear planes, similar to those found in levee formation in runout zones [Bartelt *et al.*, 2012c], were observed in the case studies ID-II, ID-III and ID-V (Fig. 3.2). For most cases, the upper surface of the wedges was close to horizontal; that is, the angle  $\gamma$  was equal to the slope angle of the terrain (Fig. 3.3a). The wedges were sometimes tilted towards the slope, especially if the snow was wet (Fig. 3.3b,c). Settling and melting affected the depositions until we reached the tracks.

The observations allow us to quantify the volume  $W$  of snow captured behind one tree or group of trees. The wedge volume for the single stem case (Fig. 3.3 a) is

$$W = \frac{d^3}{12 \tan(\gamma) \tan^2\left(\frac{\delta}{2}\right)}, \quad (3.1)$$

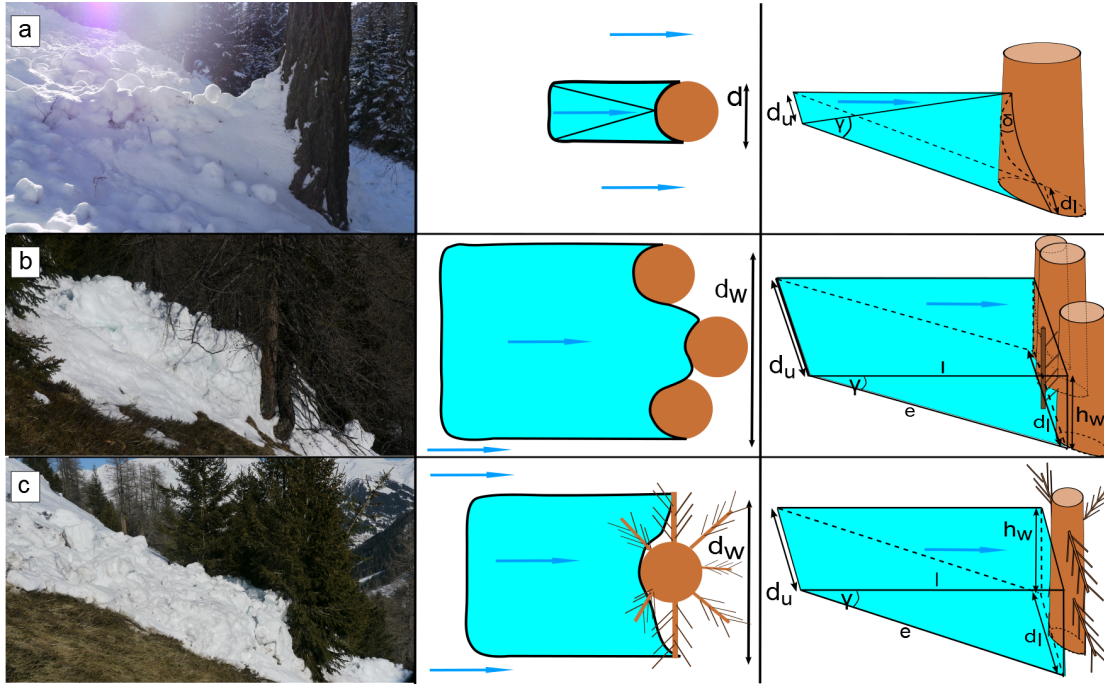


FIGURE 3.3: Typical deposition structure of avalanche snow behind trees. The second column depicts the deposition pattern from above; in the third column the approximated deposition volume is illustrated. (a) shows deposited snow behind a single trunk of approximately 100 cm diameter in relatively flat terrain ( $20^\circ$ ), whereas (b) shows deposited snow behind a group of trees. (c) depicts deposited snow behind a small tree (appr. 4 m high) in steep terrain ( $34^\circ$ ). Note the effect of branches close to the ground.

TABLE 3.2: Observed wedge dimensions and calculated volumes of the depositions in Fig. 3.3. Cases b and c catch more mass.

Observation	Slope angle $[\circ]$	Base width $d_w$ [m]	Wedge height $h_w$ [m]	Top wedge angle $\delta$ $[\circ]$	Volume $W$ [ $m^3$ ]
a	23	1	0.8	68	0.43
b	33	4	2	–	12.3
c	34	2	2	–	5.9

and for the tree group case (Fig. 3.3 b)

$$W = \frac{dh_w l}{2} = \frac{dh_w^2}{2 \tan \gamma}, \quad (3.2)$$

where  $h_w$  is the wedge height.

The latter equation can also be used for the single tree with low lying branches (Fig. 3.3 c). We provide calculated volumes of the wedges depicted in Fig. 3.3. The dimensions of the wedges are provided in Table 3.2. Note that for case b (tree groups) and c (low lying branches) the detained volumes are much larger than the single tree case.

The volume Eqs. 3.1 and 3.2 allow us to derive a first approximation of the mean deposition height  $h_d$  for different stem densities (Fig. 3.4). The mean deposition height  $h_d$  depends strongly on the deposition widths and therefore on the forest structure (Table

TABLE 3.3: Deposited snow and corresponding mean deposition height  $h_d$  for angle  $\gamma = 30^\circ$  (approximately equal to slope angle of the terrain), deposition height  $h_d = 2m$ , top wedge angle  $\delta = 60^\circ$ , tree diameter  $d = 1$  m for single tree,  $d_w = 2$  m for tree with branches reaching to the ground, and  $d_w = 4$  m for group of three trees. For single trees we used Eq. 3.1 to calculate the volume and for trees with branches and groups of trees Eq. 3.2. We assume a snow density of  $\rho = 300$  kg/m<sup>3</sup>, an avalanche length of 50 m and a velocity of 10 m/s to calculate  $K$  according to Eq. 3.14, Section 3.3.2.2.

Forest structure	Stem density	Deposition volume [m <sup>3</sup> ]	$h_d$ [m]	K-value [Pa]
Single trees	400 / ha	173	0.02	10
Group of trees	400 / ha	1842	0.18	110
Trees with branches	400 / ha	2771	0.28	166
Single trees	200 / ha	87	0.01	5
Group of trees	200 / ha	921	0.09	55
Trees with branches	200 / ha	1386	0.14	83

3.3). Assuming a dense forest (400 trees per hectare), with average stem diameters of  $d = 1$  m (for simplicity) on a slope of  $30^\circ$  with a top wedge angle of  $\delta = 60^\circ$  (from measurements), we find a rather small *mean* deposition height: only 2 cm averaged over the entire forest area struck by the avalanche. We emphasize that the stem diameter is measured at the ground, according to our observations. The snow that can be stopped by the forest can increase by over a factor 10 when wide, wedge shaped deposits are created behind groups of trees. For example, when  $d_w = 4$  m for a forest with the same stem density but trees grouped together, then the mean deposition height is 18 cm. Here, we assume that a tree group contains three trees (Fig. 3.3 b). This result reveals the importance not only of the stem diameter, but also the forest structure.

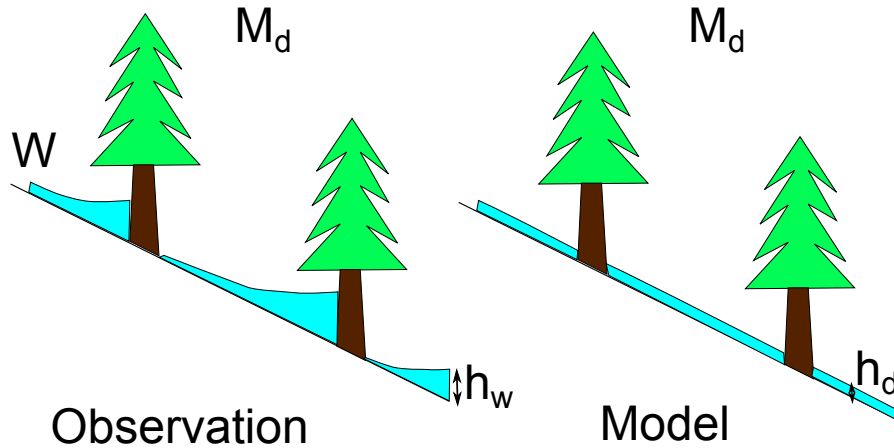


FIGURE 3.4: The goal of the forest model is to calculate the mean deposition height  $h_d$ . Wedge formation behind isolated tree stands are not predicted. The total deposited mass  $M_d$  should, however, be equal.  $W$  is the volume of snow captured behind a single tree or tree group.

Generally, we assume mean deposition heights of a few centimeters to half a meter as reasonable amounts of snow being stopped by forests,  $1 \text{ cm} < h_d < 50 \text{ cm}$ .

### 3.3 Modeling

#### 3.3.1 Avalanche modeling

We applied the numerical avalanche dynamics program **RAMMS** to simulate the observed avalanche events and to perform simulations on an ideal parabolic shaped avalanche track [Christen *et al.*, 2010b]. We describe the mountain profile in a horizontal  $X$  and  $Y$  coordinate system. The elevation of the mountain profile  $Z(X, Y)$  is defined for each coordinate pair  $(X, Y)$ . The geographic coordinates are used to construct a local surface-based coordinate system  $(x, y, z)$ . The unknown field variables are the avalanche flow height  $h(x, y, t)$  and the mean, avalanche velocities  $U(x, y, t)$  and  $V(x, y, t)$  in the  $x$  and  $y$  directions,  $\mathbf{V} = (U, V)^T$  (see Fig. 3.5). Avalanche flow is modeled using depth-averaged mass and momentum balance equations [Christen *et al.*, 2010b]:

$$\frac{\partial h}{\partial t} + (\mathbf{V} \cdot \nabla)h = \dot{Q} \quad (3.3)$$

$$\frac{\partial(h\mathbf{V})}{\partial t} + (\mathbf{V} \cdot \nabla)(h\mathbf{V}) = \mathbf{G} - \mathbf{S} - \frac{1}{2}\nabla(g_z h^2). \quad (3.4)$$

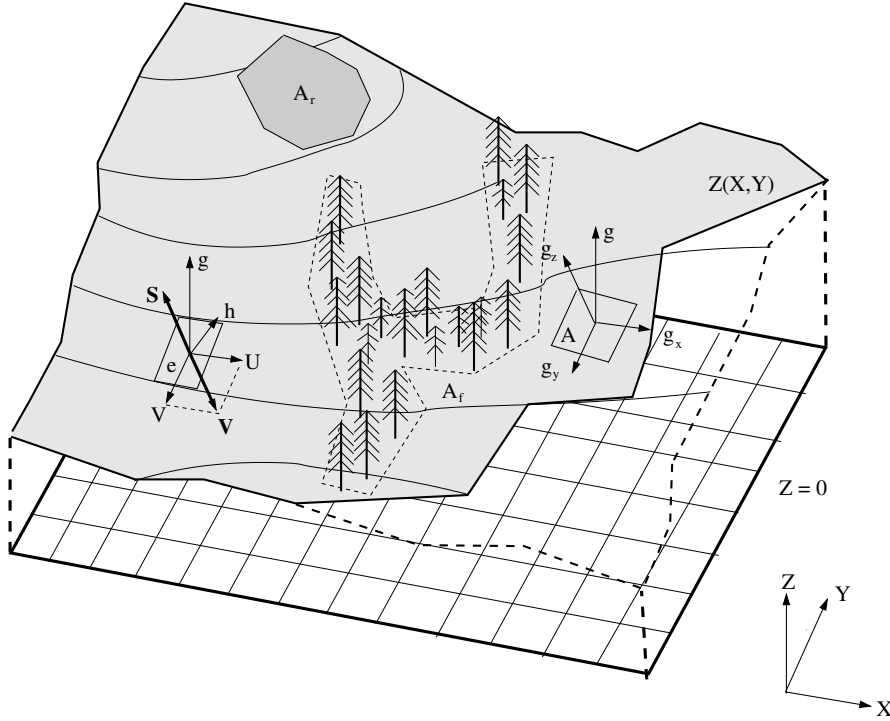


FIGURE 3.5: The model domain and definition of primary variables:  $A_r$  is the release area and  $A_f$  the forest area.  $U$  and  $V$  are the velocities in  $x$  and  $y$  direction respectively. The gravitational acceleration in  $x$ ,  $y$  and  $z$  direction is denoted by  $g_x$ ,  $g_y$  and  $g_z$ .  $\mathbf{S}$  stands for the resistance acting in the opposite direction than the velocity  $\mathbf{V}$ .

The force components associated with the gravitational acceleration  $g$  in the  $x$  and  $y$  directions are denoted  $\mathbf{G}=(G_x, G_y)^T$  and given by:

$$G_x = g_x h \quad \text{and} \quad G_y = g_y h. \quad (3.5)$$

with

$$g = g_x \mathbf{i} + g_y \mathbf{j} + g_z \mathbf{k}. \quad (3.6)$$

The corresponding resistance in the  $x$  and  $y$  directions is denoted  $S_x$  and  $S_y$ ,  $\mathbf{S} = (S_x, S_y)^T$ .

The field variables are a function of time  $t$  and thus we solve the equations from avalanche release ( $t = 0$ ) to avalanche deposition.

Let  $A_r(x, y)$  be the location of the avalanche release zone; this can be a forest opening, or, a region located above the timberline. The region  $A_f$  defines the forest. There can be multiple forest areas  $A_f$  (see Fig. 3.5). Mass uptake from the snow cover and snow detrainment from the avalanche (stopped mass) is specified by the volumetric mass flux  $\dot{Q}(x, y, t)$  defined per unit area. However, as we assume no mass uptake in forested areas, we did not account for entrainment in this study. We therefore define  $\dot{Q} = -\dot{h}_d$  as the detrainment rate. This provides the mean deposition height  $h_d$  of stopped snow mass in the forested area  $A_f$ .

An additional depth-averaged energy equation accounting for the kinetic energy  $R(x, y, t)$  associated with particle velocity fluctuations is included in the **RAMMS** model [Bartelt *et al.*, 2012a]:

$$\frac{\partial(hR)}{\partial t} + \mathbf{V} \cdot \nabla(hR) = \alpha(\mathbf{S} \cdot \mathbf{V}) - \beta(hR). \quad (3.7)$$

The parameter  $\alpha$  controls the production of random fluctuation energy  $R$  from the frictional work rate of the mean flow  $\dot{W}_f = \mathbf{S} \cdot \mathbf{V}$ . Therefore, for  $\alpha > 0$ , we have more collisional, disperse flows;  $\alpha S$  corresponds to the granular stresses caused by the fluctuating motion of particles that is not transformed into heat, which could be considered as a turbulent Reynolds stress by analogy with conventional fluids. The parameter  $\beta$  determines the dissipation of fluctuation energy by different mechanisms (collisions, plastic deformations, abrasion, fragmentation). The inclusion of the random kinetic energy in the model formulation is helpful when calculating the distribution of cold, dry avalanche deposits in the runout zone as well as the motion of small avalanches, which can stop on steep slopes [Bartelt *et al.*, 2012a].

We use the well-known Voellmy Ansatz [Völlmy, 1955; Salm, 1993] to model flow resistance. The Voellmy approach splits the total basal friction into a velocity independent dry-Coulomb term, which is proportional to the normal stress (friction coefficient  $\mu$ ) and a velocity dependent "viscous" or "turbulent" friction (friction coefficient  $\xi$ ).

$$S_x = \frac{U}{\|\mathbf{V}\|} \left[ \mu(R) g'_z h + \frac{g \|\mathbf{V}\|^2}{\xi(R)} \right] \quad (3.8)$$

and

$$S_y = \frac{V}{\|\mathbf{V}\|} \left[ \mu(R)g'_z h + \frac{g\|\mathbf{V}\|^2}{\xi(R)} \right]. \quad (3.9)$$

However, the constitutive parameters  $\mu$  and  $\xi$  are functions of the mean fluctuation energy  $Rh$  [ $\text{J m}^{-2}$ ] [Bartelt et al., 2012a]:

We use

$$\mu = \mu_0 \exp\left(-\frac{Rh}{R_0}\right) \quad (3.10)$$

$$\xi = \xi_0 \exp\left(\frac{Rh}{R_0}\right) \quad (3.11)$$

where  $R_0$  is the activation energy per unit area [ $\text{J m}^{-2}$ ] controlling the onset of the fluidized regime [Bartelt et al., 2012a]. The activation energy depends on the avalanche size (more activation energy is required to overcome the overburden pressures of thick dense avalanche cores) and cohesive properties of the flowing snow (more energy is required to break the bonds of cohesive snow). An estimate for the activation energy  $R_0$  is the sum of the mean overburden pressure and the cohesion. The parameter  $\mu_0$  is the static Coulomb friction parameter and  $\xi_0$  the speed dependent friction parameter before fluidization. When  $\alpha = 0$ , we have the standard Voellmy-Salm model (VS-model) with constant friction parameters  $\mu$  and  $\xi$ . For more information concerning the numerical implementation, see Christen et al. [2010b] and for the role of fluctuations in avalanche flow, see [Bartelt et al., 2012a].

### 3.3.2 Modeling avalanche flow in forests

The region  $A_f(x, y)$  defines the location of the forest in the model domain. The elements in this domain are assigned forest properties, depending on forest density, age and undergrowth. It is not possible to calculate each wedge-shaped deposition pattern behind individual trees or tree stands as we assume average forest values per computational element (e.g. tree density) (Fig. 3.6). Therefore, no information is needed on the position of individual trees. The forest model simulates the mean deposition height  $h_d$ , which, when multiplied with the element area, should accurately represent the total deposited volume observed at that location in the case studies (Fig. 3.4). Isolated trees are not considered to be part of  $A_f$  when they stop too little snow to have an effect on the overall flow behaviour of the avalanche.

In general, there are two possible ways to model the braking effect of forests: (1) the friction approach or (2) the detrainment approach (Fig. 3.7).

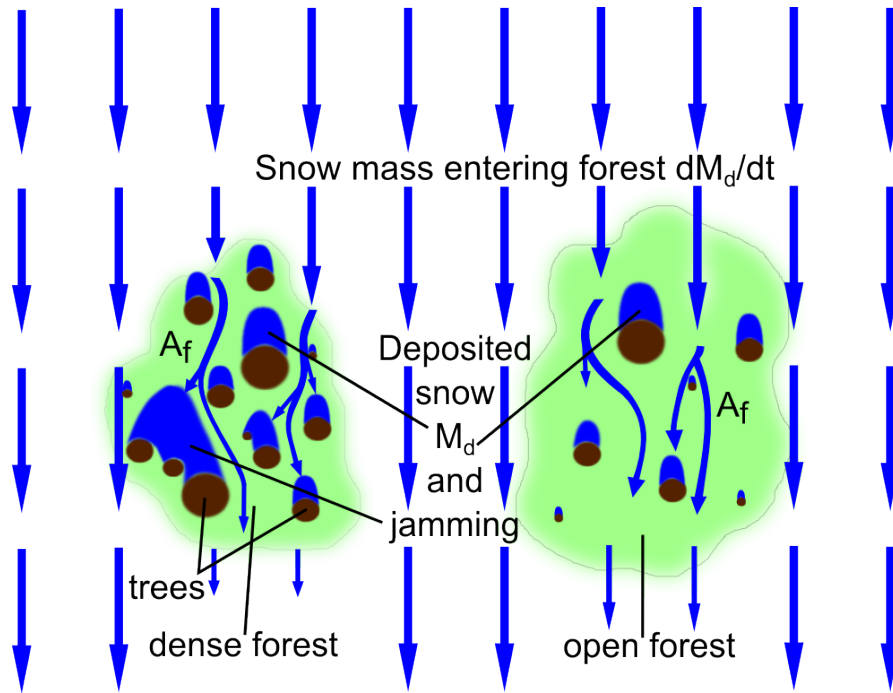


FIGURE 3.6: Schematic illustration of the mass flux before and after the interaction with forest with different densities. Snow gets deposited behind trees, most effectively if groups of trees enable jamming. Higher  $K$  values are applied for the denser forest.

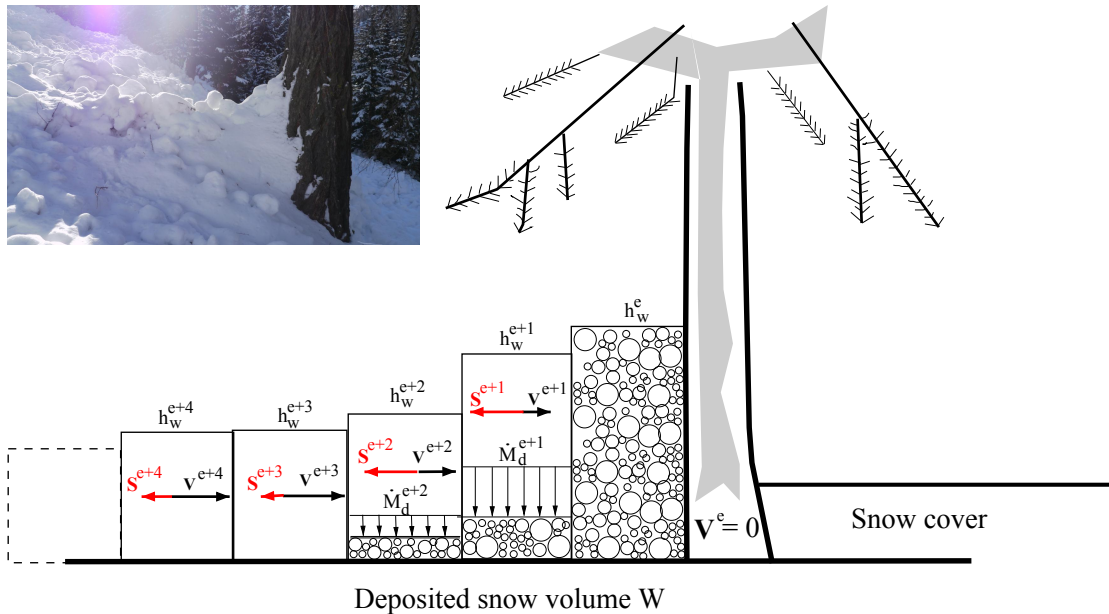


FIGURE 3.7: Two approaches can be used to model tree interaction with avalanches. The friction approach attempts to find values for  $S$  to stop the mass; the detrainment approach determines  $M_d$  and extracts the corresponding momentum from the flow.

### 3.3.2.1 Friction approach

In the friction approach, modified friction parameters  $(\mu_f, \xi_f)$  are assigned to the forest domain  $A_f$  to model the enhanced braking effect. For example, in the current version of **RAMMS** the coefficient  $\xi_f$  is assumed to be  $\xi_f = 400 \text{ m/s}^2$ , significantly smaller than the open terrain value of  $\xi = 2,000 \text{ m/s}^2$ ; the coefficient  $\mu$  is only slightly increased [Gruber and Bartelt, 2007]. These values are based on energy arguments in which different failure modes (tree overturning, trunk fracture, entrainment of woody debris) extract flow energy from the avalanche [Bartelt and Stöckli, 2001]. The fundamental assumption in this approach is that the avalanche is both large and fast enough to induce tree failure. This approach is presently employed to model all avalanche flows in forest, independent of the avalanche size. The modified  $\mu$  and  $\xi$  values are based on mechanical processes such as tree overturning or trunk fracturing. As we assume that the trees do not break, the friction parameters  $(\mu_f, \xi_f)$  should be related to non-destructive processes such as jamming.

### 3.3.2.2 Detrainment approach

Extracting mass that gets caught behind tree stands from the avalanche is an alternative approach to modeling forest-avalanche interaction. We term this method the detrainment approach, as we postulate that when mass is stopped behind dense tree stands, it is instantly subtracted from the flow. The stopping is sudden and caused primarily by material jamming which is initiated behind dense group structures of trees. The momentum of the stopped mass is removed from the total momentum of the avalanche flow (Fig. 3.7), see also Naaim *et al.* [2004] and Faug *et al.* [2004]. We assume that the trees do not break and act like obstacles causing mass to stop (Fig. 3.3). This process is difficult to model with Voellmy type parameters, because the friction coefficients, especially  $\xi$ , are designed for avalanche flow in open terrain where the dissipative processes are slow and continual: they are not designed to model tree impact. Instead of attempting to define friction values that slow the avalanche down, and therefore allow the avalanche to naturally detrain material [Naaim *et al.*, 2003], we impose a stress  $K$  [Pa] which instantly detrains mass from the flow. This stress must be in balance with the change in momentum associated with the detrained mass per unit area  $M_d$ :

$$\frac{dM_d}{dt} \|\mathbf{V}\| = -K \quad (3.12)$$

where  $\|\mathbf{V}\|$  is the depth-averaged velocity of the avalanche. We emphasize that the mass  $M_d$  is the average mass per unit area, which might differ from the height of the deposits at the tree. The stress  $K$  [Pa] is related to the forest structure and density, but also to properties of the flowing snow. Therefore,

$$\frac{dM_d}{dt} = -\frac{K}{\|\mathbf{V}\|}, \quad (3.13)$$

or, in terms of the mean deposition height

$$\rho \frac{dh_d}{dt} = \frac{K}{\|\mathbf{V}\|}, \quad (3.14)$$

where  $\rho$  is the flow density of the avalanche. The parameter  $K$  is related to non-destructive processes such as granular jamming behind tree stands. This assumption is only valid for small and medium avalanches.

## 3.4 Results

### 3.4.1 Numerical experiment

To begin our analysis, we first carried out a numerical experiment to explore the differences between the friction and detrainment approaches. The numerical experiment enabled us to perform multiple simulations with equal initial conditions and varying forest characterizations. We constructed an ideal, parabolic shaped avalanche track in order to avoid complex terrain features (Fig. 3.8). The average altitude difference between release area and runout is 380 m. The parabola is characterized by a 300 meter long runout area. In the width the parabola is flat and therefore the flow is unchanneled. We simulated avalanches with variable starting volumes and  $\alpha = 0$  (standard Voellmy model). We computed the movement of the avalanche with forest ( $A_f \neq 0$ ) and without forest ( $A_f = 0$ ). We specified a calculation grid size of 1 m.

The release area, fracture depth, snow density and the two friction parameters  $\mu = \mu_0$  and  $\xi = \xi_0$  had to be defined. To test the influence of forests on avalanches with different sizes we specified three release volumes, all with different release areas, but a constant fracture depth of 1 m for all three cases. The resulting release volumes  $\mathcal{V}_0$  were approximately 1,000 m<sup>3</sup>, 5,000 m<sup>3</sup> and 20,000 m<sup>3</sup>. The flowing snow density was set to  $\rho = 300$  kg/m<sup>3</sup>. We kept the friction parameters, except for simulations with the friction parameter approach, constant:  $\mu = 0.26$  and  $\xi = 2,000$  m/s<sup>2</sup>. These parameters are valid for frequent avalanches (10 year return period) with release volumes between 5,000 and 25,000 m<sup>3</sup> in unchanneled terrain above 1,500 m a.s.l., according to the recommended guideline values [*Buser and Frutiger, 1980; Salm et al., 1990*].

In our numerical experiment, the forest area covered the whole avalanche path below the release area (Fig. 3.8). At first we applied the friction approach and employed the  $\mu$  and  $\xi$  values that are used in the current **RAMMS** version (adding  $\Delta\mu = 0.02$  to the basic  $\mu$  value and setting  $\xi = 400$  m/s<sup>2</sup>), independent of the forest structure [*Gruber and Bartelt, 2007*]. Recall that these values are derived for extreme avalanches that destroy the forest. Next we applied the detrainment approach with five different values for parameter  $K$ : 10 Pa, 20 Pa, 50 Pa, 100 Pa and 200 Pa. These are reasonable values and are comparable to the calculated  $K$ -values of the case studies (Table 3.3): a  $K$  value of 10 Pa corresponds to an open forest, whereas a  $K$  value of 200 Pa corresponds to a dense forest with tree clusters and low-lying vegetation. As a control, we simulated the avalanches without

any forest cover. For these simulations and the detrainment simulations we specified the guideline friction parameters ( $\mu = 0.26$  and  $\xi = 2,000 \text{ m/s}^2$ ) for frequent avalanches.

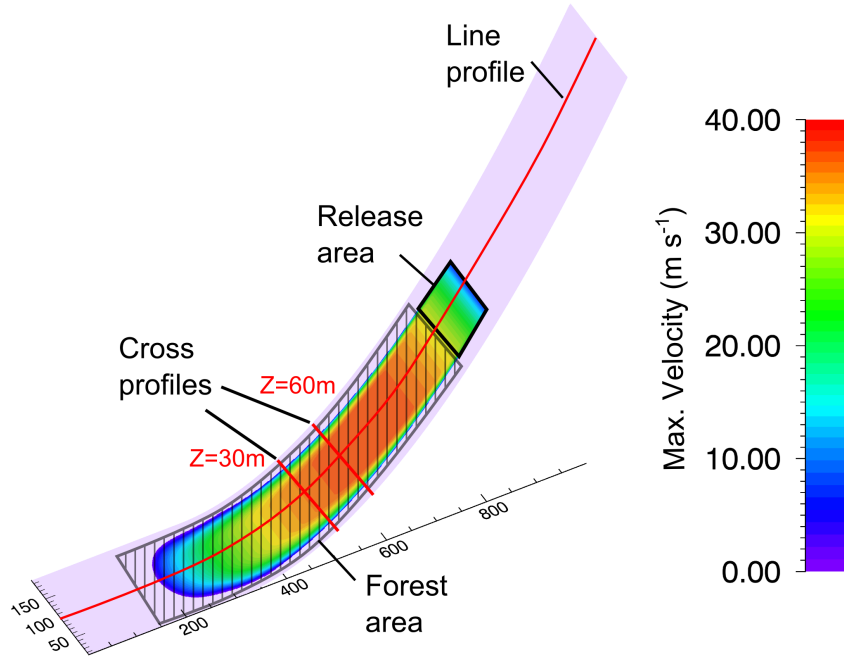


FIGURE 3.8: Simulation of avalanche on parabolic shaped avalanche track. The figure shows the maximum calculated velocity for a release volume of  $20,000 \text{ m}^3$ .

Profiles of deposition height, velocity and momentum along longitudinal and transverse sections of the avalanche track were analyzed in order to explore differences in runout length, deposition patterns, velocity distribution and the development of the total momentum of the model avalanches. Although both approaches (friction and detrainment) have the same goal to stop flowing mass, our findings reveal crucial differences.

Runout shortening was observed in the forest case for both the friction and detrainment approaches in comparison to the simulations without forest (see Fig. 3.9). We display the maximum flow height along the avalanche path for the three different flow volumes. The distance ( $x$ -axis of the plots) is measured from the starting zone ( $x = 0$ ). Simulation results of the (1) detrainment approach for different  $K$  values between  $K=10 \text{ Pa}$  (K10) and  $K=200 \text{ Pa}$  (K200) (2) the friction approach ( $\mu, \xi$  approach) and (3) results of simulations without forest are shown in the graph (Fig. 3.9). The numerical results reveal that the runout of small avalanches ( $1,000 \text{ m}^3$ , Fig. 3.9c) is barely influenced by changing the friction parameters. Conversely the detrainment approach leads to a significant runout shortening, dependent on the magnitude of the parameter  $K$ . The runout of larger avalanches ( $20,000 \text{ m}^3$ , Fig. 3.9a) is not significantly shortened when applying the detrainment approach, in contrast to the friction approach. This finding suggests that the immediate stopping and removal of flow mass because of trees has a greater influence on small avalanches than on larger avalanches.

Fig. 3.10 depicts different deposition patterns on the avalanche track with the  $\mathcal{V}_0 = 20,000 \text{ m}^3$  release volume. Most of the avalanche mass reached the flat part of the

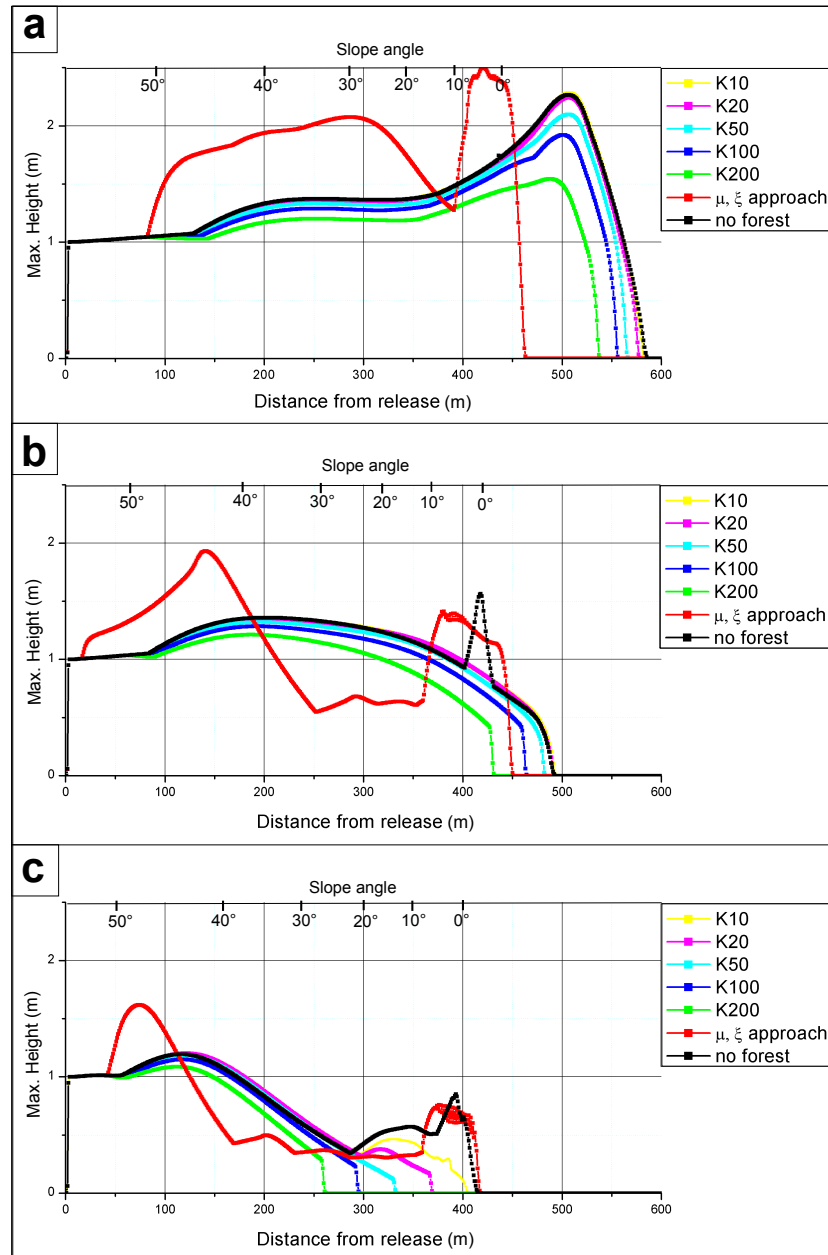


FIGURE 3.9: Profiles of max-flow-height for simulations of avalanches with different release volumes (approx. 20,000 m<sup>3</sup>, Fig. (a); approx. 5,000 m<sup>3</sup>, Fig. (b); approx. 1,000 m<sup>3</sup>, Fig. (c)). The simulations were conducted with the VS-model of **RAMMS** on a parabolic slope using both the friction and detrainment approaches. Five different values for the detrainment coefficient  $K$  [Pa] were tested ( $K10$ ,  $K20$ ,  $K50$ ,  $K100$ ,  $K200$ ). Note the significant runout shortening for smaller avalanches with the detrainment approach in contrast to the runout shortening for larger avalanches with the friction approach. The spikes in height in 400 m slope distance from release when simulating without forest and the friction approach with 5,000 m<sup>3</sup> and 1,000 m<sup>3</sup> originate from the pile up of snow at the transition of sloped and flat (0°) terrain. This spike is missing when applying the detrainment approach because of snow being already deposited on the track.

avalanche track when using either the friction approach or the detrainment approach. The results are similar for the case with no forest area. We investigated deposition heights at profile elevations  $Z = 30$  m and  $Z = 60$  m above zero (Fig. 3.8). At these altitude levels the slope angle of the track is  $27^\circ$  and  $36^\circ$ , respectively. Generally higher deposition heights were observed when applying the detrainment approach than for simulations with the friction approach. In fact, the friction approach even resulted in smaller deposition heights than for simulations without forest (because of the longer simulation times). Note the steep increase of the deposition heights at the edges of the avalanche when applying the detrainment approach, indicating that more mass is being deposited at the slower moving sides of the avalanche, as observed in the field studies. The removal of snow at the slow moving avalanche edges results in a narrower track width, especially at lower elevations.

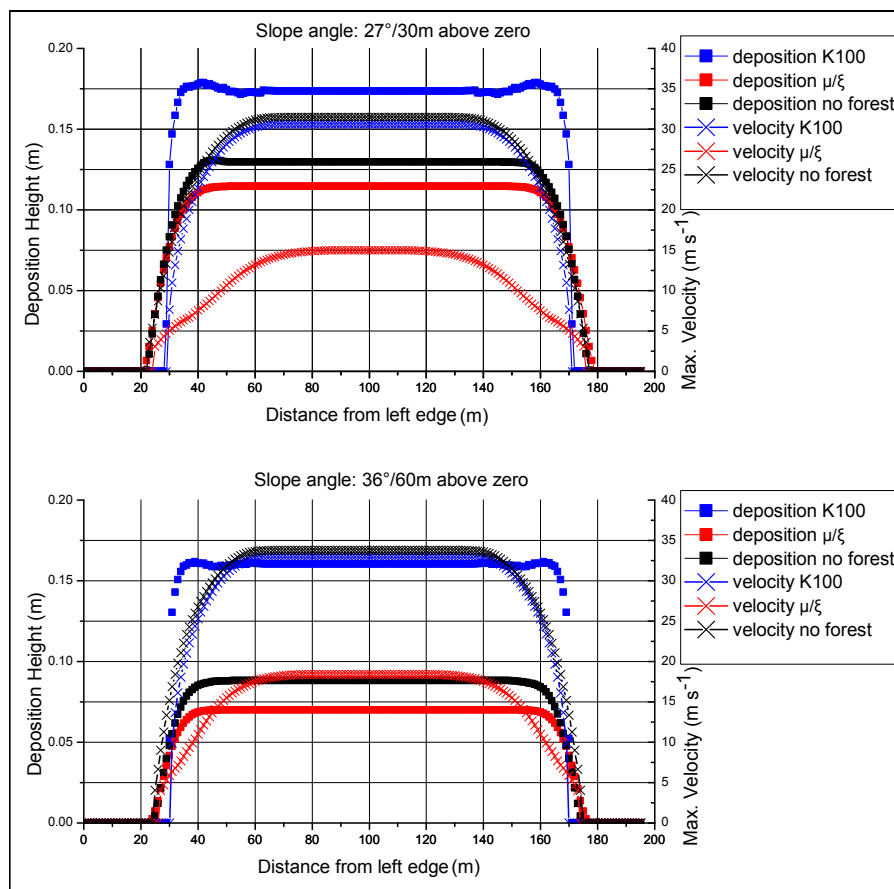


FIGURE 3.10: Cross section of the deposition heights of avalanches with friction and detrainment approach on the parabola experiment. The release volume was approximately  $\mathcal{V}_0 = 20,000$  m<sup>3</sup>; profiles are taken 30 m and 60 m above zero. Note the slow, continual increase of the deposition heights at the avalanche edges when using the friction approach in comparison to the detrainment approach. The detrainment removes mass faster at the edges, leading to smaller avalanche flow widths at lower elevations.

This agrees with the field observations.

The development of the total momentum of the avalanche over time is illustrated in Fig. 3.11. For all approaches (friction, detrainment and no forest) we observe an increase in momentum until the avalanche reaches the forest; that is, the avalanches are accelerating. After penetrating into the forest the momentum decreases. With

the friction approach the decrease of momentum starts earlier (4 s) in comparison to the detrainment approach (6-7 s) or without forest on the avalanche track (7 s). The momentum of all avalanches will decrease because the avalanche track is flattening. Although the highest decrease in momentum is reached only after 5s with the friction approach, the detrainment approach is more effective at lower slope angles. Furthermore, more mass is removed at the tail and the avalanche edges where the velocities are small. Thus, although the maximum decrease in momentum is reached later (10-11 s) with the detrainment approach, more mass is stopped. From 7 s onwards, the decrease in momentum is higher with the detrainment approach, leading to an earlier stopping of the avalanche. The detrainment approach exploits the velocity distribution between the head and tail (and sides) of the avalanche.

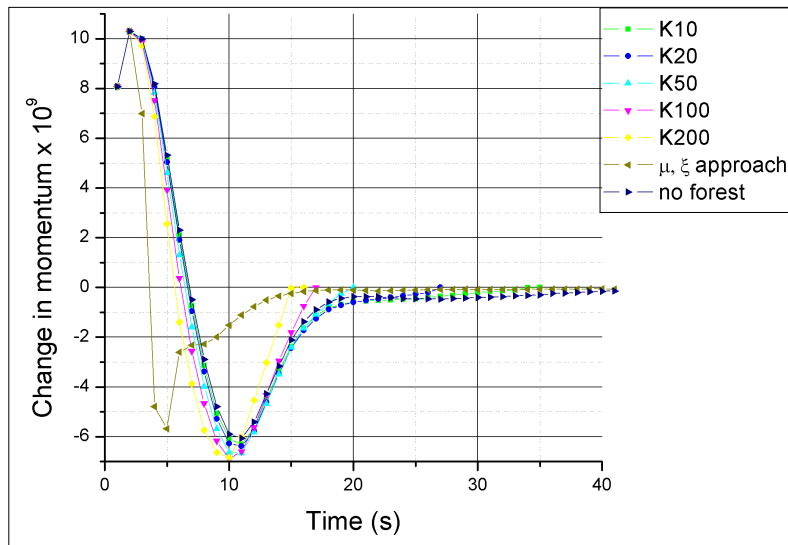


FIGURE 3.11: Development of the total momentum in time of a small avalanche (approximately  $\mathcal{V}_0 = 1,000 \text{ m}^3$ ). The plot depicts the change in momentum illustrating the braking process. Detrainment (K10, K20, K50, K100, K200) and friction approach ( $\mu, \xi$  approach) are compared to the case without forest (no forest).

### 3.4.2 Simulations of documented avalanches with $\alpha = 0$

We back-calculated the seven forest avalanche events described in Section 3.2 with the VS-version ( $\alpha = 0$ ). As in the numerical experiment, the forested region  $A_f$  was characterized by either differing friction parameters or by extracting mass with the detrainment function.

For each particular case study, the input parameters (release area  $A_r$ , forest area  $A_f$ , fracture height  $h_0$  and the  $\mu$  and  $\xi$  values for non-forested regions) were identical for all simulations. We varied only the forest friction parameters or detrainment coefficients  $K$ . Release areas and fracture heights were specified according to the observations of the field studies or, when it was impossible to enter the release zone, by applying a terrain analysis (Section 3.2). The open terrain  $\mu$  and  $\xi$  values were defined by the automatic

procedure within **RAMMS**. This feature accounts for terrain features such as gullies and flat slopes as well as altitude level, return period and avalanche size. It is based on calibrations [Buser and Frutiger, 1980; Gruber and Bartelt, 2007].

Accurate, high-precision digital elevation models were necessary to simulate the observed avalanches: Resolutions of 1 m grid size were available for the avalanches released in Germany (ID-VI, ID-VII) and a resolution of 2 m for Switzerland (ID-I, ID-II, ID-III, ID-IV, ID-V).

The forest areas  $A_f$  were specified using orthophotos taken from fixed wing, airborne flyovers. For the friction approach we set  $\xi = 400 \text{ m/s}^2$  and added  $\Delta\mu = 0.02$  to the previously defined  $\mu$  values; for the detrainment approach we did not change the friction parameters but removed mass according to the detrainment function. Forest structure and densities were not accounted for when simulating avalanches with the friction approach; we defined dense and open forest structures by varying parameter  $K$  when using the detrainment approach (Section 3.3.2.2). We selected the following values according to the field observations, Table 3.3:

- $K = 30 \text{ Pa}$  (K30) for dense forest stands with some group structures of trees and few low-lying branches that induce jamming.
- $K = 10 \text{ Pa}$  (K10) for open forest structures or older forests characterized by few branches, root plates or dead wood which serve as low-lying obstacles.

The avalanches were simulated until the final deposition patterns were reached. They were considered stopped when they flowed with less than 5% of the maximum momentum reached by the avalanches [Christen *et al.*, 2010b].

We focused our analysis on the runout distance and deposition structure of the avalanches. Both of these characteristics differed significantly for simulations with the detrainment or the friction approach, as illustrated in Fig. 3.12. The spatial distribution of deposition heights are presented for the seven avalanches (ID-I to ID-VII), for both approaches respectively (friction: a; detrainment: b). The red outlines delineate the measured runout areas.

Three findings are valid for the seven simulated avalanches:

1. The runout of simulations with the friction approach always exceeded the runout of the detrainment approach. Many times the avalanches reached the valley bottom when using the friction approach, unhindered by the forests.
2. The friction approach always overestimated the runout compared to the observations. This is plausible, because the friction parameters are valid for extreme avalanches, but highlights the difficulties of calibrating forest friction parameters for all avalanche sizes.

- More snow was deposited on the avalanche tracks when applying the detrainment approach which caused avalanches to stop on steep slopes in several cases (ID-II, ID-III, ID-VI, ID-VII).

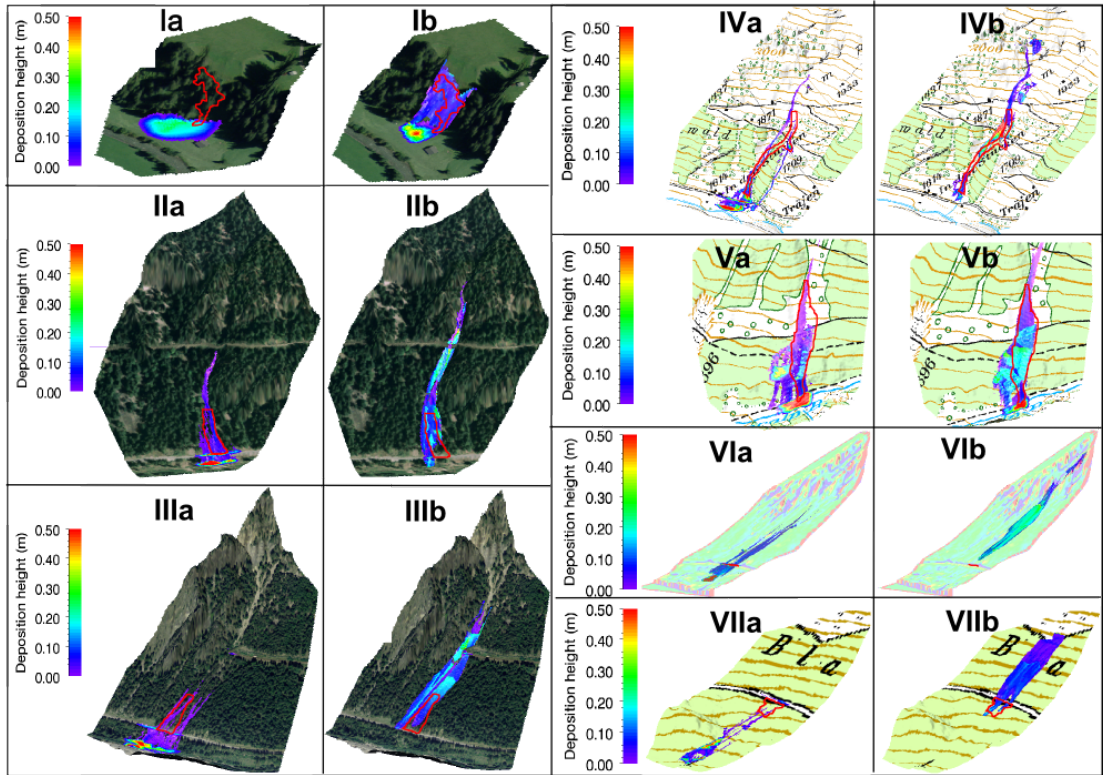


FIGURE 3.12: Comparison of the simulation results of the seven observed avalanches (I-VII). Deposition heights (up to 50 cm) are shown for the  $\mu, \xi$  approach (a) and the detrainment approach (b). The observed runout areas measured with dGNSS (I-V and VII) and photos (VI) are outlined in red. The runout for all case studies are overestimated when using the friction approach (a). The detrainment approach overestimates two cases significantly (I, V), overestimates two cases slightly (II, IV), matches the runout length in two cases (III, VII) and slightly underestimates one case (VI).

Furthermore, three characteristic deposition patterns could be distinguished for calculations with the detrainment approach:

- Avalanche runout distances and areas were considerably overestimated in two cases (ID-I, ID-V). For the avalanche ID-I at Junkerboden the very small release volume ( $V_0 = 318 \text{ m}^3$ ) might serve as an explanation. Runouts of small avalanches tend to be overestimated when using the standard VS-model [Maggioni et al., 2012]. However, the very small release volume can only partly explain the difference because the avalanche near Monstein (ID-V) had the largest release volume of the documented cases (see Table 3.1). In the Monstein case study, we had no direct measurements of the release zone dimensions (we used photographs), and therefore

we might have overestimated the release zone volume. We subsequently reduced the release zone volume and obtained the correct runout distance. This result highlights the problem of selecting the release zone dimensions correctly.

2. The calculation result of the avalanche at Hagenberg (ID-VI) was unique: the detrainment approach underestimated the runout distance. This simulation result is different in comparison to the other avalanches, which provided reasonable approximations to the observed runout distances. The avalanche released during cold weather conditions with dry, cohesionless snow flowing around the trees and therefore reaching the road. The under-prediction can be attributed to the lack of jamming of snow granules between tree stands. Therefore, we specifically simulated this avalanche assuming  $\alpha \neq 0$ , accounting for the fluidization of the flow, and obtained better results (Section 3.4.3).
3. Simulations of the other four avalanches (ID-II, ID-III, ID-IV, ID-VII) produced reasonable deposition patterns (the friction approach highly over-estimated the runout distances and areas). In all of these case studies, wedge shaped depositions were observed behind the vegetation (Table 3.4). Jammed snow mass behind tree groups appears to be the dominant stopping mechanism in all of these cases. An interesting feature of the deposition structure observed in the field campaign of avalanche ID-III could be simulated: The main depositions are concentrated on both sides of the primary flow channel, with almost no snow in the channel itself, which resembles the observations (Fig. 3.2). The main avalanche channel was unforested and mass was stopped at the forest edges.

### 3.4.3 Simulations with $\alpha \neq 0$

We simulated the case study ID-VI, Hagenberg accounting for particle velocity fluctuations ( $\alpha \neq 0$ ). The advantage of this model extension is the simplified selection of the friction parameters. They are initially constant over the whole avalanche path and change according to the generation and decay of the energy associated with particle velocity fluctuations. Therefore, defining different pairs of  $\mu$  and  $\xi$  values for different terrain features, altitude levels and return periods is unnecessary. The flow parameters should only account for snow characteristics, and not depend on avalanche size or altitude levels.

For  $\mu_0$  we chose a value of 0.55. This value can be approximated as the tangent of the angle of repose of avalanche deposits (measurable at the sides and front of avalanche depositions) [Platzter *et al.*, 2007]. In addition this value corresponds to the steepest slope angle at which snow avalanche deposits are found. It matches the tangent of  $29^\circ$ , the approximate minimum angle which allows slab avalanches to release [McClung and Schaerer, 2006]. The value also corresponds to the initial Coulomb friction values measured when a fracture slab begins to release before fragmentation [van Herwijnen and Heierli, 2009]. The value of  $\xi$  was set constant to  $500 \text{ m/s}^2$  [Völlmy, 1955]. Therefore it is between  $300 \text{ m/s}^2$  and  $700 \text{ m/s}^2$ , that is the possible range calculated by Bartelt

TABLE 3.4: Calculated avalanche characteristics of the seven case studies: mean velocity, mean flow height, detrained volume, mean deposition height  $h_d$ . Possible range of deposition widths  $d$ , calculated according to Eq. 3.1 and Eq. 3.2. From the observations we found the wedge height  $h_w$  to be approximately three times as high as the flow depths. The stem densities are taken from observations; however, we assume tree stand clusters consisting of three trees. Note the calculated widths  $d$  are in the range of observed widths. The photos show typical deposition structures of the six avalanches documented in the winter 2011/12.

Internal ID	ID-I	ID-II	ID-III	ID-IV	ID-V	ID-VI	ID-VII
Calculated mean velocity [m/s]	10	17	14	15	12	20	16
Calculated mean flow height [m]	0.4	0.8	0.5	1.3	1	0.8	0.6
Observed forest characteristics	trees with branches, 400 stems ha <sup>-1</sup>	groups of trees, 300 stems ha <sup>-1</sup>	groups of trees, 500 stems ha <sup>-1</sup>	groups of trees, 300 stems ha <sup>-1</sup>	groups of trees, 300 stems ha <sup>-1</sup>	groups of trees, 400 stems ha <sup>-1</sup>	groups of trees, 400 stems ha <sup>-1</sup>
Calculated detrained volume [m <sup>3</sup> ]	110	880	1160	2750	3180	2980	590
Calculated $h_d$ [m]	0.06	0.09	0.09	0.21	0.25	0.11	0.05
Calculated range for $d_w$ [m]	1.1 - 1.5	0.6 - 1.7	1.1 - 2.7	0.4 - 2.1	0.9 - 2.8	0.5 - 1.5	0.5 - 1.3
Observed $d_w$ [m]	< 2.0	< 3.0	< 3.2	< 5	< 3.0	< 1.5	< 1.5
Photo						–	

*et al.* [2012a], who ascertained this value using measured velocities at the avalanche tail when,  $R = 0$ .

We determined the activation energy  $R_0$  by summing the mean normal stress  $N$  and cohesion  $c$ :

$$R_0 \approx N + c = \rho gh + c \approx 2.0kPa, \quad (3.15)$$

using a flow density of 250 kg/m<sup>3</sup> and a mean flow height of  $h = 0.8$  m (Table 3.4). As the flow was dry and cold, we assumed the flow cohesionless and  $c \approx 0$ .

We took a value of  $\alpha = 0.05$  for the generation of random kinetic energy, less than *Bartelt et al.* [2012a] used for their calculations as we assume soft snow. The decay  $\beta$  was defined according to snow characteristics,  $\beta = 0.7$  [*Buser and Bartelt, 2009*]. We defined the forested regions  $A_f$  identical to simulations with the VS-model ( $\alpha = 0$ ) with  $K$  values of 10 Pa and 30 Pa depending on the forest structure.

We show the results of the simulations of avalanche ID-VI at Hagenberg Germany to highlight the differences and similarities of modeling avalanches in forested terrain with  $\alpha = 0$  and  $\alpha \neq 0$  with the detrainment approach. This avalanche was unique in the way that the runout distance was underestimated if choosing  $\alpha = 0$ . Fig. 3.13 depicts the calculation results of deposition heights and velocities for the friction and the detrainment approach with  $\alpha = 0$  and  $\alpha \neq 0$ . Generally the deposition areas of the

detrainment approach (Fig. 3.13 b1, c1) are comparable, whereas the friction approach provides the user with an avalanche reaching the valley floor (Fig. 3.13 a1). With the detrainment approach and  $\alpha = 0$  snow is lost on the steep slope, stopping the avalanche before reaching the road. For  $\alpha \neq 0$ , the avalanche overflows the road, in agreement with the observations. These significant differences can be illustrated using the calculated velocity profiles (Fig. 3.13 b2, c2). The fluctuation energy for dry snow (characterised by  $\beta = 0.7$ ) causes higher velocities for  $\alpha \neq 0$  and therefore less snow is being deposited, leading to a longer runout.

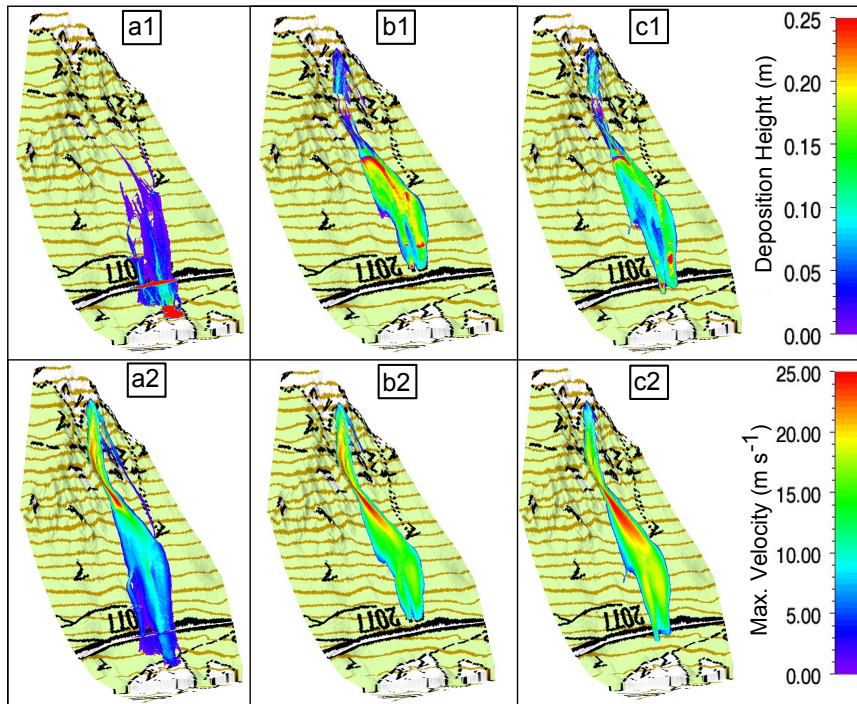


FIGURE 3.13: Comparison of the modeling results of the avalanche at Hagenberg (ID-VI). The results of the friction approach are shown in the first column (**a1**, **a2**); the detrainment approach with VS ( $\alpha = 0$ ) in the second column (**b1**, **b2**). The detrainment approach with  $\alpha \neq 0$  is shown in the third column (**c1**, **c2**). The deposition heights are presented in the upper row; the maximum velocities are presented in the lower row. Note the similar shape of the deposition areas calculated with the detrainment approach. The real avalanche reached the road and covered it with several meters of snow, not flowing further into the forest below.

### 3.5 Discussion and Conclusion

The inclusion of forest effects in avalanche dynamics simulations is an important feature for avalanche hazard analysis, especially for frequent, small to medium avalanches. Forests play a crucial protective role by shortening the runout distance of such avalanches. In this paper we have compared two different approaches to quantify this role. The first is to increase the friction parameters [Bartelt and Stöckli, 2001; Gruber and Bartelt, 2007]; the second is to directly extract mass and its momentum from the flow that has been stopped by the trees. The rate of mass extraction is parameterized by a single coefficient  $K$ , which depends on forest structure. The extraction is the result

of higher friction, so the methods are equivalent, but they lead to different parameterizations of the braking process. However, the detrainment approach is more direct and appears to account for physical processes, such as snow jamming between trees, that is not embodied in the Voellmy friction model.

We systematically tested both approaches on an ideal, parabolic shaped slope to gauge the model performance. We found that runout shortening due to detrainment depends on release volume: the smaller the release volume, the larger the decrease in runout length. This result implies that the stopping of equal mass will have a greater effect on smaller avalanches, which qualitatively agrees with observations. There is almost no effect of detrainment on larger avalanches which also agrees with observations. Additionally we investigated the deposition patterns across the avalanche track and their dependence on velocity. More snow is deposited in steep terrain when applying the detrainment approach. This result also corresponds to the field observations: Avalanches did not reach the valley floor because of snow being continuously detrained in the forest, even on steep slopes. Interestingly, our analysis of the development of the total momentum of the avalanche revealed that the deceleration and stopping of the flow is triggered later but more efficiently.

To demonstrate the applicability of the detrainment approach on real avalanche events we simulated the documented case studies. We found that the simulated mean deposition heights correspond to the observed wedge heights. This calculation requires knowing the forest structure as it involves averaging spatially inhomogeneous deposition patterns behind trees. This, coupled with a comparison of the observed runouts and lateral extension of the avalanches, is presently the only method we can apply to ascertain model performance. However, it also indicates that the parameter  $K$  can be calibrated by performing more mass balance studies in forests. These studies must involve documenting the overall mass balance of an event and relating this data to the observed deposition patterns and forest structure. The values for  $K$  can therefore be improved with future field work, but also data from past events can be employed for this purpose [Teich *et al.*, 2014]. Forest type, stem density, surface roughness and vertical structure of the forest seem to be crucial parameters to be considered [Teich *et al.*, 2014].

Runout shortening was reproduced in the simulations and a good agreement to the observed flow widths was found in four of the seven case studies. Three cases could not be reproduced with  $K$  values of 10 Pa and 30 Pa that we assume to correspond to the observed forest structure. In one case (ID-I), the starting volume was less than 500 m<sup>3</sup> and the avalanche consisted of large, moist snow granules. The simulated avalanche ran too far for  $K < 200$  Pa. This could be an indication that the model scale is not fine enough to represent forest features, terrain roughness or snow characteristics in this particular case. The size limits of depth-averaged models must clearly be established in future work [Maggioni *et al.*, 2012]. A second simulation (ID-V) also ran too far for  $K < 100$  Pa, but could be accurately simulated if the release volume was decreased. In this case, the release volume and location were determined by photographs taken from the counter slope, one kilometer distant. Our conclusion is that accurate release zone measurements, as always, are required. Again, we are confronted with documenting small release areas in inaccessible terrain. The third avalanche that could not be simulated

adequately (ID-VI), could, however, be reproduced using the Voellmy extension ( $\alpha > 0$ ). This suggests that the fluidization of the avalanche in dry/cold conditions is important, stressing the idea that jamming effects cannot develop easily in low density flows with large granular fluctuations.

The detrainment approach, based on momentum extraction, always performed better than the friction approach, based on modified friction coefficients. Nonetheless, the application of the detrainment approach has two fundamental difficulties which must be addressed in future investigations.

First, the detrainment approach is only valid for small to medium avalanches where the forest is not destroyed and the trees act as obstacles. This is not always the case and ideally the model should determine when the trees in the forest break. This is not an easy task as the breaking mode can vary from tree fracture to root upheaval and tree overturning. Furthermore, when the trees and other woody debris are entrained in the flow, they can become entangled in tree stands leading to a complex flow state that it is difficult, if not impossible, to model. If the entangled mass is stopped or if it gains more momentum, destroying still more forest, remains an open question. The application of the model is therefore restricted to a specific flow case.

Second, the model results are sensitive to the selection of the starting mass and snow characteristics. Although it is possible to back-calculate documented avalanches, the predictive capacity of the model remains limited. This is a general problem in the simulation of small and medium avalanches which depend strongly on the size and location of the release zone, entrainment processes, snow properties and terrain features (which might be modified by avalanche deposits). Because of the strong variability of the initial and boundary conditions, as well as material properties, avalanche simulations including forest effects should only be applied to selected problems. For example, to determine the general cost effectiveness of silvicultural measures, or, to determine the vulnerability of specific objects for well defined starting and boundary conditions.

Our results are however promising and will be strengthened by collecting more and specific data during future field studies. We plan to map the entire deposition area, quantifying mass piles behind individual tree clusters. The exact structure of each tree group (location in forest, relative tree composition, tree diameter, branch density, tree spacing, low-lying vegetation) will be documented and correlated to the stopped mass. This will help to calibrate the  $K$  parameter by linking structural features of the forest to mean deposition heights. Granulometry studies are needed in the deposition wedges to relate the jamming process to snow properties. To underpin the field work, small-scale granular chute experiments are conducted to investigate how detrainment in forest-like structures modifies momentum and energy fluxes of avalanches.

## Acknowledgements

The authors thank Armin Fischer, Jochen Veitinger and Irene Vassella for their help on data collection and evaluation. We also want to thank Bernhard Zenke, who made

the close cooperation with the Bavarian Avalanche Service possible. This research was funded by the Bavarian Environment Agency.



## 4. Forest damage and snow avalanche flow regime

Thomas Feistl<sup>[1,2]</sup>, Peter Bebi<sup>[1]</sup>, Marc Christen<sup>[1]</sup>, Stefan Margreth<sup>[1]</sup>, Lorenz Diefenbach<sup>[3]</sup> and Perry Bartelt<sup>[1]</sup>

<sup>[1]</sup> WSL Institute for Snow and Avalanche Research SLF, Flüelastrasse 11, 7260 Davos Dorf, Switzerland

<sup>[2]</sup> Technical University Munich (TUM), Engineering Geology and Hydrogeology, Arcisstrasse 21, 80333 Munich, Germany

<sup>[3]</sup> Swiss Federal Institute of Technology (ETH), Rämistrasse, 8092 Zurich, Switzerland

## Abstract

Snow avalanches break, uproot and overturn trees causing damage to forests. The extent of forest damage provides useful information on avalanche frequency and intensity. However, impact forces depend on avalanche flow regime. In this paper, we define avalanche loading cases representing four different avalanche flow regimes: *powder*, *intermittent*, *dry* and *wet*. In the powder regime, the blast of the cloud can produce large bending moments in the tree stem because of the impact area extending over the entire tree crown. We demonstrate that intermittent granular loadings are equivalent to low-density uniform dry snow loadings under the assumption of homogeneous particle distributions. In the wet snow case, avalanche pressure is calculated using a quasi-static model accounting for the motion of plug-like wet snow flows. Wet snow pressure depends both on avalanche volume and terrain features upstream of the tree. Using a numerical model that simulates both powder and wet snow avalanches, we study documented events with forest damage. We find (1) powder clouds with velocities over 20 m/s can break tree stems; (2) the intermittent regime seldom controls tree breakage and (3) quasi-static pressures of wet snow avalanches can be much higher than pressures calculated using dynamic pressure formulas.

## 4.1 Introduction

Forest damage caused by avalanches reveals the complex and variable nature of avalanche flow. Avalanches cut through forests leaving paths of broken and fractured tree stems, overturned root plates and torn branches [de Quervain, 1978; Bartelt and Stöckli, 2001] (Fig. 4.1). Forest destruction provides important information concerning the spatial extent of avalanche impact pressure. This information helps hazard engineers construct return periods for different avalanche release conditions. More importantly, the protective capacity of mountain forests requires distinguishing between when the avalanche destroys the forest or when trees can withstand the avalanche impact pressure. Impact pressures, however, are related to avalanche flow regime [Faug *et al.*, 2010; Sovilla *et al.*, 2014; Vera *et al.*, in press]. Both fast-moving dry avalanches and slow moving wet snow flows can lead to widespread forest destruction. Powder clouds can also cause extensive tree blow-downs. In this paper we relate forest damage to different avalanche flow regimes with the goal of quantifying the protective capacity of mountain forests.



FIGURE 4.1: Destroyed and surviving trees after avalanche impact in Täsch.

The protective capacity of forests depends on the ability of trees and tree clusters to survive avalanche loading. Forests can stop small and frequent avalanches because the trees are not destroyed [Teich *et al.*, 2012a]. Small avalanches cannot generate significant impact pressures to break and uproot trees. In this case trees serve as rigid obstacles

which cause snow to decelerate. Snow mass is stopped behind dense tree clusters and is subsequently removed from the avalanche [Feistl *et al.*, 2014b]. The avalanche starves. The protective capacity of the forest is thus related to the stem density and forest structure [Teich *et al.*, 2014]. If the trees break, they can no longer serve as rigid obstacles and other physical processes, such as entrainment of woody debris and root plates, slow the avalanche down [Bartelt and Stöckli, 2001]. The effect of tree breaking can be parameterised by increasing the velocity dependent turbulent friction [Christen *et al.*, 2010a]. Thus, to determine the protective capacity of forests requires an understanding when trees serve as rigid obstacles and when trees break. Avalanche dynamics model should distinguish between the two protective modes when predicting avalanche runout and velocity in forested terrain.

The tree breaking threshold depends on both the avalanche loading and tree strength. Trees fall if (1) the bending stress exerted by the moving snow exceeds the bending strength of the tree stem [Johnson, 1987; Peltola and Kellomäki, 1993; Peltola *et al.*, 1999; Mattheck and Breloer, 1994] or (2) if the applied torque overcomes the strength of the root-soil plate, leading to uprooting and overturning [Coutts, 1983; Jonsson *et al.*, 2006]. Avalanche loading is more difficult to quantify because it depends primarily on the avalanche flow regime. To define the avalanche loading, avalanche flow density, velocity and height must be known. These vary across the avalanche flow body and evolve along the avalanche track. The best example is the structure of a dry, mixed avalanche containing both a flowing core and powder cloud. The core velocity and density vary in the streamwise flow direction. For example, the avalanche front can have different flow characteristics than the avalanche tail. Destruction is defined by the dynamic impact pressures. In the case of wet snow avalanches, the velocities are smaller and destruction is defined by quasi-static loadings.

The primary goal of this paper is to introduce tree breaking into avalanche dynamics calculations in order to toggle between different frictional processes acting on the avalanche. We therefore define four loading cases representing four different avalanche flow regimes. These are *powder*, *intermittent*, *dry* and *wet*. We assume tree breaking is always in bending, independent of the flow regime. Failure is defined by a bending stress threshold. The bending stress for mixed dry avalanches is defined by dynamic impact pressures. The wet flow regime requires an equation to describe the indeterminate, quasi-static loading of wet avalanches. We compare the loadings to tree strength to find the critical flow properties (density, velocity, height) for a particular flow regime to break trees. Real case studies are used for this purpose. We carried out a field campaign in summer 2014 in Monbiel and Täsch (Switzerland) and investigated forest damage by avalanches in detail. We compare these observations with avalanche dynamics simulations to reconstruct the spatial extent of the pressure field. Forest damage by dry avalanches that occurred in Southern Germany, 2009 are additionally simulated to test the breaking/non-breaking bending stress thresholds.

## 4.2 Avalanche loading

### 4.2.1 Avalanche pressure and tree stress

Avalanches exert a pressure  $p$  on a tree. We make the magnitude of this pressure a function of avalanche flow regime. We consider dry (superscript  $d$ ) and wet (superscript  $w$ ) avalanche flow regimes separately (Table 4.1).

TABLE 4.1: Denotation for the different flow regimes:  $\rho$  for density,  $h$  for the flow height and  $p$  for the impact pressure per  $\text{m}^2$ . The load is distributed linearly along the tree besides the intermittent loading by the saltation-like flow which exerts the loading pointwise.

<i>Flow regime</i>	<i>Model type</i>	<i>Density</i>	<i>Flow height</i>	<i>Impact pressure</i>	<i>Loading</i>
dry, mixed	powder	$\rho_{\Pi}$	$h_{\Pi}$	dynamic, $p_{\Pi}$	linear distributed
	intermittent	$\rho_g$	$h_g$	granular impact, $p_g$	point
	dense	$\rho_{\Phi}^d$	$h_{\Phi}$	dynamic, $p_{\Phi}^d$	linear distributed
wet	creep and glide	$\rho_{\Phi}^w$	$h_{\Phi}$	quasi-static, $p_{\Phi}^w$	linear distributed
	gliding block	$\rho_{\Phi}^w$	$h_{\Phi}$	quasi-static, $p_{\Phi}^w$	linear distributed

A dry avalanche is divided into a dense flowing core (subscript  $\Phi$ ) and a powder cloud (subscript  $\Pi$ ) (Fig. 4.2). The powder cloud consists of an ice dust suspension with bulk density  $\rho_{\Pi}$ . The height of the cloud  $h_{\Pi}$  is generally larger than the height of the avalanche core  $h_{\Phi}$ . In saltation type flows, the pressure is intermittent and defined by impulsive granular impacts (subscript  $g$ ). The intermittent layer and the avalanche core contain snow granules with density  $\rho_g$ . When the spacing between the granules is small, the core pressure is uniformly distributed and defined by the bulk flow density  $\rho_{\Phi}^d$ . The bulk flow density of the core is smaller than the granule density,  $\rho_{\Phi}^d < \rho_g$ . We therefore define three impact pressures associated with the dry avalanche flow regime: powder cloud  $p_{\Pi}$ , intermittent granular impacts  $p_g$  and bulk avalanche pressure of the core  $p_{\Phi}^d$  (Table 4.1).

A wet snow avalanche contains only a dense flowing core and exerts a pressure  $p_{\Phi}^w$  on the tree. We assume for the wet snow loading case, that the avalanche does not possess a powder cloud or that the flow core is sufficiently fluidized to apply an intermittent pressure on the tree. Typically, the density of the wet snow avalanche core  $\rho_{\Phi}^w$  is higher than the density of a similar dry avalanche [McClung and Schaerer, 1985; Bozhinskiy and Losev, 1998]. The impact pressure  $p_{\Phi}^w$  arising from a wet snow avalanche is not impulsive as the flow velocity is small. The notation used to describe the four different flow regimes is summarized in Table 4.1.

Because trees grow vertical and the avalanche applies a pressure in the slope parallel flow direction the force  $F$  is related to the avalanche impact pressure  $p$  by

$$F = pA \cos \gamma, \quad (4.1)$$

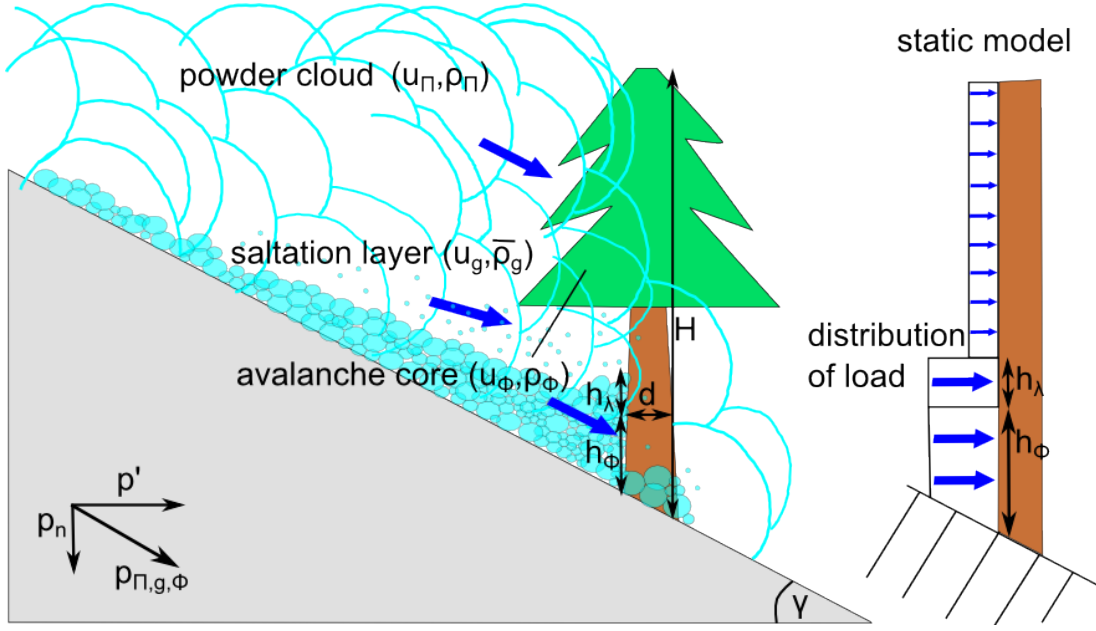


FIGURE 4.2: Schematic illustration of an avalanche with velocity  $u$  on a slope with angle  $\gamma$  hitting a tree. The avalanche has three parts: 1. the powder cloud ( $\Pi$ ), 2. the intermittent layer ( $g$ ) and 3. the wet- or dense flow avalanche core ( $\Phi$ ). The density depends on the flow regime and is denoted  $\rho_\Pi$  for powder clouds,  $\bar{\rho}_g$  for the saltation-like flow consisting of granules with density  $\rho_g$ ,  $\rho_\Phi^d$  for dry snow avalanche cores and  $\rho_\Phi^w$  for wet snow avalanches. Flow height is denoted  $h_\Phi$ , stagnation depth  $h_\lambda$  and the height of the tree  $H$ . The diameter of the stem is assumed to be constant  $d(z) = d$ . The impact pressure of the avalanche  $p_{\Pi,g,\Phi}$  is acting parallel to the slope and can be split in a vertical part due to gravitation  $p_n$  and a part perpendicular to the tree  $p'$ . The static model and the assumed distribution of the load is depicted on the right hand side.

where  $A$  is the loading area of the tree, which depends on the affected height (impact height) and width of the tree. Moreover,  $A$  depends on the avalanche flow regime. The angle  $\gamma$  defines the slope inclination (see Fig. 4.2 and Table 4.2).

The total force  $F$  with the moment arm defines the bending moment  $M$

$$M = F \frac{h_a}{2}, \quad (4.2)$$

where  $h_a$  is the impact height of the avalanche on the tree. The stress  $\sigma$  is defined by

$$\sigma = \frac{Md}{2I}, \quad (4.3)$$

where  $d$  is the diameter of the tree and  $I$  is the moment of inertia of the stem cross-section (Table 4.2). As we assume round tree trunks,

$$I = \frac{\pi d^4}{64} \quad (4.4)$$

and therefore

$$\sigma = 32 \frac{M}{\pi d^3}. \quad (4.5)$$

The bending stress is calculated from the maximum torque, which is located at the stem base. We assume a fixed support and a homogenous distribution of mass and velocity (see Fig. 4.2). We do not account for shearing. In this analysis we make use of Matthecks observation that the tree grows with respect to the applied forces imposed by the natural environment, for example wind [Mattheck and Breloer, 1994]. This implies that the tree strength  $\bar{\sigma}$  in relation to the applied moment is independent of height and therefore constant for a single tree and must only be determined at one point. We select this point to be the tree stem base. Matthecks observation also implies that the moments to break the tree in bending and to overturn the tree are similar [Bartelt and Stöckli, 2001; Peltola et al., 1999].

#### 4.2.2 Four avalanche flow regimes $p_{\Pi}$ , $p_g$ , $p_{\Phi}^d$ , $p_{\Phi}^w$

Various studies have investigated avalanche impact pressures on obstacles [Pedersen et al., 1979; Lang and Brown, 1980; Faug et al., 2004, 2010; Gray et al., 2003; Hauksson et al., 2007; Naaim et al., 2004, 2008; Sheikh et al., 2008; Teufelsbauer et al., 2011; Baroudi et al., 2011]. Pressures  $p$  from fast moving avalanches ( $Fr > 1$ ) in the dry flow regime are represented by the equation

$$p = c_d \rho \frac{u^2}{2}. \quad (4.6)$$

This formula is recommended by the Swiss guidelines on avalanche dynamics calculations [Salm et al., 1990] as well as the report from the European commission on the design of avalanche protection dams [Johannesson et al., 2009]. It describes the local momentum exchange between the avalanche and a rigid slender obstacle at impact. The drag coefficient  $c_d$  accounts for the obstacle geometry and flow regime.

The pressure formula Eq. 4.6 has been applied to back-calculate measurements of pressure exerted by wet snow avalanches on obstacles [Sovilla et al., 2010]. Application of this formula to the wet snow avalanche problem assumes that the pressures arise from a slow drag flow regime. However, to model the measured pressures with the observed avalanche velocities requires using unrealistic and non-physical drag coefficients,  $c_d > 2$ . This suggests that the nature of the wet snow avalanche pressure is not dynamic, but similar to quasi-static glide pressures exerted on pylons and defense structures. For the wet snow case  $p_{\Phi}^w$  we assume that dynamic pressures are small in comparison to the static pressure arising from the weight of the snow that loads the tree. Our assumption is based on observations of wet snow avalanche deposits and levees formation [Bartelt et al., 2012c; Feistl et al., 2014b]. Often wedges of snow pile up upstream of trees. The avalanche flows around these stationary pile-ups; shear planes develop. Any dynamic force must be transferred by frictional mechanisms across the shear planes separating the stationary and moving snow. We assume these dynamic forces to be small and that the total force acting on the tree depends on the distribution of static forces behind the obstacle. This is an indeterminate problem because it depends on the terrain and roughness in the vicinity of the obstacles. Therefore, we assume that the applied

pressure cannot be represented by Eq. 4.6 which describes only the local transfer of momentum and not the static weight of the avalanche pushing on the obstacle. We present the application of two possible alternative calculation methods. The first (we term it "creep pressure model", CPM) is based on the Swiss guidelines on avalanche protection measures [Margreth, 2007] and the report of the European commission [Johannesson et al., 2009]. The second method (we term it "sliding block model", SBM) was used to investigate the formation of glide-snow avalanches, based on the failure of the stauchwall [Bartelt et al., 2012b; Feistl et al., 2014a]. In this model the stauchwall is replaced by the tree. The model is similar to the approach developed by In der Gand and Zupančič [1966] to find glide-snow pressure acting on obstacles.

#### 4.2.2.1 Powder cloud loading $p_{\Pi}$

The pressure exerted by the powder cloud is

$$p_{\Pi} = c_{\Pi} \rho_{\Pi} \frac{u_{\Pi}^2}{2}, \quad (4.7)$$

where  $c_{\Pi}$  is the powder cloud drag coefficient of loading on the entire tree depending on tree species and wind speed [Mayhead, 1973]. Mayhead [1973] derived an average value of  $c_{\Pi} = 0.4$  for different tree species in Great Britain in wind tunnel experiments for wind speeds of  $u = 25$  m/s. We adopt this value for the powder cloud loading. Mayhead [1973] found decreasing drag coefficient values for increasing velocities. The total force is

$$F_{\Pi} = p_{\Pi} w H \cos \gamma \quad (4.8)$$

for a homogeneous distributed loading.

The total force  $F_{\Pi}$  depends on the powder cloud height  $h_{\Pi}$  and on the tree height  $H$ . We assume the powder cloud to be larger than the tree height  $h_{\Pi} > H$ , therefore is  $H$  the impact height. The quantity  $w$  is the loading width of the tree (Table 4.2). In this analysis we assume the width to be constant over height  $w(z) = w$  as indicated in Fig. 4.3. The loading width depends on the location of the tree in the forest [Indermühle, 1978]. Single trees in the avalanche path have a larger loading width than trees in dense forest stands. Leafless trees have smaller loading widths than evergreen trees (Fig. 4.3). Larch and birch trees for example have smaller loading widths than spruce or pine trees. The loading width can be estimated from aerial photographs. The relationship between stem diameter and crown diameter was evaluated by Indermühle [1978], Bürki [1981] and Pretzsch [2014].

The bending stress of a powder cloud is then

$$\sigma_{\Pi} = c_{\Pi} \rho_{\Pi} \frac{8u_{\Pi}^2}{\pi d^3} w H^2 \cos \gamma. \quad (4.9)$$

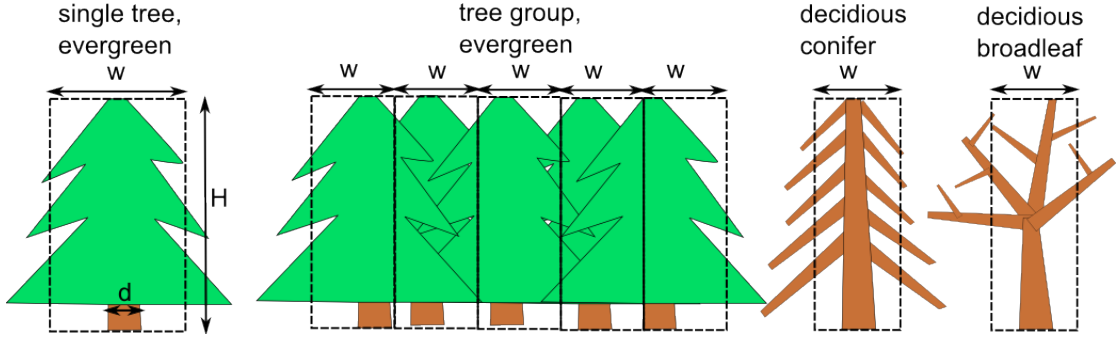


FIGURE 4.3: The loading width of the tree depends on the location in the forest. In dense forest stands tree crowns tend to be narrower than if they stand alone. Additionally the loading width  $w$  depends on the foliage of different tree species.

#### 4.2.2.2 Intermittent loading $p_g$

The pressure exerted by an individual snow granule is

$$p_g = \rho_g \frac{4u_g^2}{3} \quad (4.10)$$

[Bozhinskiy and Losev, 1998]. This equation assumes the complete destruction of the snow granule within the impact time interval  $r/u_g$  where  $r$  is the granule radius. For a granule with  $r = 0.1$  m and a velocity  $u_g = 20$  m/s the time of impact is 0.005 seconds. The force of the granule impact is applied over an area  $\pi r^2$ . The total impact pressure on the tree is the sum of the point loads exerted by the granules  $\sum p_g$ . The granule densities can be large ( $\rho_g > 300$  kg/m<sup>3</sup>). The number of granules that hit the tree per unit time depends on the speed of the avalanche and the height and average density  $\bar{\rho}_g$  of the intermittent layer. The momentum exerted by a number  $n$  of granules that hit the stem is therefore

$$M_g = p_g \pi r^2 \cos \gamma \sum_{i=1}^n h_i. \quad (4.11)$$

The total momentum of the intermittent loading case is governed by the distribution of the impact pressure exerted by the granules in height. We assume the height of the intermittent layer  $h_g$  to be as large as the flow height of the core  $h_\Phi$  plus the stagnation depth  $h_\lambda$ ,  $h_g = h_a$  (see Eq. 4.17). Certainly there are single granules hitting the tree higher up on the stem, but the number and mass of these granules is small. Additionally we assume a regular distribution of impacts, therefore

$$\sum_{i=1}^n h_i \approx n h_a / 2. \quad (4.12)$$

This assumption is conservative considering an avalanche flow with highest intensity in the lower most part. That is in contrast to loading by wind (see Fig. 4.4).

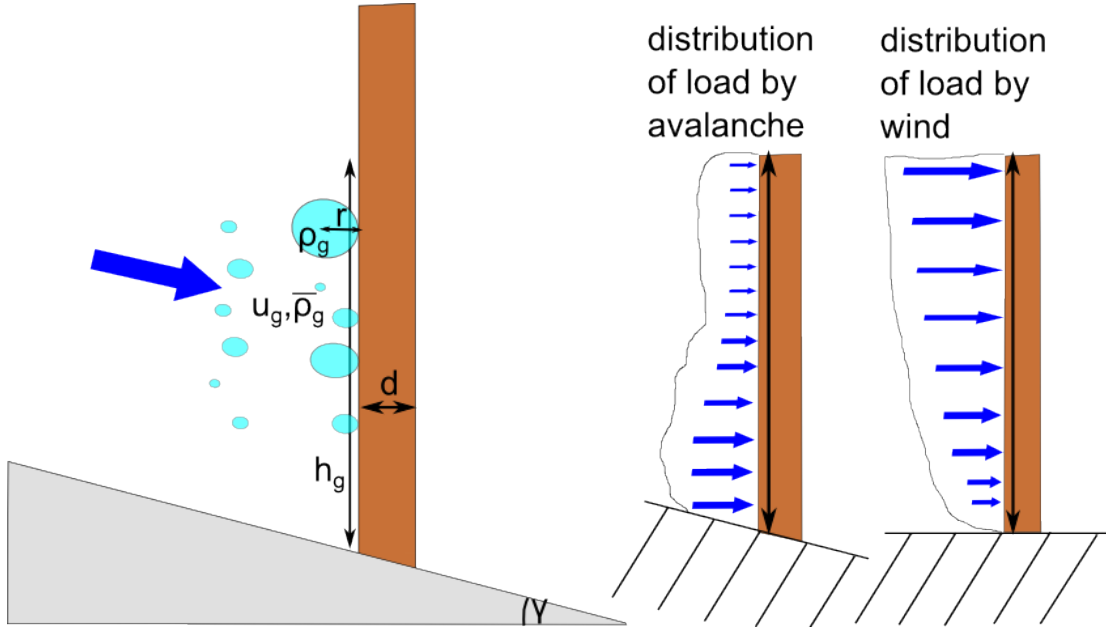


FIGURE 4.4: Granules of the intermittent layer with density  $\rho_g$  hitting a tree with diameter  $d$ . The average density  $\bar{\rho}_g$  is calculated over the whole flow height  $h_g$ . The momentum  $M_g$  is applied by the granules on an area  $\pi r^2$  on the stem for a time  $t = r/u_g$  [Bozhinskiy and Losev, 1998]. The difference between loading by an avalanche in comparison to loading by wind is depicted on the right hand side.

The average density  $\bar{\rho}_g$  times the volume with length  $r$ , height  $h_a$  and width  $d$  is equal to the mass of  $n$  granules with radius  $r$  in the identical volume; therefore

$$\bar{\rho}_g h_a d r = \rho_g \frac{4}{3} \pi r^3 n \quad (4.13)$$

(see Fig. 4.4).

We solve this equation for  $n$  and take the assumption of regular distribution (Eq. 4.12) into account. Then Eq. 4.11 results in

$$M_g = \bar{\rho}_g \frac{u_\Phi^2}{2} d h_a^2 \cos \gamma, \quad (4.14)$$

which is similar to the momentum exerted by the dense flowing core  $M_\Phi$  for a drag coefficient  $c_\Phi = 2$  and  $\bar{\rho}_g = \rho_\Phi$ . The average density of the intermittent layer will, however, always be considerably lower than the density of the flowing core. We therefore assume  $M_\Phi > M_g$  and do not consider the intermittent loading for the bending stress analysis, although we recognize that the forces from individual particles can be large.

#### 4.2.2.3 Dense flowing core loading $p_\Phi^d$

The pressure per unit area that a dense flowing avalanche exerts on a tree is calculated similarly to the powder cloud loading except that now we consider the avalanche core

$\Phi$ :

$$p_{\Phi}^d = c_{\Phi} \rho_{\Phi}^d \frac{u_{\Phi}^2}{2}. \quad (4.15)$$

Fluidization leads to bulk avalanche flow densities  $\rho_{\Phi}$  that vary in the streamwise flow direction. Values for  $c_{\Phi}$  for cylindrical obstacles (trees) are in a range between  $1 < c_{\Phi} < 2$  depending on the literature [*McClung and Schaerer, 1985; Norem, 1991*]. For our analysis we chose  $c_{\Phi} = 1.5$  according to *Johannesson et al. [2009]* for trees in dry flowing avalanches. The loading width is equal to the stem diameter  $w = d$  if the fluidized height  $h_{\Phi}$  of the avalanche is located beneath the tree crown, therefore

$$\sigma_{\Phi}^d = c_{\Phi} \rho_{\Phi}^d \frac{8u_{\Phi}^2}{\pi d^2} h_a^2 \cos \gamma. \quad (4.16)$$

The loading is adjusted to account for the stagnation height  $h_{\lambda}$

$$h_a = h_{\Phi} + h_{\lambda}, \quad (4.17)$$

and we denote  $h_a$  as impact height. The stagnation height is calculated according to the Swiss guideline formula

$$h_{\lambda} = \frac{u_{\Phi}^2}{2g\lambda} b(d, h_{\Phi}), \quad (4.18)$$

where  $b(d, h_{\Phi}) = 0.1$  for a flow height  $h_{\Phi} \gg d$  [*Salm et al., 1990*]. Furthermore,  $\lambda = 1.5$  for fluidized flows.

#### 4.2.2.4 Creep Pressure Model $p_{\Phi}^w$ (CPM)

We apply the CPM developed by *Salm [1978]* and *Häfeli [1967]*, which is applied in the Swiss Guidelines on avalanche prevention [*Margreth, 2007*] to calculate the snow pressure of snow gliding:

$$p_{\Phi}^w = \rho_{\Phi}^w g K_c N \eta \frac{h_{\Phi}}{2 \cos \gamma}, \quad (4.19)$$

where

$$K_c = \left( 2.5 \left( \frac{\rho_{\Phi}^w}{1000} \right)^3 - 1.86 \left( \frac{\rho_{\Phi}^w}{1000} \right)^2 + 1.06 \left( \frac{\rho_{\Phi}^w}{1000} \right) + 0.54 \right) \sin(2\gamma) \quad (4.20)$$

is the creep factor,  $N$  the gliding factor and

$$\eta = 1 + c^* \frac{h_{\Phi} \cos \gamma}{d} \quad (4.21)$$

the efficiency factor (Table 4.2). According to Eq. 4.5 the bending stress is calculated by

$$\sigma_{\Phi}^w = \rho_{\Phi}^w g K_c N \eta \frac{8h_{\Phi}}{\pi d^2} h_a^2. \quad (4.22)$$

#### 4.2.2.5 Sliding Block Model $p_{\Phi}^w$ (SBM)

A second method to calculate glide-snow pressure was developed by *In der Gand and Zupančič* [1966]. In this method the snow exerts a static pressure on the tree (Fig. 4.5). The magnitude of the static pressure depends on the volume of snow captured. The pressure will be highest before a wedge with shear planes develops behind the tree. The angle  $\psi$  and the length  $l_v$  are used to define the volume, see Fig. 4.5. The opening angle  $\psi$  depends on the location of the tree in the forest and the forest structure, because pressure can be distributed to other tree groups in the forest. The volume length  $l_v$  depends on the terrain and the avalanche length. It increases for open slopes and long avalanches and decreases for rough, twisted avalanche tracks where surface elements and channel sides take up the avalanche pressure. Surface roughness is parameterized with the ground friction coefficient  $\mu_m$  (Table 4.2).

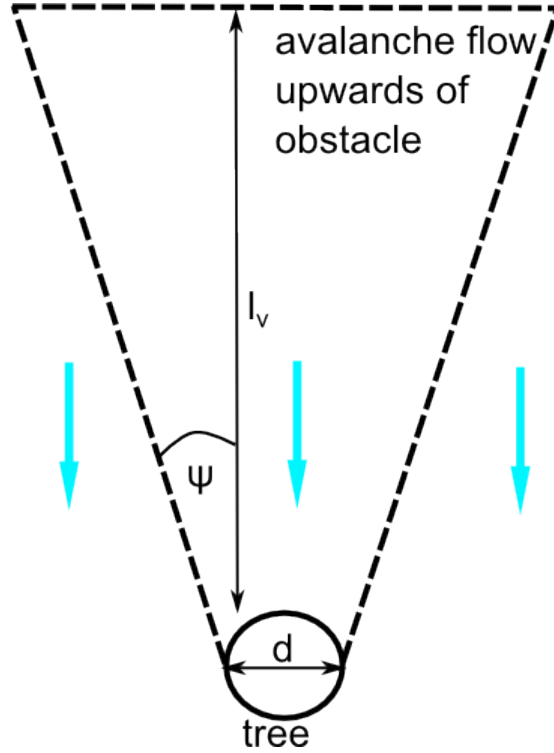


FIGURE 4.5: Schematic illustration of a wet snow accumulation behind a tree. The volume of the snow depends on the opening angle  $\psi$ , the volume length  $l_v$  and the width of the tree  $d$ .

The quasi-static pressure of the avalanche in this case is therefore

$$p_{\Phi}^w = \rho_{\Phi}^w g h_{\Phi} l_v (l_v \tan \psi + d) (\sin \gamma - \mu_m \cos \gamma) \cos \gamma. \quad (4.23)$$

The bending stress of the avalanche on the tree is then

$$\sigma_{\Phi}^w = \rho_{\Phi}^w g l_v (l_v \tan \psi + d) (\sin \gamma - \mu_m \cos \gamma) \frac{16 h_{\Phi}}{\pi d^2} h_a^2 (\cos \gamma)^2. \quad (4.24)$$

TABLE 4.2: Denotation to calculate the loading.

<i>Symbol</i>	<i>Parameter</i>	<i>Unity</i>
$\rho$	avalanche density	kg/m <sup>3</sup>
$u$	flow velocity	m/s
$h_a$	impact height	m
$\lambda$	stagnation constant	
$c_d$	drag coefficient	
$\sigma$	bending stress	Pa
$\bar{\sigma}$	bending strength of tree	Pa
$p$	applied pressure	Pa
$F$	applied force	N
$M$	bending moment	Nm
$I$	moment of inertia	m <sup>4</sup>
$A$	loading area	m <sup>2</sup>
$\gamma$	slope angle	°
$d$	stem diameter	m
$H$	tree height	m
$w$	effective crown width	m
$l_v$	volume length	m
$\psi$	opening angle	°
$\mu$	friction angle	°
$N$	gliding factor	
$K_c$	creep factor	
$\eta$	efficiency factor	
$c^*$	intensity factor	
$D$	magnification factor	
$r$	granule radius	m

### 4.2.3 Additional loading and tree breaking

The bending stress equation for powder avalanches  $\sigma_{\Pi}$  (Eq. 4.9), dry avalanches  $\sigma_{\Phi}^d$  (Eq. 4.16 and wet snow avalanches  $\sigma_{\Phi}^w$  (Eqs. 4.22 and 4.24) can be increased to include several effects that are not included in the ideal case. The stresses are magnified by the amount  $D$ . In the ideal case  $D = 1$ . Reasons for a magnification factor  $D > 1$  are:

- The avalanche exerts the pressure not only on the stem but also on low branches. Trees at the stand edge usually have branches close to the ground surface as light conditions are favorable. This effect is especially pronounced for evergreen trees such as spruces. We therefore assume that the stem diameter is a poor measure for the effective width at stand edge. For trees with low-lying branches at the forest edge, we assume a magnification factor between 1.5 (leafless trees) and 2.5 (evergreen trees),  $1.5 < D < 2.5$ . As powder clouds exert their pressure on the whole tree anyway, this does not affect Eq. 4.9,  $D = 1$ . The difference in loading

area from evergreen to leafless trees is accounted for by the varying effective width  $w$  (Fig. 4.3).

- Woody debris carried by the avalanche increases the impact pressure when hitting a tree. Similar to the additional point load exerted by single snow granules  $p_g$  (Sect. 4.2.2.2) the impact pressures can be high, especially for a wood density  $\rho_w \approx 800 \text{ kg/m}^3$ . There are countless impact scenarios of broken stems hitting trees below, leading to subsequent destruction. For the first trees at the stand edge this is not the case, however. We take this effect into account by assuming the flow density of the avalanche to contain woody debris if the avalanche has hit and entrained trees before, therefore  $1.5 < D < 2$ .
- The self weight of the tree when bending just before breaking is an additional load that increases the bending stress on the lower parts of the stem. This effect can even be higher if snow is loaded on branches and increases the tree mass. Second-order bending effects are thereby introduced into the problem [Peltola *et al.*, 1997]. We assume an increase in bending stress of approximately 10 - 20 %.
- For flexible structures such as trees, the inertial response of the tree must be considered [Clough and Penzien, 1975]. The magnification factor  $D$  depends on the mass and stiffness of the obstacle as well as the duration of the impulsive loading. Clough and Penzien [1975] calculated a value  $D \approx 1.7$ . This effect is relevant only for powder snow loading.
- We assumed in all four flow regimes that the avalanche flows close to the ground. However, an avalanche flowing over a deep snow cover will hit the tree higher up the stem. This effect can be included in the analysis by simply increasing the moment arm of applied force. Whereas the increase in momentum can be high at stand edges where deep snow covers occur, the effect is negligible where dense canopy suppresses snow accumulation on the ground. The increase of the exerted pressure is 50% if an avalanche with flow height  $h_\Phi = 3$  m hits a tree above an 80 cm deep snow cover.

Trees break if the bending stress exerted by the avalanche exceeds the bending strength of the tree  $\sigma > \bar{\sigma}$ . In forest areas the bending strength is highly variable, depending on the tree species, their location in the forest, on the soil characteristics and its nutrient content, on the trees' healthiness, on the temperature and on the moisture content of the wood [Grosser and Teetz, 1985; Götz, 2000; Peltola *et al.*, 2000; Lundström *et al.*, 2009]. Bending strengths of wood provided in literature do not only vary according to stand and tree characteristics but also depend on the measuring method, for example if the load is applied dynamically or statically. Tree pulling experiments [Peltola *et al.*, 2000; Stokes *et al.*, 2005], rock impact experiments [Lundström *et al.*, 2009], fractometer measurements by [Götz, 2000] and material testing procedures by Lavers [1983] result in different values for the bending strength: from  $\bar{\sigma} = 6 \text{ MN/m}^2$  for spruce [Götz, 2000] to  $\bar{\sigma} = 150 \text{ MN/m}^2$  for birch [Grosser and Teetz, 1985]. The values we used to predict forest damage in our model calculations are based on the study of Peltola *et al.* [2000] and are listed in Table 4.3. The bending stress of avalanches to destroy mature trees

must exceed a minimum value of  $\sigma > 30 \text{ MN/m}^2$ . According to *Peltola et al.* [2000]; *Götz* [2000] and *Stokes et al.* [2005] spruce is the species with lowest strength whereas birch is the strongest of the investigated samples.

TABLE 4.3: Bending strength of different tree species according to *Peltola et al.* [2000] who performed tree pulling experiments. Note that these values are average values and vary depending on the healthiness, the location in the forest and other stand characteristics.

	<i>Spruce</i>	<i>Scots Pine</i>	<i>Larch</i>	<i>Birch</i>
Bending strength $\bar{\sigma}$ [MN/m <sup>2</sup> ]	36	37	37	41

We only calculate the stress that is sufficient to break trees not to uproot trees. Previous studies proved, that pressures required for uprooting are in the same range or higher than for stem breakage [*Bartelt and Stöckli*, 2001; *Peltola et al.*, 1999]. Additionally we observed twice as many tree breakages than uprootings in the two documented events Täsch and Monbiel (broken: 324, uprooted: 173).

## 4.3 Modeling and results

### 4.3.1 Forest destruction modeling

To test the performance of Eq. 4.16 on forest damage by dry flowing avalanche cores we implemented a new module in the avalanche simulation program RAMMS [*Christen et al.*, 2010b]. We accounted for the turbulent movement of particles, curvature effects, snow temperature and cohesion [*Buser and Bartelt*, 2009; *Fischer et al.*, 2012; *Vera et al.*, in press; *Bartelt et al.*, accepted]. We denote this RAMMS version as “extended”.

Bending stresses exerted on trees of specific forest areas are calculated for each grid cell from flow height, density, velocity and slope angle. Additionally for each forest area an average stem diameter has to be specified. The bending strength of the predominant tree species is taken from literature (Table 4.3). The trees in an area are destroyed if  $\sigma > \bar{\sigma}$ . We denote both, broken and uprooted trees as “destroyed”. In this case the avalanche is slowed down by the increased turbulent friction and the entrainment of the woody debris in this area [*Bartelt and Stöckli*, 2001]. Detrainment of snow is dominant in areas where  $\sigma < \bar{\sigma}$  and no destruction takes place [*Feistl et al.*, 2014b].

We applied the new model approach to back calculate avalanche events with forest damage in Switzerland and Germany. Calculated forest damage was compared to the actual observed damage. Stem diameters in 1.3 m height, tree species and exact tree location were documented for two avalanche events with forest destruction in Monbiel and Täsch, Switzerland. In total we documented 1120 destructed or non-destructed trees in the avalanche paths. Six avalanches with forest destruction, that released in an avalanche cycle in winter 2009 in Germany were additionally simulated to test on the model performance.

### 4.3.2 Wet snow avalanche Monbiel, 2008

A large wet snow avalanche (release volume approx. 150000 m<sup>3</sup>) released on 23rd April 2008 near Monbiel, Switzerland and destroyed a small spruce forest before it stopped in the river bed of the Landquart. An approximation of the flow velocity ( $u = 5$  m/s) and flow height ( $h_{\Phi} = 3$  m) was possible by analyzing a movie documentation [Sovilla *et al.*, 2012]. The deposition height was measured using laser scan (between 2 m and 7 m). Subsequently this avalanche was simulated by Vera *et al.* [in press] with the avalanche modeling software RAMMS, applying a new model extension that accounts for random kinetic energy fluxes, cohesion and snow temperature [Buser and Bartelt, 2009; Bartelt *et al.*, accepted]. They compared the model results with the data and Vera *et al.* [in press] found the calculated velocities, flow heights and deposition heights to resemble the real avalanche flow (Fig. 4.6). These calculations allowed us to determine the impact pressure  $p_{\Phi}^w$  in the area of forest destruction. The slope angle at the location of the spruces was  $10^{\circ} < \gamma < 20^{\circ}$ . We assume the density of the snow  $\rho_{\Phi}^w = 450$  kg/m<sup>3</sup> as the avalanche was wet. The average stem diameter of the lower spruce stand was approximately  $d = 0.5$  m (Fig. 4.6). We calculated the impact pressures  $p_{\Phi}^w$  and the resulting bending stresses  $1MN/m^2 < \sigma < 8MN/m^2$  with the dynamic approach (Eq. 4.16) for all damaged trees. These values are far below the bending strength  $\bar{\sigma} = 36MN/m^2$  of spruces. For one spruce, marked with a red cross in Fig. 4.6 we additionally calculated the bending stress with the CPM and the SBM (Table 4.4).

### 4.3.3 Powder snow avalanche Täsch, 2014

A cold powder snow avalanche released on March 4th, 2014 in Täsch in Wallis, Switzerland. The road and the rail tracks to Zermatt were buried in deep snow. Aerial pictures and the insight of our visit to the site the next day allowed us to reconstruct the avalanche release volume (approx. 80000 m<sup>3</sup>), deposition patterns and forest damage along the track (Fig. 4.7). We used a dGNSS (differential Global Navigation Satellite System) device to measure the deposition heights. In summer 2014 we carried out a field campaign to document the forest destruction in detail. Approximately 1000 uprooted, broken, bent and still healthy trees were mapped, their stem diameter measured and their species noted. The location of the trees and their characteristics are depicted in Fig. 4.7. Due to terrain undulations the avalanche split in two parts in the lower part of the slope leaving trees in the central area untouched. Two old larch trees (at least 200 years old, measured with a pole testing drill) with stem diameters of 88 and 95 cm resisted the impact pressure in the main avalanche path (pink crosses in Fig. 4.7).

Approximately 10 m high deflecting dams were built along the north side of the avalanche path to protect the village Täsch from being hit by extreme avalanche events. These dams worked well in the upper part of the avalanche path where the avalanche hardly overflowed the dam. In the lower part, however, the dam lost its deflecting effect because of avalanche depositions of earlier events. The channel was almost filled up to the dam crown and the avalanche from March 4th partly went straight down the slope. A young forest, consisting mainly of birches and larches was destroyed and the avalanche hit the

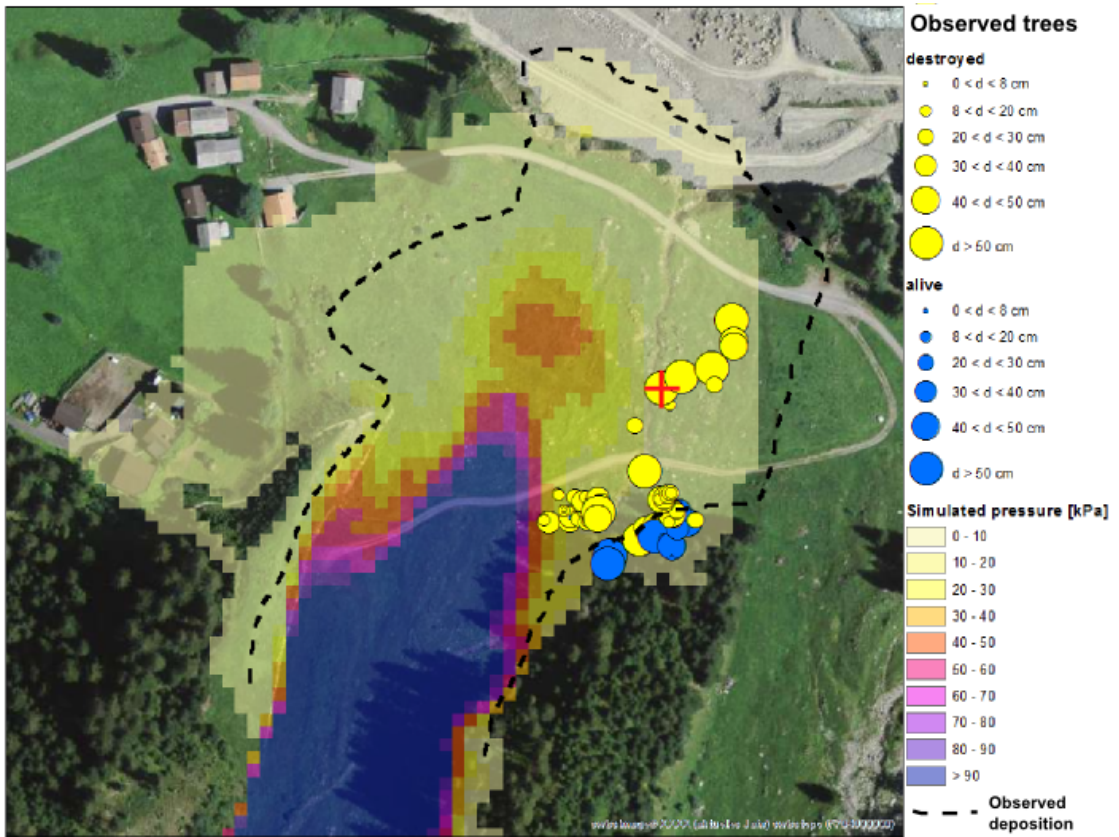


FIGURE 4.6: Simulated dynamic impact pressure  $p_{\Phi}$  of the wet snow avalanche in Monbiel, calculated with RAMMS taking snow temperature and cohesion [Vera *et al.*, in press; Bartelt *et al.*, accepted] into account. The tree species and stem diameters were measured during a field campaign in summer 2014. The tree location was measured with a dGNSS device. The red cross denotes the spruce that we calculated the bending stress  $\sigma$  for (Sect. 4.4)(Swissimage ©, DV 033594, 2014). Note that the calculated velocity and runout distance agreed well with the observations.

road north of the gallery, went through the river bed and hit the rail tracks on the other side (see Fig. 4.7).

Velocities, flow height and the powder cloud diffusion were modeled with the extended RAMMS version. The simulations enabled us to calculate bending stresses caused by the dry flowing avalanche core  $\sigma_{\Phi}^d$  and the powder part  $\sigma_{\Pi}$ . The avalanche core was flowing with an approximate speed,  $u_{\Phi}^d = 17$  m/s, flow height  $h_{\Phi} = 2$  m and we assumed a density of  $\rho_{\Phi}^d = 300$  kg/m<sup>3</sup>. For the powder cloud we calculated a density  $\rho_{\Pi} = 5$  kg/m<sup>3</sup>, velocity  $u_{\Pi} = 25$  m/s and a flow height  $h_{\Pi} \approx 40$  m, which was higher than the trees it passed and destroyed.

We calculated the forest destruction and compared the results with the actual observed tree damage (Fig. 4.7). Our simulation results correspond well with the observed destruction. The two old larches remain standing whereas the young trees below the dam were broken (see Fig. 4.1). The forest in the lower central deposition area remained standing as observed. The avalanche turned right in the lower slope, shortly before the gallery and caused tree destruction in a forest stand shortly above the river bed (red

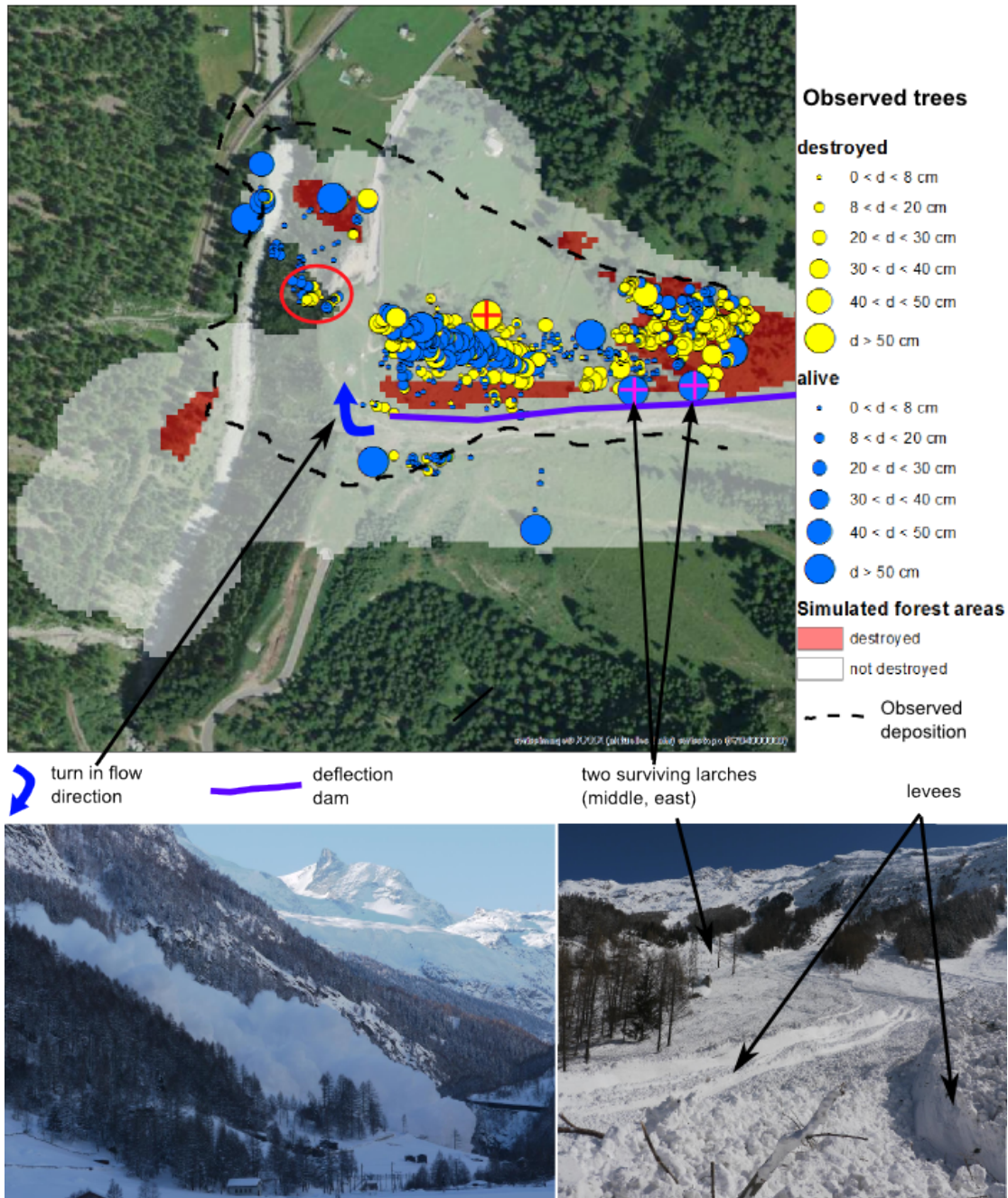


FIGURE 4.7: The calculated forest destruction with the new RAMMS module (red areas) in comparison to the observed forest stand (blue and yellow dots) and deposition area in Täsch. The simulated extent of the avalanche is underlaid with white. We chose the following parameter values to calculate this avalanche:  $\xi = 1500$ ,  $\mu = 0.55$ ,  $\alpha = 6\%$ ,  $\beta = 0.9$ ,  $R_0 = 2$  and entrainment along the track. The broken larch is marked with a red cross (west), whereas the two old larches in the upper part of the slope are marked with pink crosses (middle, east). A photo of the levees that lead to the direction change is added as well as the forest damage that followed (red circle). The avalanche ran over depositions of earlier events and overflow the dam (violet line)(Swissimage ©, DV 033594, 2014).

circle in Fig. 4.7) before it went up the counter slope and hit the rail tracks. This turn in flow direction was caused by levee formation which could not be simulated with the avalanche modeling software. The levee formation is also the reason, why the avalanche did not reach as far as highlighted in the lower left corner of Fig. 4.7. The red cross denotes a broken larch we calculated the pressure for (see Sect. 4.4). The overflowing of the lower dam could be calculated assuming snow depositions of earlier events of approx. 5 m height.

#### 4.3.4 Powder snow avalanches Germany, 2009

We simulated six avalanches that released in Germany end of February 2009 and tested the new model approach (Fig. 4.8). We chose  $\mu$  and  $\xi$  values according to an automatic procedure in RAMMS which takes terrain features, such as channels, gullies and flat areas into account [Christen *et al.*, 2010b]. We did not consider the random movement of particles ( $\alpha = 0$ ) for these avalanches. We accounted for cohesion ( $c = 50$  Pa) according to Dreier *et al.* [2014]; Bartelt *et al.* [accepted]. The meteorological conditions for these six avalanches were similar: Cold temperatures (- 5 °), a release height of approximately 80 cm and snow entrainment along the avalanche path. The avalanches all released shortly above or below the treeline and caused massive forest destruction. From the forest damage the return period of these events was estimated to be at least 100 years. The damaged forest was mainly spruce with some areas of larch at higher elevations. The stem diameters  $d$  and tree species were defined according to orthoimages [Bebi *et al.*, 2001]. Runout areas were overestimated if not taking forest into account (see pictures (a) in Fig. 4.8) with Frillensee as an exception. In average the runout was overestimated by approx. 200 m. When taking forest into account the the runout was in average well reproduced (in average 30 m too short). Generally forest damage by the dense flowing core was underestimated especially in the lower part of the avalanche paths. Large powder clouds were observed, however, especially in the lower avalanche paths.

## 4.4 Discussion

Using the standard dynamic calculation formula for  $\sigma_{\Phi}^d$  (Eq. 4.6), we were able to reproduce the observed forest damage in the central and upper parts of the avalanche tracks in Täsch and Germany (see Sect. 4.3.3, 4.3.4). In these regions the calculated avalanches reached high velocities and therefore exerted large dynamic pressures on the trees. However, it was not possible to reproduce the observed forest damage in the runout zone or lateral edges of the flow without taking into account the avalanche flow regime, specifically using the formulas for powder snow pressure  $\sigma_{\Pi}$  or wet snow avalanche pressure  $\sigma_{\Phi}^w$ . In the runout zone the standard pressure formula *underestimated* the pressures required to break trees.

The avalanches in Täsch and Germany consisted of cold snow and were accompanied by large powder clouds. At Täsch the powder cloud was higher than the trees (see Fig.

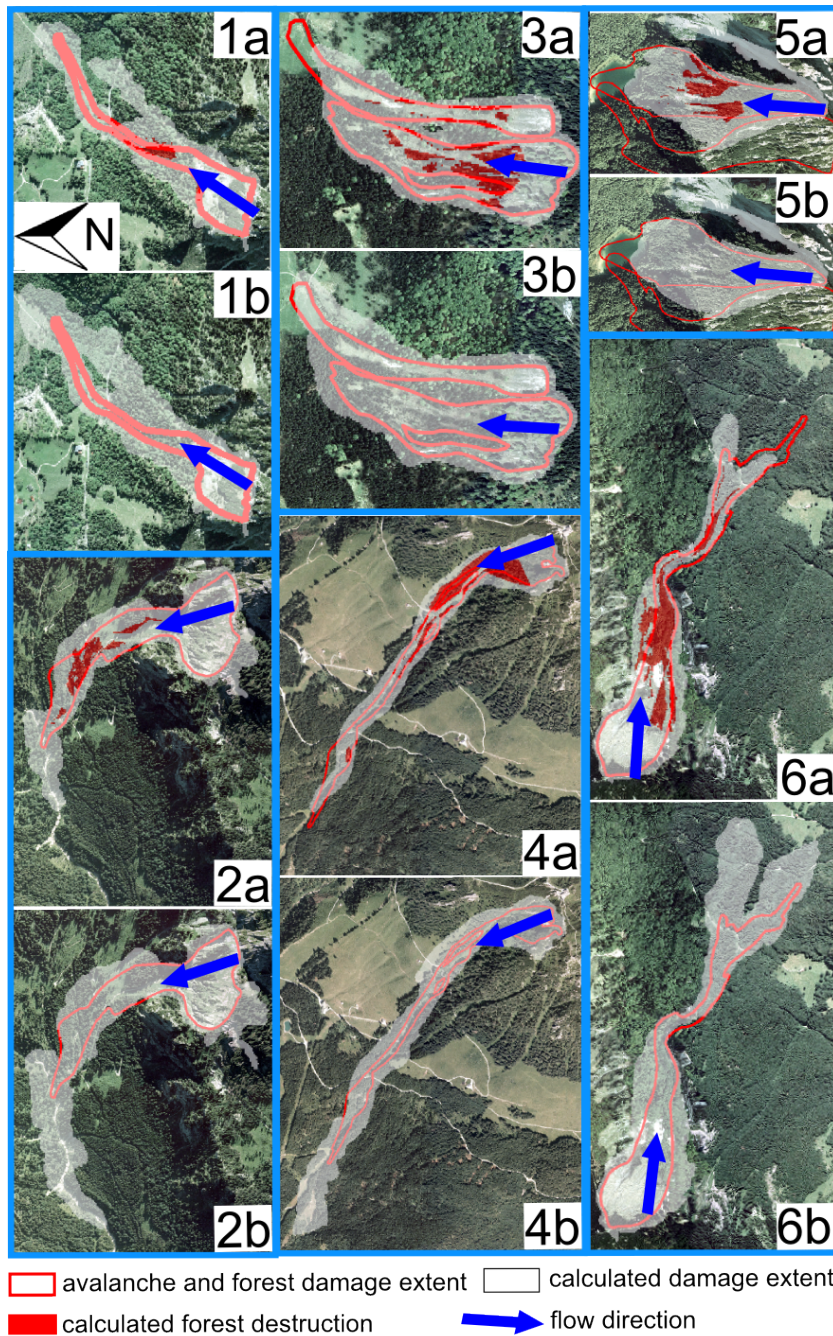


FIGURE 4.8: Simulation results for the dense flowing core for six avalanches with forest damage in Germany. The avalanches released at Wendelstein (1), Ahornalpe (2), Hochries (3), Spinnergraben (4), Frillensee (5) and Zwillingwand (6). In (a) forest was taken into account whereas (b) was modeled without forest. If bending stresses of the dry flowing core exceed the bending strength of trees (red areas) the turbulent friction increases and the avalanche is slowed down. Detrainment occurs if the avalanche enters a forest area without damaging the trees. Note that the runout is shortened significantly if forest is taken into account. Forest destruction is well modeled in the upper parts of the avalanche paths and is underestimated in the lower parts. Large powder clouds developed in the lower avalanche paths and probably caused extensive destruction (Geobasisdaten ©Bayerische Vermessungsverwaltung, Bayerisches Landesamt für Umwelt).

4.7). The simulated velocity north of the deflecting dam in the runout zone was  $20 < u_{\Pi} < 30$  m/s. We could therefore calculate the bending stresses  $\sigma_{\Pi}$  that were exerted by the powder cloud on both the destroyed and surviving larch trees ( $\rho_{\Pi} \approx 5$  kg/m<sup>3</sup>) (Table 4.4). The effective width  $w$  of the trees was small as the larches were leafless. For the destroyed tree (west) we found bending stresses  $\sigma_{\Pi} = 45$  MN/m<sup>2</sup> (see Fig. 4.7). For the two surviving trees, middle and east, we found  $\sigma_{\Pi} = 34$  MN/m<sup>2</sup> and  $\sigma_{\Pi} = 31$  MN/m<sup>2</sup>. In comparison, the dense flowing core exerted pressures  $\sigma_{\Phi}^d = 18$  MN/m<sup>2</sup> on the destroyed tree and  $\sigma_{\Phi} = 10$  MN/m<sup>2</sup> (middle) and  $\sigma_{\Phi} = 9$  MN/m<sup>2</sup> (east) on the two surviving larches (Table 4.4). Thus, in the runout zone the bending stresses from the powder cloud were larger than the bending stresses produced by the core. This result was duplicated in the German case studies, where the trees were mainly spruce. Bending stresses exerted by the powder cloud were larger than those of the dry core  $\sigma_{\Pi} > \sigma_{\Phi}^d$ .

TABLE 4.4: Bending stress  $\sigma$  and impact pressure  $p$  that was exerted on three larches in Täsch and one spruce in Monbiel (Figs. 4.6, 4.7) for constant slope angle  $\gamma = 25^\circ$  in Täsch and  $\gamma = 10^\circ$  for the avalanche in Monbiel. The drag coefficient was  $c_{\Phi} = 1.5$  for the avalanche core and  $c_{\Pi} = 0.4$  for the powder snow avalanche. For the CPM we assume  $c^* = 2$ ,  $N = 3.0$ . To calculate the stagnation height  $h_{\lambda}$  we chose  $\lambda = 1.5$  and  $b(h_{\Phi}, d) = 0.1$  according to the Swiss guidelines [Margreth, 2007]. To calculate the pressure with the SBM we assume a volume length  $l_v = 20$  m,  $\psi = 15^\circ$  and the friction on the ground or on the gliding surface  $\mu = 0.1$ . The trees in Täsch were approximately  $H = 28$  m (west),  $H = 30$  m (middle) and  $H = 32$  m (east) high and had a width  $w = 3$  m (west),  $w = 3$  m (middle) and  $w = 3$  m (east) [Indermühle, 1978]. The stem diameters of the larches in Täsch were  $d = 0.66$  m (west),  $d = 0.88$  m (middle) and  $d = 0.95$  m (east) and the stem diameter of the spruce in Monbiel was  $d = 0.75$  m.

Avalanche type	Location	$\rho$ [kg/m <sup>3</sup> ]	$H, h_{\Phi}$ [m]	$u$ [m/s]	$d$ [m]	$\sigma$ [MN/m <sup>2</sup> ]	$p$ [kN/m <sup>2</sup> ]
powder	Täsch west	5	28	20	0.66	45	< 1
	Täsch middle	5	30	25	0.88	34	< 1
	Täsch east	5	32	25	0.95	31	< 1
dry core	Täsch west	300	2	17	0.66	18	65
	Täsch middle	300	2	17	0.88	10	65
	Täsch east	300	2	17	0.95	9	65
wet (dynamic)		450	3	5	0.75	3	8
wet (CPM)	Monbiel	450	3	5	0.75	18	53
wet (SBM)		450	3	5	0.75	41	120

For the Monbiel case study, the standard dynamic pressure formula underestimated the forest damage over the entire slope, including the transition and runout zones. We therefore tested the three proposed approaches to calculate the wet snow pressure on the trees: (1) the sliding block model (SBM),  $\sigma_{\Phi}^w = 41$  MN/m<sup>2</sup>, (2) the creep pressure model (CPM),  $\sigma_{\Phi}^w = 18$  MN/m<sup>2</sup> and (3) the standard dynamic approach,  $\sigma_{\Phi}^d = 3$  MN/m<sup>2</sup>, assuming  $c_{\Phi} = 1.5$  (Table 4.4). For the SBM model a volume length of  $l_v = 20$  m is required to overcome the bending strength of spruces. The opening angle above the trees was taken to be only  $\psi = 15^\circ$ . Creep pressures were calculated assuming extreme gliding ( $N = 3$ ,  $c = 2$ ) according to the Swiss guidelines [Margreth, 2007]. Pressures exerted by the quasi-static SBM and CPM approaches were in general one magnitude larger than the pressure calculated with the dynamic approach. Forest damage by the

wet snow avalanche in Monbiel could not be simulated with velocity dependent pressure formulas. Even for  $c_{\Phi} = 5$ , is  $\sigma_{\Phi}^w < 30 \text{ MN/m}^2$  for velocities below 8 m/s. Wet snow, plug-like avalanches hardly exceed velocities of  $u_{\Phi}^w = 8 \text{ m/s}$ . Our calculations correspond to pressure measurements captured in the Vallee de la Sionne test site [Sovilla *et al.*, 2010, 2014], that could not be explained with dynamic drag terms.

## 4.5 Conclusions

To investigate how snow avalanches destroy forests, we developed four flow regime dependent impact formulas. These are *powder*, *intermittent*, *dry dense* and *wet dense*. The impact formulas were tested on two case studies in Switzerland, Monbiel and Täsch and six avalanches that released in Germany during the winter 2009. The formula parameters (flow velocity, density, height) were obtained from avalanche dynamics calculations and observations. The eight avalanche case studies consisted of seven dry mixed flowing avalanches and one wet snow avalanche. In all cases the forest damage was documented. The standard approach to predict forest damage is to calculate the pressure exerted by the core of a fast moving dry dense avalanche. This case can lead to widespread forest damage; however, it does not explain the damage caused by powder blasts or slow moving wet snow avalanches.

Dry, powder snow avalanches exert dynamic pressures on the tree stem and the crown. Although the applied impact pressures can be small (less than 3 kPa), bending stresses in the stem can be large due to the torque action of the blast. The impact pressure, cloud height and impact area must be taken into account to predict forest destruction. Destructive bending stresses can easily be reached even if the density of the snow-air mixture is low. The destructive potential depends on the crown area that is affected by the snow blast and not only on the velocity and density of the powder cloud. The crown area varies with tree position in the forest and on the foliage. Single, evergreen trees are exposed to the full avalanche blast and bending stresses are higher in comparison to leafless trees sheltered in clustered forest stands. The presence of deciduous conifer (larch) and broadleaf (birch) trees in an avalanche track is a possible indication of powder snow activity. These tree types can survive powder avalanche blasts because their effective crown areas are small, in contrast to evergreen trees.

The impact pressure formula for the intermittent case was derived by considering individual granule impacts. Interestingly, if we assume a homogeneous velocity and density distribution in the avalanche core, the formula is the same as the standard impact pressure formula used in practice. The density of the flow, however, is considerably smaller in the intermittent case. Therefore, the intermittent case seldom provides pressures higher than the dense case for dry avalanches. However, the intermittent impact formula should be modified to include the effect of particle clusters and uneven velocity distributions. This case could also be modified to include impacts caused by entrained woody debris or rocks. More real examples where these effects could be documented are needed to test a modified formula.

Destructive pressures of wet snow avalanches were back-calculated using two quasi-static modeling approaches, the “sliding block model” (SBM) and the “creep pressure model” (CPM). The results were compared to the standard dynamic approach used for dry snow avalanches. Dynamic models severely underestimated the applied pressures and cannot reproduce the bending stresses required for tree breakage. The sliding block model provided the highest bending stresses and the more realistic results. The creep pressure model underestimated the applied loading in the Monbiel case study. To apply the sliding block model, engineers must estimate the avalanche volume length  $l_v$  and the angle  $\psi$ , which depend on the location of the tree in the forest, terrain and avalanche dimensions. Unlike the dynamic impact loading, the intensity of the wet snow avalanche loading is therefore influenced by the spatial distribution of trees, terrain features and surface roughness. The loading cannot be determined exclusively from the avalanche flow parameters, but requires an understanding of the terrain features upstream of the tree. It is a statically indeterminate problem. Clearly, more case studies are required to validate this approach. However, our initial results suggest that the dynamic pressure can be neglected for large wet snow avalanches flowing with a velocity  $u_{\Phi}^w < 5\text{m/s}$ . Below this value, static pressures are at least a factor 10 larger than dynamic pressures.

A primary goal of our work is to underscore the importance of field surveys to document forest damage by avalanches. These surveys can provide valuable information on avalanche characteristics and return periods that are needed to formulate hazard scenarios. Broken trees serve as valuable sensors that record avalanche intensity. Our results, however, indicate that impact pressures on trees depend on the avalanche flow regime. For wet snow avalanches, the pressure additionally depends on the distribution of trees in the forest and on terrain features. By differentiating between four different avalanche flow regimes, a more inclusive and reliable analysis of forest damage is possible.

## Acknowledgements

This work was funded by the Bavarian Environment Agency. We would especially like to thank Armin Fischer from the Bavarian avalanche service who provided the data of the avalanche events in Bavaria. Leo Jörger and Christian Rüschi from the forest department in Randa and Klosters provided us with valuable information on the forest cover in Monbiel and Täsch and made the field work possible.



## 5. Discussion

At the onset of this dissertation, four key questions concerning forest-avalanche interaction were posed (Chapter 1). The results of the experimental, numerical and theoretical investigations carried out in this dissertation are now discussed in relation to existing literature.

1. *What physical processes prevent snow gliding in forests?*

There is general agreement that trees stabilize the snow cover on steep slopes and prevent snow gliding [McClung, 1975; Salm, 1978; Frey et al., 1987; Gubler and Rychetnik, 1991; Höller, 2001; Schneebeli and Bebi, 2004; Höller, 2014b]. However avalanches release in forest gaps. The maximum gap sizes mentioned by Gubler and Rychetnik [1991]; Frehner et al. [2005] and Teich et al. [2012a] to prevent avalanche formation are based on observations. The large discrepancy in the recommended maximum gap lengths (20 m to 200 m [Bebi et al., 2009]) arises from varying basal friction. Basal friction depends on the terrain and the vegetation cover in the gap. It has been identified as a crucial parameter in glide-snow avalanche formation in previous studies [In der Gand and Zupančič, 1966; Newsely et al., 2000; Leuenberger, 2003; McClung and Schaerer, 2006; Leitinger et al., 2008; Höller, 2012a]. Attempts to quantify basal friction theoretically [McClung, 1975; Salm, 1978; Höller, 2012b] and with measurements [Leitinger et al., 2008] have been performed. However, the magnitude of basal friction could never be linked to glide-snow avalanche release. To address this problem, the stauhwall/basal friction model developed by Bartelt et al. [2012b] was applied in Chapter 2 to assess the formation of glide-snow avalanches in forest gaps. Forest management guidelines that define a maximum allowable gap size were compared to glide-snow avalanche release thresholds supplied by the mechanical model. The calculations fit the guideline values only if the ground roughness is relatively high.

By applying the stauhwall model, a link between terrain characteristics (slope angle, roughness, friction, slab length) and the formation of glide-snow avalanches was accomplished. The stauhwall is fixed to the ground by trees at the lower edge of the forest gap and must fail for glide-snow avalanche release. The elastic and viscous mechanical properties of the snowpack are decisive parameters because they define the strength of the stauhwall. The assumption that a compressive zone within the snow cover (stauhwall) exists at the lower edge of a forest gap is

in accordance with previous studies. The application of the stauchwall model to investigate potential glide-snow avalanche formation is only possible if the exact location of the stauchwall and the extent of the release slab in uphill direction are known. Forest gaps, however, have well defined borders. Therefore an application of stauchwall mechanics for the definition of potential glide-snow avalanche release is justifiable. The basal friction values used in the modeling are minimum values derived from field observation of different terrain and vegetation types. As glide-snow avalanches tend to release at the same locations, the influence of terrain (slope angle, undulations) can be separated from the influence of vegetation type. By quantifying the influence of vegetation, it can be better managed to stabilize the snow cover or reduce potential release area size. In our investigations a wet soil surface was always assumed (Chapter 2). The prediction of an exact time of release remains difficult [Lackinger, 1987; Clarke and McClung, 1999; Reardon et al., 2006; Stimberis and Rubin, 2011; Peitzsch et al., 2012; Dreier, 2013] and was not addressed in this study.

2. *What is the influence of forest density and structure on avalanche dynamics? How can it be quantified?*

In existing avalanche models forest areas are characterized by increasing the value of the turbulent friction (friction approach) [Schaerer, 1973; Buser and Frutiger, 1980; Sampl and Zwinger, 2004; Takeuchi et al., 2011]. This friction approach is based on the assumption of forest destruction and was verified by calculations on the energy loss associated with tree breakage, overturning, uprooting and entrainment of woody debris in the avalanche flow [Bartelt and Stöckli, 2001]. The friction approach cannot explain the observed runout shortening of small avalanche events [Teich et al., 2012b, 2014], as an increase in turbulent friction does not lead to significant runout shortening as observed in field studies. In a first step, avalanche snow depositions in forest stands were observed and quantified in a field campaign that was carried out within the framework of this thesis. The avalanche deposition field is not homogeneous: wedge-like depositions behind tree stands were observed. The heterogeneous structure of the mountain forest appears to play a significant role in stopping avalanches. Significant snow mass detrainment behind tree stands appears to be the key process to stop small avalanches on steep slopes [McClung and Schaerer, 2006] (Chapter 3).

Modeling the avalanche stopping process in forests can be accomplished either by increasing friction or directly by removing mass from the avalanche. Both processes lead to a loss of avalanche flow momentum. The friction approach, however, is based on the assumption that woody debris entrainment is the primary physical mechanism causing the avalanche deceleration. This assumes the forest is destroyed. Because woody debris must be accelerated, the avalanche slows down. Detrainment is associated with the sudden stopping of snow clods by jamming and collisions. It results in instant loss of flow momentum, which is taken up by the tree/vegetation and is transferred directly to the ground. The trees are not destroyed. Therefore, entrainment of woody debris is dominant when trees are broken, uprooted and overturned; detrainment is dominant in forest stands where trees withstand the avalanche pressure.

The limits of forest destruction and non-destruction can usually be clearly distinguished. Forest boundaries are therefore a good indicator that there is a threshold value for the avalanche impact pressure that separates forest destruction from non-destruction. The dominant mechanism that stops small avalanches running through forests is the “drowning” due to the loss of avalanche mass. Structural parameters of forest control the amount of snow that is stopped. *Teich et al.* [2012a, 2014] showed in their statistical analysis of forest avalanche runouts that structural parameters of forest have a significant influence on runout shortening of small to medium size avalanches. By implementing the detrainment approach in avalanche dynamics modeling the snow mass that is extracted by remaining trees and the resulting runout shortening could be determined (Chapter 3). This approach was tested with RAMMS and enables the reconstruction of small and medium size forest-avalanche events. The application of the friction and the detrainment approach depends on forest damage. In Chapter 4, calculations of bending stresses on trees exerted by avalanches with four different flow regimes are presented. A threshold value for tree breakage is adapted from literature for certain tree species [*Peltola et al.*, 2000]. Forest destruction can be predicted if the flow regime of the avalanche and the stem diameter are considered.

In modeling forest-avalanche interaction, trees are often disregarded, especially if the avalanche is large and releases high above the tree line. To neglect forest for the simulation of extreme events with return periods of 300 or more years is a simplification but reasonable [*Christen et al.*, 2010a]. The protective function of forest may be strongly reduced due to forest fire, bark beetle outbreaks and due to secondary destructive avalanche events. In addition, an avalanche will only lose energy until the trees are broken and entrained. The increase in turbulent friction is therefore a local effect, constrained to the avalanche front where entrainment occurs. In this thesis, neglecting forest for hazard zoning is not questioned as forests cannot be treated as an everlasting terrain feature. However, *for the runout of small and frequent avalanches forest plays a crucial role.*

3. *How can forest-avalanche interaction be calculated and implemented in existing avalanche modeling systems?*

The friction and the detrainment approaches were implemented in the avalanche simulation program RAMMS. The friction approach is applied if the calculated bending stresses exceed the bending strength of the trees in a certain forest area. The user must define the tree species and an average stem diameter, which are the controlling parameters for forest destruction. The dynamic impact pressure of the avalanche is calculated from flow height, velocity and density for each grid cell. In the current version of RAMMS only bending stresses of the dry flowing avalanche core that act on the trees are calculated automatically. Importantly a more detailed physical description of different flow regimes will lead to further improvements. In the latest scientific version of RAMMS powder clouds, wet snow avalanches and the cohesive behavior of snow are implemented [*Bartelt et al.*, 2006; *Buser and Bartelt*, 2009; *Vera et al.*, in press; *Bartelt et al.*, accepted]. Forest destruction by avalanches depends on the flow regime, therefore these advances in avalanche modeling are important for the correct prediction of forest destruction.

The detrainment and friction approaches are applicable for any model extension and influence the avalanche dynamics according to the forest characteristics. Back-calculations of forest avalanche events in Switzerland, Germany, Austria, Norway, Slovakia and USA produced promising results regarding runout distance and forest destruction.

4. *What are the crucial forest parameters that define the protective effect against avalanches?*

For the release of glide-snow avalanches the basal friction assigned to the vegetation cover plays an important role. Four characteristic types of vegetation cover were identified on glide-snow avalanche release areas during a field study on the Dorfberg in Davos: long compacted grass, short upright grass, low dwarf shrubs and strong lignified shrubs. In the study of *Leitinger et al.* [2008] they found corresponding vegetation covers for managed and abandoned meadows and measured their static friction coefficients. The measures values were higher compared to the values that were found in Chapter 2. However, in this thesis a wet soil surface was assumed which decreases the basal friction significantly. Dead wood, small trees, rootstocks or stumps are characterized by high basal friction values. The minimum slab length for glide-snow avalanche release for a certain slope angle depends on the type of vegetation cover in combination with the underlying terrain. In general the basal friction of any kind of vegetation cover can be quantified and its influence on glide-snow avalanche formation can be calculated with the stauchwall model.

Basal friction and therefore ground roughness plays also an important role in stopping small and medium size avalanches. Additionally *Teich et al.* [2014] found forest type, crown closure, and vertical structure to be crucial forest parameters with a significant influence on the runout distance of avalanches. These parameters govern the amount of mass that is detraind by forest. They can be determined by forest managers for affected forest areas from orthoimages or field surveys and can then be delineated in RAMMS. Based on the study of *Teich et al.* [2014] and the results of Chapter 3, a dense, evergreen forest, with tree regeneration, dead wood and additional roughness elements is ideal in stopping small to medium size avalanches. The amount of snow that is detraind in a forest area then depends on these parameters. If trees are destroyed the friction approach can be applied but only in the moment of tree breakage and entrainment. Then the forest is destroyed and remains an area with increased surface roughness as stumps and rootstocks remain standing.

To predict forest damage, the tree species and stem diameter must be known. Knowledge of the exact impact area (low branches, width and height) would increase the performance of the calculations in Chapter 4, especially for powder snow avalanches. If trees are destroyed the friction approach is applied and forest structural parameters are of minor importance.

A combination of closed forest with adult trees that withstand high avalanche impact pressures and high ground roughness that prevents snow gliding is assumed to be the most effective forest against avalanches. Dead wood on the forest floor is useful in terms of glide-snow avalanche prevention and increases the ground

roughness also for small avalanches. If entrained by the avalanche though, it can cause even more destruction, for example when large tree stems flowing with the avalanche impact a building or power lines.



# 6. Conclusion

## 6.1 Overview of results

### 6.1.1 Vegetation effects on glide-snow avalanche release

How basal friction influences stauchwall failure and therefore glide-snow avalanche release is presented in Chapter 2. The main findings are:

1. The stauchwall model enables the prediction of slab failure and therefore the release of glide-snow avalanches.
2. Stauchwall mechanics link slope angle, slab length, snow cover characteristics and basal friction with glide-snow avalanche formation.
3. Basal friction depends on wetness, vegetation cover and topography and a minimum value for different terrain and vegetation height categories can be defined from observations.
4. The wide range of basal friction values for different vegetation covers is not addressed in existing avalanche prevention guidelines in Switzerland.
5. Modeling stauchwall failure allows the identification of potential glide-snow avalanche release areas in forest gaps.
6. Depending on the slope angle, even low vegetation can contribute to the prevention of avalanche formation .

### 6.1.2 Detrainment approach to model forest-avalanche interaction

A new approach to model forest-avalanche interaction is presented in Chapter 3. The main findings are:

1. There is field evidence that detrainment is the key process that leads to the runout shortening of small avalanches in forests.

2. The removal of avalanche snow by trees can be quantified and depends on forest structural parameters and on the avalanche velocity.
3. The stopping behavior of avalanches that run through forest without breaking or overturning trees can be modeled with the detrainment approach.
4. A one-parameter function describes avalanche snow detrainment by forest and allows the back-calculation of forest-avalanche events.

### 6.1.3 Tree breakage and avalanche flow regime

In Chapter 4 the complex and variable nature of avalanche flow is revealed by calculating tree breakage in reference to tree strength. The main findings are:

1. Bending stresses exerted by avalanches on trees depend on the avalanche flow regime.
2. Crown area is the crucial parameter to predict tree damage from powder snow avalanche blasts.
3. Bending stresses produced by wet snow avalanches cannot be described with velocity dependent pressure laws.
4. The Sliding Block Model (SBM) enables the calculation of static impact pressures of slow moving plug-like wet snow avalanches.
5. Stem diameter, tree species and crown area define the potential of trees to be damaged by avalanches.
6. Vegetation patterns in avalanche prone areas can be explained taking tree statics into account.

## 6.2 Main conclusions

The purpose of this thesis was to identify, understand and model the main processes involved in vegetation-avalanche interaction. Natural hazard and protection forest management should be supported in their decision-making process with practical tools that enable quantitative analysis. In this respect the main conclusions can be summarized as follows:

- Vegetation cover can hinder the formation of glide-snow avalanches by increasing the basal friction. Modeling the mechanical behavior of the stauhwall unites the main parameters for slab failure together: slope angle, slab length, snow cover properties and basal friction. By defining a threshold strain rate for slab failure, statements on the maximum allowable forest gap size for a certain slope angle and vegetation cover are possible. The benefit of avalanche mitigation measures such as timber jacks or piles of dead wood can therefore be evaluated.

- Snow detrainment by trees is the main process that leads to avalanche runout shortening. The amount of mass that is stopped depends on the forest structure and tree destruction. Modeling the runout distance of small to medium size avalanches that run through forest is possible with the detrainment approach.
- Tree breakage can only be calculated *if the avalanche flow regime is considered*. The bending stress exerted on a tree depends on the stem diameter, impact area, snow density, slope angle, velocity if dynamic impact is assumed and the terrain and stand characteristics if static impact is assumed. The degree of forest damage is used to distinguish between the application of a friction (forest destroyed, entrainment of woody debris) and detrainment approach (forest survives, mass caught behind trees).

Despite its protective function, forest and low lying vegetation can not hinder the formation of large, destructive avalanches that release high above the treeline. Trees are broken, uprooted and entrained into the avalanche flow, runout distances are hardly shortened and people and infrastructure are under considerable danger. Forest is an important avalanche hazard mitigation measure, especially in elevations between 1000 - 2200 m a.s.l., where most of the traffic routes and settlements are located in the European Alps. This thesis contributes insights to the complex physical interaction between a mechanical and a biological system, that is the movement of snow in forested terrain. In addition, novel calculation tools and model extensions are provided. These enable the quantification of the protective capacity of forests.



# 7. Applications and Outlook

## 7.1 Applications for avalanche hazard management in forested terrain

The stauchwall modeling approach presented in Chapter 2 can be used to delineate potential glide-snow avalanche release areas in forest gaps. Transitions of the vegetation cover, for example when managed meadows are abandoned and short upright grass develops to long compacted grass, can be implemented by decreasing the value of the basal friction. This will result in a shorter allowable gap length for constant slope angle and snow characteristics. Knowledge on the slope angle, gap length, vegetation cover and small-scale topography is required to calculate the strain rate of the stauchwall. The calculated strain rate can be compared to a threshold value for failure. The stauchwall model presented in Chapter 2 was calibrated with data from the Dorfberg in Davos only and further validation is recommended for the daily practical use. However, the necessity and effectiveness of glide-snow avalanche prevention measures such as timber jacks, piles of dead wood, root stocks and stems in upright or horizontal position can be evaluated with the stauchwall model. Existing guidelines on glide-snow prevention measures and forest management guidelines can be evaluated and extended. The theoretical description of the mechanical behavior of the stauchwall provides a physical explanation for the guidelines which are based on observations [Leuenberger, 2003; Frehner *et al.*, 2005]. The importance of shrubs, lying stems and rootstocks to prevent snow gliding can be demonstrated to forest managers.

If avalanche formation in forest gaps cannot be excluded, natural hazard- and forest management profit from assessing the deceleration and stopping of avalanches that run through forest below the gap. Therefore, the next step in evaluating the protective effect of forest stands is the simulation of forest-avalanche interaction. Characterization of forest effects on avalanche dynamics was restrained to increase the turbulent friction to account for the breakage, uprooting, overturning and entrainment of woody debris. The friction approach is limited to large avalanche events where forest damage can be assumed. Consideration of the mass removal by surviving trees was introduced in avalanche modeling by implementing a detrainment function in RAMMS in the framework of this thesis (Chapter 3). Detrainment depends on avalanche flow velocity and forest structural parameters. The detrainment coefficient  $K$  defines the amount of mass that

is removed during one time step on a certain grid cell. Areas with different forest cover characteristics are delineated by the RAMMS user. Practitioners distinguish between tree types (evergreen, leafless), crown coverage (dense, scattered, open) and surface roughness classes (rough, knobby, smooth) to determine the value for  $K$ . A look-up table was developed to simplify this procedure (see Fig. 7.1).

To distinguish between friction and detrainment approach one needs to know if forest is destroyed or not. Bending stresses that are exerted on trees by avalanches with different flow regimes were calculated and compared to the bending strength of certain tree species (Chapter 4). Impact pressures of the dry flowing core of an avalanche can be calculated and modeled in RAMMS with flow velocity, flow height and slope angle. To calculate the bending stress that acts on the tree one needs to specify the tree species and stem diameter. Forest areas can now be tested on their ability to withstand avalanche impact. The RAMMS user defines a representative stem diameter and the dominant tree species for a certain forest area that is affected by an avalanche and RAMMS calculates the resulting bending stresses. If the bending stresses exceed the bending strength of the trees, they are assumed to break, to be overturned and to be entrained in the avalanche flow. The friction approach is consequently applied for these areas for the first time step. Increased turbulent friction occurs until the woody debris is entrained. Subsequently an increased surface roughness caused by rootstocks, remnant stumps and woody debris remains and leads to moderate detrainment ( $K = 10 \text{ Pa}$ ). If the bending stress does not exceed the bending strength of the affected trees the detrainment approach is applied. Detrainment then depends on the forest structural parameters.

This model extension of RAMMS allows to calculate forest destruction, velocity reduction and runout shortening of avalanches. A powerful tool is provided to the RAMMS user that enables a detailed analysis of forest effects on avalanche dynamics. Consequences of changes in forest cover and forest structure by management interventions (clear-cuts, regeneration gaps) or natural disturbances can be evaluated. On the other hand afforestations and their potential to protect houses, roads and ski runs can be demonstrated.

## 7.2 Outlook

The well-established Voellmy-Salm model is used in Switzerland since decades and the calibrated friction parameters were constantly tested and evaluated with numerous back-calculations of large avalanche events. Extensive validation is necessary to guarantee a reliable model performance. The novel forest module in RAMMS was tested by back-calculating real avalanche events in Switzerland and Germany (Chapter 3, *Teich et al.* [2014]). Currently case studies from Norway, Austria, USA and Slovakia are simulated with RAMMS. Forest is characterized with increased turbulent friction and detrainment, and forest destruction is considered. The simulation results are promising and indicate the applicability of this model extension. However, further extensive testing is necessary to confirm that modeling results are resilient and that over- or underestimations of avalanche runouts and velocities can be eliminated. The forest extension of RAMMS was

Look-up table of K-values for forest shape files

Choose the characteristics of forest area to obtain the corresponding K-value or Code.

forest type	crown coverage*	roughness**	K-value***
evergreen/ mixed	dense (> 70%) coverage	rough (stumps/shrubs/saplings); height > 100 cm	48
		knobby (scree/stepped/seedlings); height 20 - 100 cm	38
		smooth (grass/leaves/smooth rock); height < 20 cm	28
	scattered, grouped (40% - 70%) coverage	rough (stumps/shrubs/saplings); height > 100 cm	43
		knobby (scree/stepped/seedlings); height 20 - 100 cm	33
		smooth (grass/leaves/smooth rock); height < 20 cm	23
	open (20% - 40%) coverage	rough (stumps/shrubs/saplings); height > 100 cm	38
		knobby (scree/stepped/seedlings); height 20 - 100 cm	28
		smooth (grass/leaves/smooth rock); height < 20 cm	18
larch / deciduous trees	dense (> 70%) coverage	rough (stumps/shrubs/saplings); height > 100 cm	35
		knobby (scree/stepped/seedlings); height 20 - 100 cm	25
		smooth (grass/leaves/smooth rock); height < 20 cm	15
	scattered, grouped (40% - 70%) coverage	rough (stumps/shrubs/saplings); height > 100 cm	30
		knobby (scree/stepped/seedlings); height 20 - 100 cm	20
		smooth (grass/leaves/smooth rock); height < 20 cm	10
	open (20% - 40%) coverage	rough (stumps/shrubs/saplings); height > 100 cm	25
		knobby (scree/stepped/seedlings); height 20 - 100 cm	15
		smooth (grass/leaves/smooth rock); height < 20 cm	5

\* Can be determined analysing orthophotos. Pictures below show example cases.

\*\* Quantity for ground roughness as well as small vegetation and dead wood in the avalanche path. Examples below.

\*\*\* K in [Pa] represents the braking power per square meter that the forest exerts on the avalanche flow. It can be chosen manually if forest structure is not clear or in between two classes.

Crown coverage:

dense



scattered, grouped



open



Roughness:

rough



knobby



smooth



Features of ground roughness should be present every few meters. If there are only few large obstacles the roughness can be classified as knobby.

FIGURE 7.1: K-value look-up table. Forest structures are specified with different values for the detrainment coefficient  $K$ .

provided to scientists and engineers in Europe and America to test its performance. An optimization of this model extension, for example with a procedure which was introduced by *Fischer* [2013] and *Teich et al.* [2014] would be of considerable value. The overall goal should be to implement detailed forest-avalanche interaction in RAMMS for all RAMMS users.

Large-scale experiments to determine the deceleration of avalanches in forests, to measure deposition volumes behind trees in detail and to study tree breakage would be of major importance. To perform such experiments is difficult though. Forest damage must be accepted and the repeatability cannot be guaranteed. The challenge of how to measure avalanche velocity in forest stands has not been solved yet. Laboratory experiments on the other hand could provide valuable indications on the avalanche flow behavior around trees. Granular chute experiments were performed at the SLF during the course of this thesis. Forest was introduced with treenails on a rough runout zone (Fig. 7.2). Preliminary results suggest that forest-like structures stop cohesive, wet granular material more effective than dry material. Details on the experimental setup and analysis on the stopping behavior of dry and wet granular material were summarized by *Carisch* [2013]. Back-calculations of the experiments with RAMMS and finite elements models could help to validate the governing parameters.



FIGURE 7.2: Deposition patterns of wet granular material stopping between forest-like treenails.

Tree breakage by powder clouds is influenced by the dynamical response of trees to avalanche impacts. The effect of the blast depends strongly on the mechanical response of the tree, which is characterized by the natural sway frequency (eigenfrequency) of the tree, which is given by the tree height, stiffness and mass distribution. To calculate and quantify this effect could improve predictions on the destructive power of powder snow avalanche blasts. In Chapter 4 the influence of the magnification factor was assumed to be approximately  $D = 1.7$ . A detailed analysis on the response of tree stems on avalanche blasts would help to understand forest destruction and to precisely quantify the impact of powder clouds.

A further calibration of the stauchwall model to predict glide-snow avalanche formation could help to establish a tool for practitioners. To gain basal friction values for more characteristic vegetation covers, field studies are needed. The basal friction values that are mentioned in Chapter 2 are based on observations that were carried out on the Dorfberg in Davos. They are good indicators but for a validation, more data from different study sites would be necessary. A simple calculator for practitioners where slope angle, slab length and basal friction (topographic features in combination with vegetation cover) must be specified, could be the goal for an operationalization of the stauchwall model. The output would be a statement on the potential release of glide-snow avalanches (yes or no).

In this thesis new modeling approaches are presented that enable the mathematical description of the interaction and interference of a mechanical and a biological system. Whereas further calibration and validation are required for a final operationalization, the collected data confirms the newly developed model approaches. Forest-avalanche interaction continues to be a highly complex research area and further studies must be carried out to fully understand and quantify all involved processes. I hope that the findings and new approaches, presented in this thesis will help to answer the most urgent questions and provide the basis for further investigations.



# Bibliography

- Ammer, C., 1996: Impact of ungulates on structure and dynamics of natural regeneration of mixed mountain forests in the Bavarian Alps. *Forest Ecology and Management*, **88** (1), 43–53.
- Anderson, G. and D. McClung, 2012: Snow avalanche penetration into mature forest from timber-harvested terrain. *Canadian Geotechnical Journal*, **49** (4), 477–484.
- Austrian Standard Institute, 2011: *ONR 24806 - Permanenter technischer Lawinenschutz - Bemessung und konstruktive Ausgestaltung*.
- BAFU, 2008: *Sturmschaden-Handbuch. Vollzugshilfe für die Bewältigung von Sturmschadenereignissen von nationaler Bedeutung im Wald*. Bundesamt für Umwelt, Bern. 3. überarbeitete Auflage.
- Barbeito, I., R. L. Brücker, C. Rixen, and P. Bebi, 2013: Snow fungi-induced mortality of *Pinus cembra* at the alpine treeline: evidence from plantations. *Arctic, Antarctic, and Alpine Research*, **45** (4), 455–470.
- Baroudi, D., B. Sovilla, and E. Thibert, 2011: Effects of flow regime and sensor geometry on snow avalanche impact-pressure measurements. *Journal of Glaciology*, **57** (202), 277–288.
- Bartelt, P., Y. Bühler, O. Buser, M. Christen, and L. Meier, 2012a: Modeling mass-dependent flow regime transitions to predict the stopping and depositional behavior of snow avalanches. *Journal of Geophysical Research-earth Surface*, **117**, F01015.
- Bartelt, P., O. Buser, and K. Platzer, 2006: Fluctuation–dissipation relations for granular snow avalanches. *Journal of Glaciology*, **52** (179), 631–643.
- Bartelt, P., T. Feistl, Y. Bühler, and O. Buser, 2012b: Overcoming the stauchwall: Viscoelastic stress redistribution and the start of full-depth gliding snow avalanches. *Geophysical Research Letters*, **39** (L16501), 16.
- Bartelt, P., J. Glover, T. Feistl, Y. Bühler, and O. Buser, 2012c: Formation of levees and en-echelon shear planes during snow avalanche run-out. *Journal of Glaciology*, **58** (211), 980–992.
- Bartelt, P., L. Meier, and O. Buser, 2011: Snow avalanche flow-regime transitions induced by mass and random kinetic energy fluxes. *Annals of Glaciology*, **52**, 159–164.

- Bartelt, P., L. B. Salm, and U. Gruber, 1999: Calculating dense-snow avalanche runout using a Voellmyfluid model with active/passive longitudinal straining. *Journal of Glaciology*, **45** (150), 242–254.
- Bartelt, P. and V. Stöckli, 2001: The influence of tree and branch fracture, overturning and debris on snow avalanche flow. *Annals of Glaciology*, **32**, 209–216.
- Bartelt, P., C. Vera, T. Feistl, M. Christen, Y. Bühler, and O. Buser, accepted: A model of cohesion in snow avalanche flow. *Journal of Glaciology*.
- Bebi, P., F. Kienast, and W. Schönenberger, 2001: Assessing structures in mountain forests as a basis for investigating the forests dynamics and protective function. *Forest Ecology and Management*, **145**, 3–14.
- Bebi, P., D. Kulakowski, and C. Rixen, 2009: Snow avalanche disturbances in forest ecosystems—State of research and implications for management. *Forest Ecology and Management*, **257**, 1883–1892.
- Berger, F., C. Quetel, and L. K. Dorren, 2002: Forest: a natural protection mean against rockfalls, but with which efficiency. *International Congress Interpraevent*, 815–826.
- Bovet, E., B. Chiaia, and B. Frigo, 2011: Modelling and testing of avalanche impact on structures. *Proceedings XX Congresso AIMETA*.
- Bozhinskiy, A. and K. Losev, 1998: *The fundamentals of avalanche science*. Mitteilungen Eidgenössisches Institut für Schnee- und Lawinenforschung SLF, Davos, 280 pp.
- Brändli, U., 2010: Schweizerisches Landesforstinventar: Ergebnisse der dritten Erhebung 2004–2006: Birmensdorf, Eidgenössische Forschungsanstalt für Wald, Schnee und Landschaft WSL. Bern, Bundesamt für Umwelt, BAFU.
- Brang, P., W. Schönenberger, M. Frehner, R. Schwitter, J.-J. Thormann, and B. Wasser, 2006: Management of protection forests in the European Alps: an overview. *Forest Snow Landscape Research*, **80**, 23–44.
- Briukhanov, A., S. Grigorian, S. Miagkov, M. Y. Plam, I. Y. Shurova, M. Eglit, and Y. L. Yakimov, 1967: On some new approaches to the dynamics of snow avalanches. *Physics of Snow and Ice: proceedings*, **1** (2), 1223–1241.
- Bründl, M., P. Bartelt, M. Schneebeli, and H. Flühler, 1999: Measuring branch deflection of spruce branches caused by intercepted snow load. *Hydrological Processes*, **13** (14-15), 2357–2369.
- Bühler, Y., M. Christen, J. Kowalski, and P. Bartelt, 2011: Sensitivity of snow avalanche simulations to digital elevation model quality and resolution. *Annals of Glaciology*, **52** (58), 72–80.
- Bühler, Y., M. Marty, and C. Ginzler, 2012: High resolution DEM generation in high-alpine terrain using airborne remote sensing techniques. *Transactions in GIS*, **16** (5), 635–647.

- Bürki, A. F., 1981: Bestandesstrukturen im Gebirgsfichtenwald. Ph.D. thesis, Eidgenössische Technische Hochschule Zürich.
- Buser, O. and P. Bartelt, 2009: Production and decay of random kinetic energy in granular snow avalanches. *Journal of Glaciology*, **55** (189), 3–12.
- Buser, O. and P. Bartelt, submitted: Streamwise density variations in a granular flow. *Journal of Glaciology*.
- Buser, O. and H. Frutiger, 1980: Observed maximum run-out distance of snow avalanches and the determination of the friction coefficients  $\mu$  and  $\xi$ . *Journal of Glaciology*, **26**, 121–130.
- Butler, D. R., 1979: Snow avalanche path terrain and vegetation, Glacier National Park, Montana. *Arctic and Alpine Research*, **11**, 17–32.
- Carisch, L., 2013: Stopping behavior of dry and wet granular avalanches. M.S. thesis, Eidgenössische Technische Hochschule Zürich.
- Casteller, A., M. Christen, R. Villalba, H. Martinez, V. Stöckli, J. C. Leiva, and P. Bartelt, 2008: Validating numerical simulations of snow avalanches using dendrochronology: the Cerro Ventana event in Northern Patagonia, Argentina. *Natural Hazards and Earth System Sciences*, **8**, 433–443.
- Casteller, A., R. Villalba, D. Araneo, and V. Stöckli, 2011: Reconstructing temporal patterns of snow avalanches at Lago del Desierto, southern Patagonian Andes. *Cold Regions Science and Technology*, **67** (1), 68–78.
- Christen, M., P. Bartelt, and U. Gruber, 2002: Aval-1d: An avalanche dynamics program for the practice. *International Congress Interpraevent*, 715–725.
- Christen, M., P. Bartelt, and J. Kowalski, 2010a: Back calculation of the In den Arenen avalanche with RAMMS: interpretation of model results. *Annals of Glaciology*, **51** (54), 161–168.
- Christen, M., J. Kowalski, and P. Bartelt, 2010b: RAMMS: Numerical simulation of dense snow avalanches in three-dimensional terrain. *Cold Regions Science and Technology*, **63** (1), 1–14.
- Clarke, J. and D. McClung, 1999: Full-depth avalanche occurrences caused by snow gliding, Coquihalla, British Columbia, Canada. *Journal of Glaciology*, **45** (151), 539–546.
- Clough, R. W. and J. Penzien, 1975: *Dynamics of structures*. Mc Gray-Hill, Incorporated.
- Corona, C., J. Lopez Saez, M. Stoffel, M. Bonnefoy, D. Richard, L. Astrade, and F. Berger, 2012: How much of the real avalanche activity can be captured with tree rings? An evaluation of classic dendrogeomorphic approaches and comparison with historical archives. *Cold Regions Science and Technology*, **74**, 31–42.

- Coutts, M., 1983: Root architecture and tree stability. *Plant and Soil*, **71** (1-3), 171–188.
- de Quervain, M., 1978: Wald und Lawinen. *Proceedings of the IUFRO Seminar Mountain Forests and Avalanches, Davos, Switzerland*, 219–231.
- de Quervain, M. and B. Salm, 1963: *Lawinenverbau im Anbruchgebiet: Kommentar zu den Richtlinien für den permanenten Stützverbau vom Februar 1961*. Eidg. Inspektion für Forstwesen.
- Dorren, L. K. and F. Berger, 2006: Stem breakage of trees and energy dissipation during rockfall impacts. *Tree Physiology*, **26** (1), 63–71.
- Dorren, L. K., F. Berger, C. le Hir, E. Mermin, and P. Tardif, 2005: Mechanisms, effects and management implications of rockfall in forests. *Forest Ecology and Management*, **215** (1), 183–195.
- Dorren, L. K. A., F. Berger, A. C. Imeson, B. Maier, and F. Rey, 2004: Integrity, stability and management of protection forests in the European Alps. *Forest Ecology and Management*, **195**, 165–176.
- Dreier, L., 2013: Einfluss von Wetter und Gelände auf Gleitschneelawinen. M.S. thesis, Friedrich-Alexander-Universität Erlangen-Nürnberg.
- Dreier, L., Y. Bühler, C. Ginzler, and P. Bartelt, submitted: Comparison of simulated powder snow avalanches with photogrammetric measurements. *Annals of Glaciology*.
- Dreier, L., Y. Bühler, W. Steinkogler, T. Feistl, and P. Bartelt, 2014: Modelling small and frequent avalanches. *Proceedings of the International Snow Science Workshop, Banff, Canada*.
- Dreier, L., C. Mitterer, S. Feick, and S. Harvey, 2013: The influence of weather on glide-snow avalanches. *Proceedings of the International Snow Science Workshop, Grenoble, France*.
- EAWS, 2013: *European avalanche size classification*. <http://www.avalanches.org>, URL [www.avalanches.org](http://www.avalanches.org).
- Faug, T., B. Chanut, R. Beguin, M. Naaim, E. Thibert, and D. Baroudi, 2010: A simple analytical model for pressure on obstacles induced by snow avalanches. *Annals of Glaciology*, **51** (54), 1–8.
- Faug, T., B. Chanut, M. Naaim, and B. Perrin, 2008: Avalanches overflowing a dam: dead zone, granular bore and run-out shortening. *Annals of Glaciology*, **49** (1), 77–82.
- Faug, T., M. Naaim, D. Bertrand, P. Lachamp, and F. Naaim-Bouvet, 2003: Varying dam height to shorten the run-out of dense avalanche flows: Developing a scaling law from laboratory experiments. *Surveys in Geophysics*, **24** (5-6), 555–568.
- Faug, T., M. Naaim, and F. Naaim-Bouvet, 2004: Experimental and numerical study of granular flow and fence interaction. *Annals of Glaciology*, **38** (1), 135–138.

- Feistl, T., 2010: Schneehöhenverteilung im bayerischen Alpenraum: Die Durchführung einer Messkampagne zur kleinräumigen Analyse. M.S. thesis, Ludwigs-Maximilians-Universität München.
- Feistl, T., P. Bebi, L. Dreier, M. Hanewinkel, and P. Bartelt, 2014a: Quantification of basal friction for technical and silvicultural glide-snow avalanche mitigation measures. *Natural Hazards and Earth System Sciences*, **14** (4), 2921–2931.
- Feistl, T., P. Bebi, M. Teich, Y. Bühler, M. Christen, K. Thuro, and P. Bartelt, 2014b: Observations and modeling of the braking effect of forests on small and medium avalanches. *Journal of Glaciology*, **60** (219), 124–138.
- Fiebiger, G., 1978: Ursachen von Waldlawinen im Bereich der nordöstlichen Randalpen und ihre Behandlung durch forsttechnische Massnahmen. Ph.D. thesis, Universität für Bodenkultur, Wien.
- Fischer, J.-T., 2013: A novel approach to evaluate and compare computational snow avalanche simulation. *Natural Hazards and Earth System Science*, **13** (6), 1655–1667.
- Fischer, J.-T., J. Kowalski, and S. Pudasaini, 2012: Topographic curvature effects in applied avalanche modeling. *Cold Regions Science and Technology*, **74–75**, 21–30.
- Frehner, M., B. Wasser, and R. Schwitter, 2005: Nachhaltigkeit und Erfolgskontrolle im Schutzwald. *Wegleitung für Pflegemassnahmen in Wäldern mit Schutzfunktion, Vollzug Umwelt. Bundesamt für Umwelt, Wald und Landschaft, Bern*, **564**.
- Frey, W., H. Frutiger, W. Good, F. T., and M. Kimura, 1987: Openings in the forest caused by forest deperishment and their influence on avalanche danger. In: *Human Impacts and Management of Mountain Forests*, 223–238.
- Frey, W. and P. Thee, 2002: Avalanche protection of windthrow areas: A ten year comparison of cleared and uncleared starting zones. *Forest Snow Landscape Research*, **77** (1), 2.
- Gellrich, M., P. Baur, B. Koch, and N. E. Zimmermann, 2007: Agricultural land abandonment and natural forest re-growth in the Swiss mountains: a spatially explicit economic analysis. *Agriculture, Ecosystems & Environment*, **118** (1), 93–108.
- Germain, D., L. Filion, and B. Hétu, 2005: Snow avalanche activity after fire and logging disturbances, northern Gaspé Peninsula, Quebec, Canada. *Canadian Journal of Earth Sciences*, **42** (12), 2103–2116.
- Götz, K., 2000: Die innere Optimierung der Bäume als Vorbild für technische Faserverbunde-eine lokale Approximation. Tech. rep., Forschungszentrum Karlsruhe.
- Gray, J., Y.-C. Tai, and S. Noelle, 2003: Shock waves, dead zones and particle-free regions in rapid granular free-surface flows. *Journal of Fluid Mechanics*, **491**, 161–181.
- Grosser, D. and W. Teetz, 1985: Einheimische Nutzhölzer. Tech. rep., Centrale Marketinggesellschaft der deutschen Agrarwirtschaft GmbH (CMA), Bonn, und Arbeitsgemeinschaft Holz e. V., Düsseldorf.

- Gruber, U. and P. Bartelt, 2007: Snow avalanche hazard modelling of large areas using shallow water numerical methods and GIS. *Environmental Modelling & Software*, **22** (10), 1472–1481.
- Gubler, H. and J. Rychetnik, 1991: Effects of forests near timberline on avalanche formation. *Snow, Hydrology and Forests in High Alpine Areas*, **205**, 19–38.
- Häfeli, R., 1967: Kriechen und progressiver Bruch in Schnee, Boden, Fels und Eis. *Schweizerische Bauzeitung*, **85** (1), 1–9.
- Hauksson, S., M. Pagliardi, M. Barbolini, and T. Johannesson, 2007: Laboratory measurements of impact forces of supercritical granular flow against mast-like obstacles. *Cold Regions Science and Technology*, **49** (1), 54–63.
- Höller, P., 2001: Snow gliding and avalanches in a south-facing larch stand. *IAHS Publ.*, **270** (270), 355–358.
- Höller, P., 2004: Untersuchungen zum Schneegleiten in einem Lärchenwald nahe der Waldgrenze. *BFW-Berichte*, Bundesministerium für Land- und Forstwirtschaft Umwelt und Wasserwirtschaft.
- Höller, P., 2012a: On the identification of snow gliding areas and planning of control measures to protect high-altitude afforestations. *Allgemeine Forst- und Jagdzeitung*, **183** (5/6), 94–100.
- Höller, P., 2012b: Zur Bestimmung schneegleitgefährdeter Standorte und Planung von Gleitschutzmaßnahmen und Hochlagenaufforstungen. *Allg. Forst und Jagdzeitschrift*, **183**, 94–100.
- Höller, P., 2014a: Snow gliding and glide avalanches: a review. *Natural Hazards*, **71** (71), 1259–1288.
- Höller, P., 2014b: Snow gliding on a south-facing slope covered with larch trees. *Annals of Forest Science*, **71** (1), 81–89.
- Höller, P., R. Fromm, and G. Leitinger, 2009: Snow forces on forest plants due to creep and glide. *Forest Ecology and Management*, **257** (2), 546 – 552.
- Imbeck, H., 1984: Lawinenbildung im Wald und deren Wirkung im Raum Davos. Tech. rep., Eidgenössisches Institut für Schnee- und Lawinenforschung SLF, Davos.
- Imbeck, H., 1987: Schneeprofile im Wald. *Schnee und Lawinen in den Schweizer Alpen Winter 1985/1986. Winterbericht des Eidgenössisches Instituts für Schnee- und Lawinenforschung EISLF. 50:177-183.*
- Imbeck, H. and M. Meyer-Grass, 1988: Waldlawinen am Gugelberg. *Schweizer Zentrales Forstwesen*, **139**, 145–152.
- In der Gand, H. and M. Zupančič, 1966: Snow gliding and avalanches. *IAHS-AISH Publ.*, **69**, 230–242.

- Indermühle, M., 1978: Struktur-, Alters- und Zuwachsuntersuchungen in einem Fichten-Plenterwald der subalpinen Stufe. Ph.D. thesis, Eidgenössische Technische Hochschule Zürich.
- Johannesson, T., P. Gauer, P. Issler, and K. Lied, 2009: *The design of avalanche protection dams. Recent practical and theoretical developments*, chap. 12, 95–107. European Commission.
- Johnson, E. A., 1987: The relative importance of snow avalanche disturbance and thinning on canopy plant populations. *Ecology*, **68** (1), pp. 43–53.
- Jonsson, M., A. Foetzki, M. Kalberer, T. Lundström, W. Ammann, and V. Stöckli, 2006: Root-soil rotation stiffness of Norway spruce (*Picea abies* (L.) Karst) growing on subalpine forested slopes. *Plant and Soil*, **285** (1-2), 267–277.
- Kajimoto, T., H. Daimaru, T. Okamoto, T. Otani, and H. Onodera, 2004: Effects of snow avalanche disturbance on regeneration of subalpine *Abies mariesii* forest, northern Japan. *Arctic, Antarctic, and Alpine Research*, **36** (4), 436–445.
- Kazakova, E. and V. Lobkina, 2013: Distribution of the population and enterprises in avalanche-hazardous zones of Sakhalin oblast. *Geography and Natural Resources*, **34** (4), 345–349.
- Kienholz, R., 1940: Frost depth in forest and open in Connecticut. *Journal of Forestry*, **38** (4), 346–350.
- Konetschny, H., 1990: *Schneebewegungen und Lawinentätigkeit in zerfallenen Bergwäldern*. Bayerisches Landesamt für Wasserwirtschaft.
- Kozik, S., 1962: Calculation of movement of snow avalanches. *Gidrometeoizdat, Leningrad*.
- Kräuchi, N., P. Brang, and W. Schönenberger, 2000: Forests of mountainous regions: gaps in knowledge and research needs. *Forest Ecology and Management*, **132** (1), 73–82.
- Kupferschmid Albisetti, A. D., P. Brang, W. Schönenberger, and H. Bugmann, 2003: Decay of *Picea abies* snag stands on steep mountain slopes. *The Forestry Chronicle*, **79** (2), 247–252.
- Lackinger, B., 1987: Stability and fracture of the snow pack for glide avalanches. *International Association of Hydrological Sciences Publication*, **162**, 229–240.
- Lang, T. E. and R. L. Brown, 1980: Snow avalanche impact on structures. *Journal of Glaciology*, **25** (93), 445–455.
- Lavers, G. M., 1983: *The strength properties of timber, Building Research Establishment Report, 3rd edition*,. Her Majesty's Stationery Office, London.
- Leitinger, G., P. Höller, E. Tasser, J. Walde, and U. Tappeiner, 2008: Development and validation of a spatial snow-glide model. *Ecological Modelling*, **211** (34), 363 – 374.

- Leuenberger, F., 2003: Bauanleitung Gleitschneeschutz und temporärer Stützverbau. Tech. rep., Eidgenössisches Institut für Schnee- und Lawinenforschung SLF, Davos.
- Löfvenius, M. O., M. Kluge, and T. Lundmark, 2003: Snow and soil frost depth in two types of shelterwood and a clear-cut area. *Scandinavian Journal of Forest Research*, **18** (1), 54–63.
- Logan, J. A., J. Regniere, and J. A. Powell, 2003: Assessing the impacts of global warming on forest pest dynamics. *Frontiers in Ecology and the Environment*, **1** (3), 130–137.
- Losey, S. and A. Wehrli, 2013: Schutzwald in der Schweiz. *Vom Projekt SilvaProtect-CH zum harmonisierten Schutzwald*. Bundesamt für Umwelt, Bern.
- Lundström, T., M. J. Jonsson, A. Volkwein, and M. Stoffel, 2009: Reactions and energy absorption of trees subject to rockfall: a detailed assessment using a new experimental method. *Tree Physiology*, **29** (3), 345–359.
- MacKinney, A., 1929: Effects of forest litter on soil temperature and soil freezing in autumn and winter. *Ecology*, **10** (3), 312–321.
- Maggioni, M., M. Freppaz, M. Christen, P. Bartelt, and E. Zanini, 2012: Back calculation of small avalanches with the 2D avalanche dynamics model RAMMS: Four events artificially triggered at the Seehore test site in Aosta Valley (NW-Italy). *Proceedings of the International Snow Science Workshop*, Anchorage, Alaska.
- Margreth, S., 2004: Die Wirkung des Waldes bei Lawinen. *Forum für Wissen*, 21–26.
- Margreth, S., 2007: Lawinenverbau im Anbruchgebiet. *Technische Richtlinie als Volzugshilfe*. Bundesamt für Umwelt, Bern.
- Margreth, S., A. Burkard, and H. Buri, 2008: Teil b: Lawinen. *Wirkung von Schutzmassnahmen*. National Platform for Natural Hazards PLANAT, Bern, 1–51.
- Matsushita, H., M. Matsuzawa, and H. Nakamura, 2012: Possibility of increasing the slope distance between avalanche prevention bridges. *Proceedings of the International Snow Science Workshop*, Anchorage, Alaska.
- Mattheck, C. and H. Breloer, 1994: *Handbuch der Schadenskunde von Bäumen: Der Baumbruch in Mechanik und Rechtsprechung*. Rombach.
- Mayhead, G., 1973: Some drag coefficients for British forest trees derived from wind tunnel studies. *Agricultural Meteorology*, **12**, 123–130.
- McClung, D., 1975: Creep and the snow-earth interface condition in the seasonal alpine snowpack. *IAHS-AISH Publ*, **114**, 236–248.
- McClung, D. and P. Schaerer, 1985: Characteristics of flowing snow and avalanche impact pressures. *Annals of Glaciology*, **6**, 9–14.
- McClung, D. and P. Schaerer, 2006: *The avalanche handbook*. The Mountaineers Books.

- McClung, D., S. Walker, and W. Golley, 1994: Characteristics of snow gliding on rock. *Annals of Glaciology*, **19**, 97–97.
- Mears, A. I., 1975: Dynamics of dense-snow avalanches interpreted from broken trees. *Geology*, **3** (9), 521–523.
- Mellor, M., 1974: *A review of basic snow mechanics*. US Army Cold Regions Research and Engineering Laboratory.
- Meyer-Grass, M. and M. Schneebeli, 1992: Die Abhängigkeit der Waldlawinen von Standorts-, Bestandes-, und Schneesverhältnissen. *Internationales Symposium Interpraevent - Bern*.
- Mitterer, C., H. Hirashima, and J. Schweizer, 2011: Wet-snow instabilities: comparison of measured and modelled liquid water content and snow stratigraphy. *Annals of Glaciology*, **52** (58), 201–208.
- Naaim, M., T. Faug, and F. Naaim-Bouvet, 2003: Dry granular flow modelling including erosion and deposition. *Surveys in Geophysics*, **24** (5-6), 569–585.
- Naaim, M., T. Faug, E. Thibert, N. Eckert, G. Chambon, F. Naaim, and H. Bellot, 2008: Snow avalanche pressure on obstacles. *Proceedings of the International Snow Science Workshop, Whistler, Canada*.
- Naaim, M., F. Naaim-Bouvet, T. Faug, and A. Bouchet, 2004: Dense snow avalanche modeling: flow, erosion, deposition and obstacle effects. *Cold Regions Science and Technology*, **39** (2-3), 193–204.
- Newesely, C., E. Tasser, P. Spadinger, and A. Cernusca, 2000: Effects of land-use changes on snow gliding processes in alpine ecosystems. *Basic and Applied Ecology*, **1** (1), 61–67.
- Norem, H., 1991: Estimating snow avalanche pressures on towers. *Proceedings of a Workshop on Avalanche Dynamics*.
- Olschewski, R., P. Bebi, M. Teich, U. Wissen Hayek, and A. Grêt-Regamey, 2012: Avalanche protection by forests - A choice experiment in the Swiss Alps. *Forest Policy and Economics*, **17**, 19–24.
- Pedersen, R., J. Dent, and T. Lang, 1979: Forces on structures impacted and enveloped by avalanches. *Journal of Glaciology*, **22** (88), 529–534.
- Peitzsch, E. H., J. Hendrikx, D. B. Fagre, and B. Reardon, 2012: Examining spring wet slab and glide avalanche occurrence along the Going-to-the-Sun Road corridor, Glacier National Park, Montana, USA. *Cold Regions Science and Technology*, **78**, 73–81.
- Peltola, H. and S. Kellomäki, 1993: A mechanistic model for calculating windthrow and stem breakage of Scots pines at stand edge. *Silva Fennica*, **24-31**.
- Peltola, H., S. Kellomäki, A. Hassinen, and M. Granander, 2000: Mechanical stability of Scots pine, Norway spruce and birch: an analysis of tree-pulling experiments in Finland. *Forest Ecology and Management*, **135** (1), 143–153.

- Peltola, H., S. Kellomäki, H. Väisänen, and V.-P. Ikonen, 1999: A mechanistic model for assessing the risk of wind and snow damage to single trees and stands of Scots pine, Norway spruce, and birch. *Canadian Journal of Forest Research*, **29** (6), 647–661.
- Peltola, H., M.-L. Nykänen, and S. Kellomäki, 1997: Model computations on the critical combination of snow loading and windspeed for snow damage of Scots pine, Norway spruce and birch sp. at stand edge. *Forest Ecology and Management*, **95** (3), 229–241.
- Platzer, K., P. Bartelt, and M. Kern, 2007: Measurements of dense snow avalanche basal shear to normal stress ratios (S/N). *Geophysical Research Letters*, **34** (7).
- Podolskiy, E. A., K. Izumi, V. E. Suchkov, and N. Eckert, 2014: Physical and societal statistics for a century of snow-avalanche hazards on Sakhalin and the Kuril Islands (1910–2010). *Journal of Glaciology*, **60** (221), 409.
- Potter, N., 1969: Tree-ring dating of snow avalanche tracks and the geomorphic activity of avalanches, northern Absaroka Mountains, Wyoming. *Geological Society of America Special Papers*, **123**, 141–166.
- Pretzsch, H., 2014: Canopy space filling and tree crown morphology in mixed-species stands compared with monocultures. *Forest Ecology and Management*, **327**, 251–264.
- Ragaz, C., 1972: *Lawinenschutz in der Schweiz*, chap. 16, 211–219. Zeitschrift des Bündner Forstvereins SELVA.
- Rammig, A., L. Fahse, P. Bebi, and H. Bugmann, 2007: Wind disturbance in mountain forests: Simulating the impact of management strategies, seed supply, and ungulate browsing on forest succession. *Forest Ecology and Management*, **242** (2), 142–154.
- Reardon, B. A., D. B. Fagre, M. Dundas, and C. Lundy, 2006: Natural Glide Slab Avalanches, Glacier National Park, USA: a unique hazard and forecasting challenge. *Proceedings of the International Snow Science Workshop, Telluride, Colorado*.
- Rixen, C., S. Haag, D. Kulakowski, and P. Bebi, 2007: Natural avalanche disturbance shapes plant diversity and species composition in subalpine forest belt. *Journal of Vegetation Science*, **18** (5), 735–742.
- Salm, B., 1977: Snow forces. *Journal of Glaciology*, **19**(81), 67 – 100.
- Salm, B., 1978: Snow forces on forest plants. *Mountain Forests and Avalanches*, 157–181.
- Salm, B., 1982: Mechanical properties of snow. *Reviews of Geophysics*, **20** (1), 1–19.
- Salm, B., 1993: Flow, flow transition and runout distances of flowing avalanches. *Annals of Glaciology*, **18**, 221–221.
- Salm, B., A. Burkard, and H. Gubler, 1990: *Berechnung von Fließlawinen: eine Anleitung für Praktiker mit Beispielen*. Eidgenössisches Institut für Schnee-und Lawinenforschung SLF, Davos.
- Sampl, P. and T. Zwinger, 2004: Avalanche simulation with SAMOS. *Annals of Glaciology*, **38** (1), 393–398.

- Scapozza, C. and P. Bartelt, 2003: Triaxial tests on snow at low strain rate. Part II. Constitutive behaviour. *Journal of Glaciology*, **49** (164), 91–101.
- Schaerer, P. A., 1973: Observations of avalanche impact pressures. *USDA For Serv Gen Tech Rep RM Rocky Mt For Range Exp Stn For Serv US Dep Agric*.
- Schneebeli, M. and P. Bebi, 2004: *Snow and Avalanche Control*, 397–402. Elsevier.
- Schneebeli, M. and M. Meyer-Grass, 1993: Avalanche starting zones below the timberline-structure of forest. *Proceedings of the International Snow Science Workshop*, Breckenridge, Colorado.
- Schoennagel, T., T. T. Veblen, D. Kulakowski, and A. Holz, 2007: Multidecadal climate variability and climate interactions affect subalpine fire occurrence, western Colorado (USA). *Ecology*, **88** (11), 2891–2902.
- Schweingruber, F. H. et al., 1996: *Tree rings and environment: dendroecology*. Paul Haupt AG Bern.
- Schweizer, J., J. Bruce Jamieson, and M. Schneebeli, 2003: Snow avalanche formation. *Reviews of Geophysics*, **41** (4).
- Schweizer, J., K. Kronholm, J. B. Jamieson, and K. W. Birkeland, 2008: Review of spatial variability of snowpack properties and its importance for avalanche formation. *Cold Regions Science and Technology*, **51** (2-3), 253–272.
- Sheikh, A. H., S. C. Verma, and A. Kumar, 2008: Interaction of retarding structures with simulated avalanches in snow chute. *Current Science*, **94** (7), 916–921.
- SLF, 2000: *Der Lawinenwinter 1999. Ereignisanalyse*. Eidgenössisches Institut für Schnee- und Lawinenforschung SLF, Davos, 588 pp.
- Sovilla, B., P. Burlando, and P. Bartelt, 2006: Field experiments and numerical modeling of mass entrainment in snow avalanches. *Journal of Geophysical Research-earth Surface*, **111** (F3), F03007.
- Sovilla, B., M. Kern, and M. Schär, 2010: Slow drag in wet-snow avalanche flow. *Journal of Glaciology*, **56** (198), 587–592.
- Sovilla, B., S. Margreth, M. Schaer, E. Thiebert, J.-T. Fischer, D. Baroudi, and C. Ancey, 2014: Taking into account wet avalanche load for the design of tower-like structures. *Proceedings of the International Snow Science Workshop, Banff, Canada*.
- Sovilla, B., M. Schaer, and L. Rammer, 2008: Measurements and analysis of full-scale avalanche impact pressure at the Vallée de la Sionne test site. *Cold Regions Science and Technology*, **51** (2-3), 122 – 137.
- Sovilla, B., I. Sonatore, Y. Bühler, and S. Margreth, 2012: Wet-snow avalanche interaction with a deflecting dam: field observations and numerical simulations in a case study. *Natural Hazards and Earth System Sciences*, **12** (5), 1407–1423.

- Steinkogler, W., B. Sovilla, and M. Lehning, 2014: Influence of snow cover properties on avalanche dynamics. *Cold Regions Science and Technology*, **97**, 121–131.
- Stethem, C., B. Jamieson, P. Schaerer, D. Liverman, D. Germain, and S. Walker, 2003: Snow avalanche hazard in Canada—a review. *Natural Hazards*, **28 (2-3)**, 487–515.
- Stimberis, J. and C. Rubin, 2011: Glide avalanche response to an extreme rain-on-snow event, Snoqualmie Pass, Washington, USA. *Journal of Glaciology*, **57 (203)**, 468–474.
- Stokes, A., et al., 2005: Mechanical resistance of different tree species to rockfall in the French Alps. *Plant and Soil*, **278 (1-2)**, 107–117.
- Takeuchi, Y., H. Torita, K. Nishimura, and H. Hirashima, 2011: Study of a large-scale dry slab avalanche and the extent of damage to a cedar forest in the Makunosawa valley, Myoko, Japan. *Annals of Glaciology*, **52 (58)**, 119–128.
- Teich, M., P. Bartelt, A. Grêt-Regamey, and P. Bebi, 2012a: Snow avalanches in forested terrain: influence of forest parameters, topography and avalanche characteristics on runout distance. *Arctic, Antarctic, and Alpine Research*, **44 (4)**, 509–519.
- Teich, M. and P. Bebi, 2009: Evaluating the benefit of avalanche protection forest with GIS-based risk analyses—A case study in Switzerland. *Forest Ecology and Management*, **257**, 1910–1919.
- Teich, M., J.-T. Fischer, T. Feistl, P. Bebi, M. Christen, and A. Grêt-Regamey, 2014: Computational snow avalanche simulation in forested terrain. *Natural Hazards and Earth System Sciences*, **14 (8)**, 2233–2248.
- Teich, M., I. Vassella, P. Bartelt, P. Bebi, T. Feistl, and A. Grêt-Regamey, 2012b: Avalanche simulations in forested terrain: A framework towards a bayesian probabilistic model calibration. *Proceedings of the International Snow Science Workshop, Anchorage, Alaska*.
- Teufelsbauer, H., Y. Wang, S. Pudasaini, R. Borja, and W. Wu, 2011: DEM simulation of impact force exerted by granular flow on rigid structures. *Acta Geotechnica*, **6 (3)**, 119–133.
- Tiri, R., 2009: Interaktionen zwischen verschiedenen Baumeigenschaften und Lawinen. M.S. thesis, Eidgenössische Technische Hochschule Zürich.
- Trujillo, E., N. P. Molotch, M. L. Goulden, A. E. Kelly, and R. C. Bales, 2012: Elevation-dependent influence of snow accumulation on forest greening. *Nature Geoscience*, **5 (10)**, 705–709.
- van Herwijnen, A. and J. Heierli, 2009: Measurement of crack-face friction in collapsed weak snow layers. *Geophysical Research Letters*, **36**, L23 502.
- van Herwijnen, A. and R. Simenhois, 2012: Monitoring glide avalanches using time-lapse photography. *Proceedings of the International Snow Science Workshop, Anchorage, Alaska*.

- Veitinger, J., B. Sovilla, and R. Purves, 2014: Influence of snow depth distribution on surface roughness in alpine terrain: a multi-scale approach. *The Cryosphere*, **8**, 547–569.
- Vera, C., K. Wikstroem, Y. Bühler, and P. Bartelt, in press: Release temperature, snowcover entrainment and the thermal flow regime of snow avalanches. *Journal of Glaciology*.
- Viglietti, D., S. Letey, R. Motta, M. Maggioni, and M. Freppaz, 2010: Snow avalanche release in forest ecosystems: A case study in the Aosta Valley Region (NW-Italy). *Cold Regions Science and Technology*, **64**, 167–173.
- Völlmy, A., 1955: Über die Zerstörungskraft von Lawinen. *Schweizer Bauzeitung*, **73(12/15/17/19)**, 159–162, 212–217, 246–249.
- Von Moos, M., P. Bartelt, A. Zweidler, and E. Bleiker, 2003: Triaxial tests on snow at low strain rate. Part I. Experimental device. *Journal of Glaciology*, **49 (164)**, 81–90.
- Voytkovskiy, K., 1977: Mekhanicheskiye svoystva snega [mechanical properties of snow]. *CE Bartelt (trans.)*, Moscow, Nauka. Sibirskoye Otdeleniye. Institut Merzlotovedeniya.
- Weir, P., 2002: *Snow avalanche management in forested terrain*. B.C. Government Publication Services.
- Zenke, B., 1978: *Das Schneegleiten auf der Plaick: seine Ursachen und seine Auswirkungen auf Boden und Vegetation*.
- Zenke, B., 1989: Die Lawinensituation im bayerischen Alpenraum. *Schutz vor Wildbächen und Lawinen - Auswirkungen der Waldschäden -*, Informationsbericht des Bayerischen Landesamtes für Wasserwirtschaft, München, 163–182.